

FLORIDA INTERNATIONAL UNIVERSITY

Miami, Florida

DEVELOPMENT OF HUMAN VALVULAR CALCIFICATION VIA FLUID-
INDUCED OSCILLATORY SHEAR STRESS-BASED CELL AND TISSUE
CULTURE

A dissertation submitted in partial fulfillment of

the requirements for the degree of

DOCTOR OF PHILOSOPHY

in

BIOMEDICAL ENGINEERING

by

Chia-Pei Denise Hsu

2022

To: Dean John L. Volakis
College of Engineering and Computing

This dissertation, written by Chia-Pei Denise Hsu, and entitled Development of Valvular Cell and Tissue Calcification from Fluid-Induced Oscillatory Shear Stresses, having been approved in respect to style and intellectual content, is referred to you for judgment.

We have read this dissertation and recommend that it be approved.

Nikolaos Tsoukias

Florence George

Elena Aikawa

Sharan Ramaswamy, Co-Major Professor

Joshua Hutcheson, Co-Major Professor

Date of Defense: October 21, 2022

The dissertation of Chia-Pei Denise Hsu is approved.

Dean John L. Volakis
College of Engineering and Computing

Andres G. Gil
Vice President for Research and Economic Development
And Dean of the University Graduate School

Florida International University, 2022

© Copyright 2022 by Chia-Pei Denise Hsu

All rights reserved.

DEDICATION

To Mom and Dad.

ACKNOWLEDGMENTS

When I first joined the program, the journey was joyful and exciting yet somewhat solitary. Then over the semesters the circle began to expand, encompassing people of whom contributed their expertise, until finally I am holding the creation of a new dissertation in my hands. Thank you, thank you, and thank you: to my major and co-major professors, Dr. Sharan Ramaswamy and Dr. Joshua Hutcheson, who provided scientific knowledge and helped me formulate this part of my life. To my dissertation committee members as well as mentors and colleagues from CV-PEUTICS and Cardiovascular Matrix Remodeling Laboratory (CMRL), thank you all for sharing your research skills to help me complete my goals. Many thanks to CorMatrix Cardiovascular, Inc. for sponsoring a portion of this dissertation, the Teaching Assistant Fellowships provided by the Department of Biomedical Engineering at Florida International University, and my Dissertation Year Fellowship award from the University Graduate School at Florida International University.

ABSTRACT OF THE DISSERTATION
DEVELOPMENT OF HUMAN VALVULAR CALCIFICATION VIA FLUID-
INDUCED OSCILLATORY SHEAR STRESS-BASED CELL AND TISSUE
CULTURE

by

Chia-Pei Denise Hsu

Florida International University, 2022

Miami, Florida

Professor Sharan Ramaswamy, Co-Major Professor

Professor Joshua Hutcheson, Co-Major Professor

Cardiovascular diseases are the global leading causes of morbidity and mortality that includes conditions affecting the heart and blood vessels, with little or no treatment options in many severe cases. Calcific aortic valve disease (CAVD) is one of the most common chronic heart problems that involves build-up of calcified deposits on the aortic valve leaflet, resulting in hardening of valve leaflets and inefficient valve function, thereby severely compromising the systemic blood circulation. Currently, there are no treatment options or diagnostic tools for early and intermediate stages of CAVD, and the main factors associated with early formation of CAVD remain unclear. Severe treatment options for CAVD include transcatheter aortic valve replacements (TAVR) and surgical aortic valve replacements (SAVR) with mechanical or bioprosthetic valves, which involve various potential risks and are therefore limited to a selective patient subset.

A major obstacle in developing therapeutic targets for early CAVD intervention is an absence of human tissue model systems that can assess the responses to potential treatments.

While forces generated by blood flow are known to affect cardiovascular development and remodeling, these hemodynamic forces induce molecular cues that are often communicated amongst various cell types, and the links between flow patterns and development of CAVD requires further investigation. Common animal models for cardiovascular diseases such as ovine and porcine models, do not mimic the human response following heart valve therapeutics. Therefore, understanding the specific effects of flow oscillations on human valve pathology can also help to establish the foundation for developing a human engineered tissue model system for early stages of CAVD, thereby forming a testbed for effective drug discovery. Using the oscillatory shear index (OSI) as a parameter to quantify the degree of flow oscillations, this PhD dissertation provides identification between a specific OSI-level and the clear induction of CAVD. In this regard, for 3D tissue culture assessment, an oscillatory flow bioreactor was built and used. This bioreactor facilitates a controlled oscillatory flow environment that allows mechanistic and longitudinal studies of evolving CAVD at the organ-level and may serve as a potential platform to facilitate drug discovery for effective pharmaceutical management of CAVD.

TABLE OF CONTENTS

CHAPTER	PAGE
Chapter I: Introduction and Motivation	1
1.1. Statement of Problem	1
1.2. Specific Aims	3
Chapter II: Background.....	7
2.1. Unidirectional Laminar Flow vs. Oscillatory Laminar Flow	7
2.2 Transition and Flow Turbulence	8
2.3. Vascular Anatomy and Hemodynamics	9
2.4. Aortic Valve Anatomy and Hemodynamics	10
2.5. Vasculature Plaques vs. Valve Calcification.....	11
2.5.1. Vascular Pathology.....	12
2.5.2. Biomechanical Context in the Vasculature	13
2.5.3. Valvular Pathology	15
2.5.4. Biomechanical Context in Heart Valves	15
2.6. Bioreactor Systems.....	16
2.7. Summary	17
Chapter III: Aim 1 – Effect of OSI on vascular pathology at the cellular level	18
3.1. Introduction	18
3.2. Methods.....	19
3.3. Results	21
3.4. Discussion	26
3.5. Summary	27
Chapter IV: Aim 2 – Effect of OSI on valvular calcification at the cellular level	29
4.1. Introduction	29
4.2. Methods.....	31
4.2.1. <i>In Vitro</i> Experiments and Calcification Assessments Using Rat Cells	31
4.2.2. <i>In Vitro</i> Experiments and Calcification Assessments Using Human Cells	33
4.3. Results	34
4.3.1. Rat Valvular Cell Assessments.....	34
4.3.2. Human Valvular Cell Assessments	36
4.4. Discussion	38
4.5. Summary	39
Chapter V: Aim 3 – An <i>in vitro</i> engineered tissue model system to recreate the etiology of valve calcification.....	41
5.1. Introduction	41
5.1.1. Bio-scaffolds vs. Synthetic Scaffolds.....	41

5.1.2. Cardiac Output, GOA, and EOA	43
5.1.3. Bernoulli's Principle and Modified Bernoulli's Equation.....	44
5.1.4. Elastic Modulus (Young's Modulus) and Hertzian Theory	45
5.2. Methods	46
5.2.1. Bioreactor Design and CFD	46
5.2.2. Valvular Cell Seeding and Valve Tissue Conditioning in Bioreactor.....	48
5.2.3. Valve Hydrodynamic Assessments	52
5.2.4. Mechanical Properties of Conditioned Valves	54
5.3. Results	55
5.3.1. CFD Results and Cell Seeding Verification.....	55
5.3.2. Valve Hydrodynamic Assessments	57
5.3.3. Mechanical Properties of Conditioned Valves	60
5.3.4. Calcification Assessments of Conditioned Valves.....	60
5.4. Discussion	61
5.5. Summary	67
Impact and Future Studies	67
References.....	70
APPENDICES	79
VITA.....	104

LIST OF TABLES

TABLE	PAGE
Table 1. HAEC Top 15 Genes in Order of Significance between Flow Groups	23
Table 2. HASMC Top 15 Genes in Order of Significance between Flow Groups.....	24
Table 3. Valve in open and closed configurations during hydrodynamic testing.....	53
Table 4. ARS Quantification - Bioreactor Conditioned Samples	89
Table 5. ARS Quantification - Raw PSIS Samples	90
Table 6. ARS Quantification - Static Conditioned Samples.....	91

LIST OF FIGURES

FIGURE	PAGE
Figure 1. Flowrate over time.....	7
Figure 2. Flowrate profile under turbulent flow conditions.....	9
Figure 3. Structure of the arterial wall.....	10
Figure 4. A straight segment of vasculature	10
Figure 5. Aortic valve anatomy and valve hemodynamics.....	11
Figure 6. Plaque formation in blood vessels.....	12
Figure 7. Healthy (A) and calcified (B) aortic valves in the closed configuration.....	12
Figure 8. HAEC Log ₂ fold change gene expression comparisons.....	21
Figure 9. HASMC Log ₂ fold change gene expression comparisons	22
Figure 10. HAEC gene expression of CDH5, MMP10, and SELE	26
Figure 11. HASMC gene expression of ACTA2, MYH11, and TAGLN	26
Figure 12. Rat VIC calcification.....	34
Figure 13. Rat VIC gene expression.....	35
Figure 14. Human VIC calcification 1.....	36
Figure 15. Human VIC calcification 2.....	37
Figure 16. Human VIC calcification 3.....	38
Figure 17. Elastin (green) deposition in PSIS (top) vs. in PGA-PLLA (bottom).....	42
Figure 18. GOA vs. EOA.....	43
Figure 19. Young's modulus	45
Figure 20. Overview of the Young's Modulus of different materials.....	46
Figure 21. Bioreactor flow domain (top) and meshed elements (bottom).....	47

Figure 22. Input square waveform of 1 cardiac cycle.....	48
Figure 23. Bioreactor schematic	48
Figure 24. PSIS geometry and material texture	49
Figure 25. 3D printed valve holders in aortic tri-leaflet configuration with three posts ..	49
Figure 26. Conditioned Bioreactor Valves.	50
Figure 27. Embedding of samples in OCT compound	51
Figure 28. Schematic of the Vivitro pulse duplicator for valve hydrodynamic testing	52
Figure 29. Flat-end circular indenter over a PSIS sample	54
Figure 30. CFD simulation results	55
Figure 31. Immunofluorescent staining of bioreactor and static samples	56
Figure 32. Regurgitation factor.....	57
Figure 33. Transvalvular pressures	58
Figure 34. EOA.....	58
Figure 35. Volumetric flowrates.....	59
Figure 36. Young's moduli of PSIS valves	60
Figure 37. ARS images of valves	61
Figure 42. Hydrodynamic results.....	63
Figure 43. GOA of bioreactor PSIS valve in the open configuration.....	68
Figure 44. CFD velocity profile (top) and measured volumetric flow rates.....	82
Figure 45. ARS images of bioreactor-conditioned valves	89
Figure 46. ARS images of raw PSIS.....	90
Figure 47. ARS images of statically conditioned valves	91
Figure 48. CD31 (green) and α SMA (red) immunofluorescent stains 1	98

Figure 49. CD31 (green) and α SMA (red) immunofluorescent stains 2 99

ABBREVIATIONS AND ACRONYMS

AA2P	L-Ascorbic acid 2-phosphate
ARS	Alizarin red staining
bFGF	Basic fibroblast growth factor
BPM	Beats per minute
CAVD	Calcific aortic valve disease
CFD	Computational fluid dynamics
CO	Cardiac output
DAPI	4',6-diamidino-2-phenylindole
DEPC	Diethylpyrocarbonate
DMEM	Dulbecco's modified eagle medium
DNA	Deoxyribonucleic acid
ECHO	Echocardiogram
ECM	Extracellular matrix
EOA	Effective orifice area
EX	Exosome or exosomal
GOA	Geometric orifice area
FBS	Fetal bovine serum
HAEC	Human aortic endothelial cells
HASMC	Human aortic smooth muscle cells
HBMSC	Human bone marrow stem cells
HR	Heart rate
NonEX	Non-exosome or non-exosomal

OCT	Optimal cutting temperature
OSI	Oscillatory shear index
PC	Pro-calcific
PGA-PLLA	Poly glycolic acid-poly L-lactic acid
PS	Penicillin streptomycin
PSIS	Porcine small intestinal submucosa
Re	Reynolds Number
RF	Regurgitation factor
RNA	Ribonucleic acid
RT-qPCR	Real-time quantitative polymerase chain reaction
SAVR	Surgical aortic valve replacement
SEM	Standard error of the mean
SV	Stroke volume
TAVR	Transcatheter aortic valve replacement
TAWSS	Time-averaged wall shear stress
VasEC	Vascular endothelial cells
VasSMC	Vascular smooth muscle cells
VEC	Valvular endothelial cells
VIC	Valvular interstitial cells

Chapter I: Introduction and Motivation

1.1. Statement of Problem

The cardiovascular system is comprised of the heart and blood vessels that provide nutrients and remove wastes throughout the systemic circulation. While heart valves and vasculature differ in cell types and are subject to different environmental forces, they both undergo continuous remodeling that involve paracrine regulation between respective cell types and can become susceptible to calcification due to improper cell communication. Cardiovascular diseases are global leading causes of morbidity and mortality that includes conditions affecting the heart, blood vessels, and heart valves. While plaque morphology in valvular and vascular diseases are similar, current available therapeutic targets for vascular calcification are ineffective in treating heart valve calcification. Understanding the similarities and differences in the development of calcification between valvular and vascular systems due to environmental factors can help provide insights to identify future treatment options, particularly valvular pathologies that are less studied in comparison to vascular diseases. Heart valve complications such as calcific aortic valve disease (CAVD) are one of the most prevalent conditions involving hardening of valve leaflets due to mineral deposition, which can lead to reduced cardiac output, increased regurgitation, and eventually heart failure. Statistical data show a worldwide increase of CAVD cases by 124% between 1990 and 2017 [1]. Currently, there are no treatment options or diagnostic tools for early and intermediate stages of CAVD, and the main factors associated with early formation of CAVD remain unclear. Treatment options for severe CAVD include transcatheter aortic valve replacements (TAVR) and surgical aortic valve replacements (SAVR) with mechanical or bioprosthetic valves. However, these treatment options

involve various potential risks and are often limited to a selective patient subset. A major obstacle in developing therapeutic targets for early CAVD intervention is an absence of human tissue model systems that can assess the responses to potential treatments, recognizing that animal models are unable to adequately mimic the human response [2].

The aortic valve consists of three equal-sized leaflets that form three lines of coaptation. In some cases, two or more than three leaflets are found. Each valve leaflet contains a ventricularis layer that faces the heart's ventricle, a fibrosa layer that faces the aorta, and a spongiosa layer that is sandwiched between the ventricularis and fibrosa layers. Due to the valve structure and direction of blood flow, the ventricularis layer is mainly dominated by laminar flow with high shear stress, whereas the fibrosa layer is subject to low shear stress and oscillatory flow. While clinical observations have mainly correlated CAVD with the fibrosa layer [3] [4], the links between flow patterns and development of CAVD need further investigation. We have identified flow oscillation as a factor and regulator for valve calcification, and we showed that valve tissue exposure to high flow oscillations under low shear stresses can lead to substantial risk of valve calcification.

A monolayer of valve endothelial cells (VECs) resides on the outer surfaces of aortic valve leaflets. Deeper within the leaflets are sublayers of valve interstitial cells (VICs). Valve remodeling is a continuous physiological response that involves paracrine regulation between VECs and VICs, and diseases such as CAVD can result from abnormal communication between these cell types. VECs are known to respond to hemodynamic stimuli and can result in pro-inflammatory phenotypic changes under disturbed flow [5]. Using the oscillatory shear index (OSI) as a parameter to quantify the degree of flow oscillations [6], we studied the effects of various OSI flow profiles on VECs, and their

communication with VICs that leads to valve calcification. We demonstrated that VECs exposed to high oscillation leads to higher risk of VIC calcification compared to exposure to low or moderate flow oscillation. Furthermore, we introduced a novel oscillatory bioreactor model system that allows mechanistic and longitudinal studies of evolving CAVD at the organ-level that can be used as a potential platform to facilitate drug discovery to prevent or slow the progression of severe valve calcification.

1.2. Specific Aims

Flow environments on cardiovascular tissues can significantly impact cellular interactions, including paracrine regulation in both the vasculature, as well as in heart valves. While plaque morphology in the vascular and valvular systems are similar as they both involve calcific mineral deposition and undergo pathological remodeling due to environmental forces, the etiology of valve calcification can be quite distinct from vascular calcification. Of particular focus is the effect of oscillatory flow from blood flow patterns on biomechanical-induced pathology in vascular versus valvular components in the systemic circulation. In addition, currently available therapeutic targets for vascular calcification are ineffective in the management of valvular calcification.

Clinical observations have shown atherosclerotic plaque formation mainly on vascular bifurcation sites [7]. Bifurcations regions also exhibit higher variations of flow oscillation compared to straight segments [8]. In heart valves, previous studies have shown that oscillatory flow can result in pro-inflammatory responses and VEC dysfunction, which can lead to phenotypic switching of quiescent VICs to osteogenic phenotypes [5] [9]. To further determine the magnitude of oscillatory flow patterns under a low, but nonetheless physiologically relevant level of time-averaged valve leaflet shear stress (1 dyne/cm²) and

its association with pathology, an OSI parameter is used to quantify changes in the direction of shear stress [6]. The effect of valve tissue calcification due to OSI as a key regulator of shear-dependent mechanotransduction has not been studied. We hypothesize that a combination of high degrees of flow oscillations trigger pathological events, as clinical observations have correlated plaque formation mainly on regions that are subject to oscillatory flow environments.

Specific Aim 1. Evaluate the extent to which paracrine signaling-mediated events from VasECs cultured under dynamic conditions in low (OSI = 0), moderate (OSI = 0.25), and high (OSI = 0.50) OSI environments alter VasSMC gene expression. Human aortic endothelial cells (HAECs) will be conditioned under different OSI environments at a physiologically relevant magnitude of time-averaged shear stress (1 dyne/cm^2) for arterial tissues. To establish paracrine communication by exposing biochemical end-products from HAECs to its sublayer cell type, human aortic smooth muscle cells (HASMCs), conditioned media of each OSI group from HAECs will be collected and subsequently reused to culture HASMCs. We expect that HAECs exposed to high OSIs and HASMCs exposed to HAEC end-products generated from conditioning under high OSI (OSI = 0.50) will significantly induce more pro-remodeling gene expressions compared to other OSI groups. This aim is a non-biased approach that seeks to establish a database of cellular responses in the vascular endothelium due to exposure to various oscillatory flow environments, as well as paracrine regulation between HAECs and HASMCs in response to inflammation or pathology in the vascular system.

Specific Aim 2. Evaluate the extent to which paracrine signaling-mediated events from VECs cultured under dynamic conditions in low (OSI = 0), moderate (OSI = 0.25), and

high (OSI = 0.50) OSI environments lead to VIC calcification. VECs will be conditioned under different OSI environments at a physiologically relevant magnitude of time-averaged shear stress (1 dyne/cm^2) for aortic valve leaflet tissues. To establish paracrine communication by exposing biochemical end-products from VECs to VICs, conditioned media of each OSI group from VECs will be collected and subsequently reused to culture VICs with PC ingredients. We expect that VICs exposed to VEC end-products generated from conditioning under high OSI (OSI = 0.50) in conjunction with PC environments will exhibit significantly higher calcification levels compared to other OSI groups. The goal of this aim is to identify OSI-mediated paracrine signaling between VECs and VICs that promotes valvular calcification by focusing on the endpoint responses and genes of interest.

Specific Aim 3. Assess calcification and impact on valve performance in tri-leaflet engineered valve tissue (3-dimensional) culture consisting of bio-scaffolds seeded with valvular cells conditioned *in vitro* under dynamic fluid-induced mechanical environments with time-averaged shear stress and the most calcific OSI from Aim 2 in PC media in a bioreactor system. Using computational fluid dynamics (CFD), OSI environments in the bioreactor chamber will be quantified and validated using pressure and flow probes. VECs and VICs will be seeded in cylindrical porcine small intestinal submucosa (PSIS) bio-scaffolds and sutured in tri-leaflet configurations to be conditioned in PC environments under a valve-relevant magnitude of time-averaged shear stress (1 dyne/cm^2) in conjunction with static and most pro-calcific OSI determined from Aims 1 and 2 in the bioreactor system. Histological assessments, mechanical properties, and valve hydrodynamic functions will be evaluated on conditioned tissues to determine level of calcification and effect on valve performance. Under a physiologically relevant magnitude

of time-averaged aortic leaflet shear stress, we expect that tissues exposed to high OSI (OSI = 0.50) in a PC environment will exhibit significantly higher calcification compared to static conditions. The goal of this aim is to formulate an *in vitro* framework for our engineered tissue model system for recreating the etiology of human aortic valve calcification.

Impact. The proposed study will provide an insight to relation between OSI and the development of CAVD in aortic valves. In addition, the study will introduce a novel bioreactor system that provides an environment to recapitulate progression of human aortic valve calcification. The bioreactor system can serve as a future testbed for drug discovery that targets calcific bio-molecular cues to prevent or slow the progression of CAVD.

Chapter II: Background

2.1. Unidirectional Laminar Flow vs. Oscillatory Laminar Flow

Laminar flow is a type of flow pattern characterized by smooth and parallel movement of fluid particles with little or no mixing between adjacent layers. This flow type is deterministic, in which future fluid behavior can be determined by specifications of fluid flow at an earlier time point. In most areas of the circulatory system, laminar flow is the normal condition of blood flow, consisting of concentric layers of blood movement with the highest velocity at the center of the vessel. Fluid velocity is generally determined by the viscosity based on laminar flow conditions. High fluid viscosity indicates higher resistance between each layer of flow, while low viscosity generally implies lower resistance. Laminar flow can be categorized as unidirectional laminar flow and oscillatory laminar flow (Figure 1) [10] [11] based on Reynold's number [12].

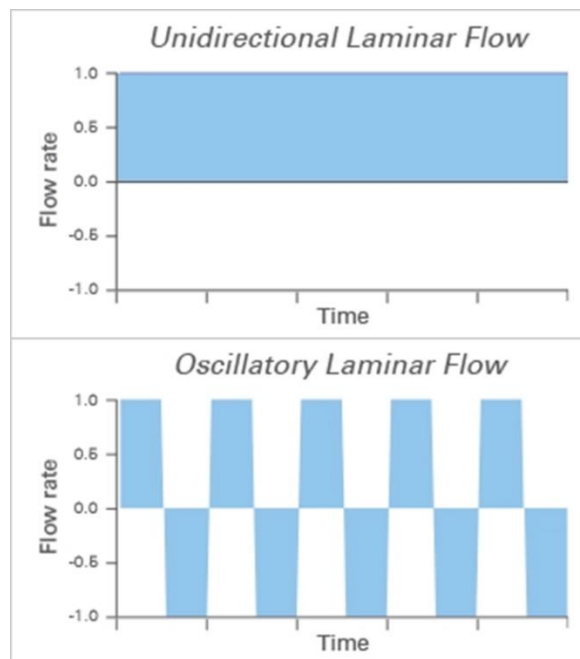


Figure 1. Flowrate over time under unidirectional laminar flow vs. oscillatory laminar flow conditions [13].

Unidirectional laminar flow consists of a constant flow rate and a constant steady flow direction, whereas fluid motion from oscillatory laminar flow is subject to a dominant frequency that is present throughout the overall flow movement due to an external force or a boundary condition while simultaneously maintaining a constant overall flow rate.

To quantify the level or intensity of oscillatory flow, an oscillatory shear index (OSI) parameter is used [6]:

$$OSI = \frac{1}{2} \left(1 - \frac{\left| \int_0^T \tau_w dt \right|}{\int_0^T |\tau_w| dt} \right)$$

Equation 1. OSI equation, T = cycle duration, t = time, and τ_w = wall shear stress [6].

The OSI equation (Equation 1) is defined by the ratio between the net temporal shear stresses in the forward direction to the total temporal shear stress magnitude, which can be in both forward and reverse directions. The OSI values range between 0 (no oscillation) to 0.50 (full oscillation), and the values in between are mainly moderate oscillation. This dissertation utilizes various OSI values to determine their effects on cardiovascular tissue remodeling.

2.2 Transition and Flow Turbulence

While a non-zero OSI flow pattern describes flow disturbance, this flow pattern remains distinct from flow turbulence. Flow turbulence occurs as flow pattern becomes irregular, such that future flow path becomes unpredictable based on previous fluid specifications, and a transitional flow is the presence of both laminar and turbulent characteristics (Figure 2). Laminar and turbulent flows in pipelines are generally determined by the Reynolds Number (Re, Equation 2), which is a dimensionless ratio between inertial forces and dynamic viscosity within the fluid.

$$Re = \frac{\rho V D}{\mu}$$

Equation 2. Reynolds Number, Re. ρ = fluid density, V = flow velocity, D = characteristic linear dimension, and μ = dynamic viscosity.

The flow is laminar when $Re < 2300$, transient when $2300 < Re < 3500$, and turbulent when $Re > 3500$ [12]. Laminar flow is mainly observed in most cardiovascular regions, however, locations such as branching of vessels, changes in boundary conditions such as stenosis or protruding plaques, turbulent flow can be observed even under normal physiological flow velocities [14]. Typical range of Re of blood through aorta varies between 10 to 4000 [15]. However, due to the pulsatile nature blood flow combined with curvature and presence of stenosis, flow can become transient and turbulent at lower Re [16].

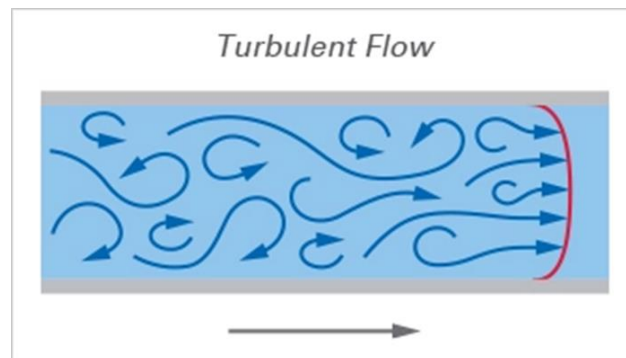


Figure 2. Flowrate profile under turbulent flow conditions [13]. Flow pattern becomes irregular and cannot be predicted based on previous flow path.

2.3. Vascular Anatomy and Hemodynamics

The vascular wall consists of vascular endothelial cells (VasEC) in the tunica intima layer, in which are directly in contact with blood flow, and a sublayer of vascular smooth muscle cells (VasSMC) in the tunica media layer (Figure 3). The outermost layer, tunica adventitia, serves as an external coat on the vasculature consisting of connective tissues and nerves that are responsible for vasodilation and vasoconstriction [17]. Vascular remodeling

involves paracrine signaling between VasECs and VasSMCs, and diseases such as atherosclerosis can result from improper communication between these cell types.

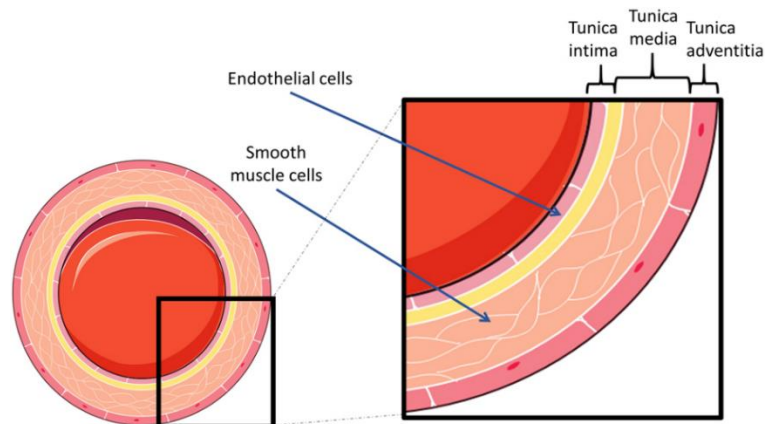


Figure 3. Structure of the arterial wall comprising of vascular endothelial cells in the tunica intima layer and vascular smooth muscle cells in the tunica media layer [18].

Clinical observations show that regions exposed to oscillatory shear are most affected by plaque formation [19]. Most oscillatory shear stresses are found in arterial bifurcation sites (Figure 4), and these sites are more susceptible to developing atherosclerosis [20].

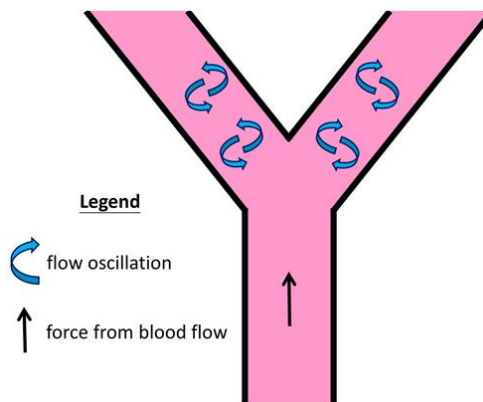


Figure 4. A straight segment of vasculature with laminar flow on the upstream and a bifurcation site on the downstream that is subject to oscillatory flow [18].

2.4. Aortic Valve Anatomy and Hemodynamics

The aortic valve facilitates unidirectional blood movement from the heart ventricles to the aortas to provide systemic blood distribution. Aortic valve function relies on the action of

thin, membranous leaflets that open and close in each cardiac cycle. Each leaflet consists of three layers: the ventricularis, the spongiosa, and the fibrosa layers (Figure 5). The ventricularis faces the ventricle compartment of the heart and is mainly comprised of elastin that is aligned in the radial direction. The fibrosa layer faces the aortic side of the leaflet and consists of mainly collagen aligned in the circumferential direction [21]. The spongiosa layer is sandwiched between the ventricularis and fibrosa layers and are mainly comprised of glycosaminoglycans (GAGs) [22].

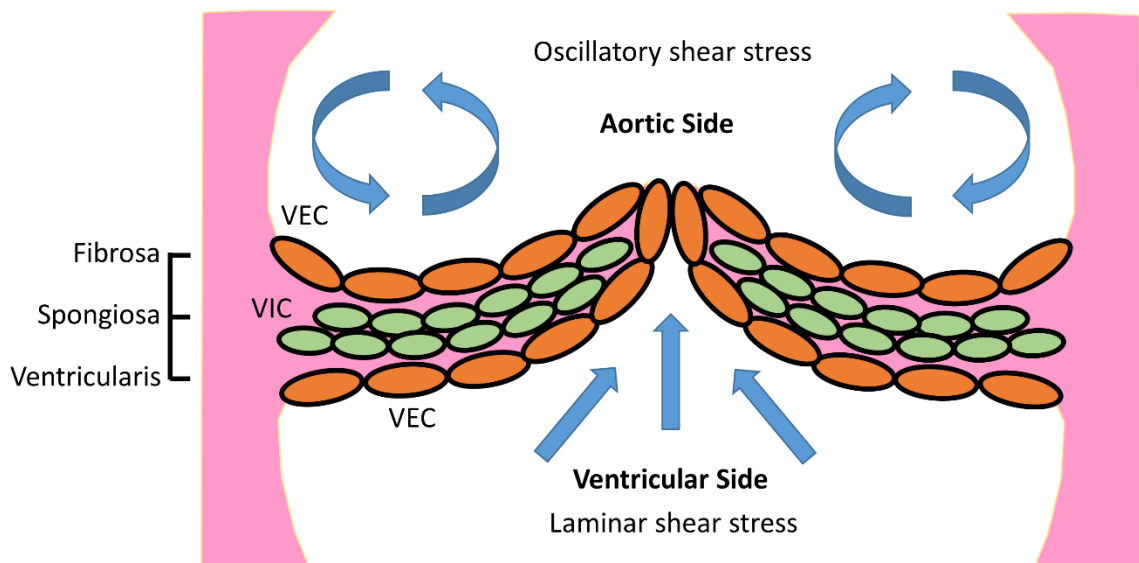


Figure 5. Aortic valve anatomy and valve hemodynamics. Valve tissues consist of fibrosa, spongiosa, and ventricularis layers. Oscillatory flow is commonly found on the fibrosa layers while laminar flow mainly dominates the ventricularis layers [23].

Due to the valve structure and blood flow direction, the ventricularis layer is mainly dominated by high shear stress and unidirectional laminar flow, while the fibrosa layer is subject to low shear stress and oscillatory flow [23].

2.5. Vasculature Plaques vs. Valve Calcification

Clinical observations have shown that regions exposed to oscillatory shear forces are most affected by plaque development or formation of calcification in both vascular and valvular

systems [19]. Vascular atherogenesis often initiates from endothelium dysfunction, which leads to unbalanced production of nitric oxide and formation of atherosclerotic plaques due to smooth muscle cell infiltration and proliferation (Figure 6) [24] [25].

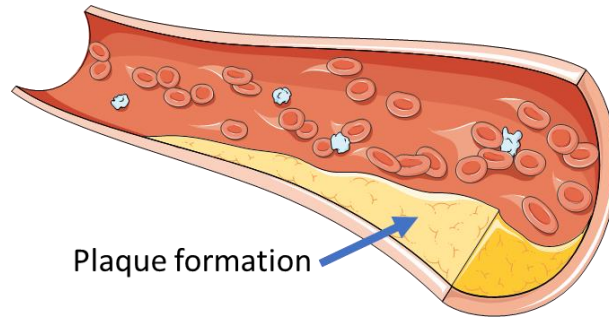


Figure 6. Plaque formation in blood vessels. Image was created from Servier Medical Art Commons (<http://smart.servier.com>). Servier Medical Art by Servier is licensed under a Creative Commons Attribution 3.0 Unported License.

Valve pathology often begins with injury in the valve endothelium, in which increases production of inflammatory cytokines that trigger lipid accumulation, resulting in eventual valve calcification (Figure 7) and valve tissue degeneration [26] [27]. In both vascular and valvular pathologies, the processes involve injury on the respective endothelium, leading to inflammatory responses and increased immune cell activities.

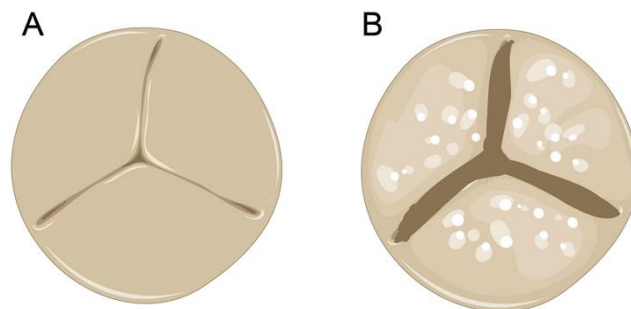


Figure 7. Healthy (A) and calcified (B) aortic valves in the closed configuration [18].

2.5.1. Vascular Pathology

Text for the following subsection taken from:

[18] C. Hsu, J. Hutcheson and S. Ramaswamy, "Oscillatory Fluid-Induced Mechanobiology in Heart Valves with Parallels to the Vasculature," *Vascular Biology*, vol. 2, no. 1, pp. R59-R71, 2020.

Vascular diseases often initiate with damage to the endothelium. The vessel wall consists of two major cell types, VasECs and VasSMCs. VasECs form monolayers that line blood vessel walls, while VasSMCs form multiple layers that cover the outer surface of the lumen. The VasECs secrete signals required for migration and proliferation of VasSMCs [28]. The endothelium is known to play critical roles in initiation and progression of diseases [29]. During vascular injury, smooth muscle cells undergo a process of contractile-to-synthetic phenotypic switching. The synthetic vascular smooth muscle cells tend to migrate and proliferate to enhance vascular repair [30]. Under normal conditions, the synthetic phenotype returns to the non-proliferative, contractile state. However, this plasticity in smooth muscle cells allows cells to respond, resulting in remodeling or, in some cases, pathology, which leads to atherosclerosis, stenosis, or hypertension [31]. Environmental cues including growth factors, inflammatory mediators, and mechanical stresses may trigger phenotypic changes in vascular smooth muscle cells. Disruption of VasEC-VasSMC paracrine communication can also lead to arterial tissue destabilization and regression [28].

2.5.2. Biomechanical Context in the Vasculature

Text for the following subsection taken from:

[18] C. Hsu, J. Hutcheson and S. Ramaswamy, "Oscillatory Fluid-Induced Mechanobiology in Heart Valves with Parallels to the Vasculature," *Vascular Biology*, vol. 2, no. 1, pp. R59-R71, 2020.

Blood vessels maintain integrity and function via VasSMC contractions and relaxations [32]. Studies have found that large production of basal nitric oxide in combination with α 1-

adrenergic responses facilitates high compliance and prevents stiffening effects of VasSMC contractions at high pressures [33]. Other studies have suggested a significant correlation between arterial stiffness and blood pressure, smoking, and circadian rhythms [34] [35] [36]. Nonetheless, the hemodynamics have shown to influence plaque formation and regression in blood vessels, specifically the effects of absolute wall shear stresses and levels of oscillations on vascular lesions [37]. The linkage between blood flow oscillations and atherosclerosis are based on two premises: the mass transport theory and the shear stress theory [38]. The mass transport theory suggests that prolonged contact between blood components and the vessel wall under oscillatory flow conditions increases transport of certain substances. For instance, transport of bioactive compounds such as low-density lipoproteins may increase at sites of high oscillatory flow due to prolonged exposure of these compounds to the vessel wall. The shear stress theory, on the other hand, focuses on the effects of mechanical forces due to blood flow on vascular physiology. Some studies suggest that regions exposed to low wall shear stress magnitudes in combination with blood flow oscillations promote plaque progression [39]. Other studies showed an inconclusive correlation between oscillatory wall shear stress and intimal thickening [40]. The two theories are not mutually exclusive, as both influence plaque formation. Shear stresses can also alter the permeability of blood vessel walls, thereby indirectly affecting molecular mass transport [41]. The combined effects of both hemodynamic parameters in the initiation of atherosclerosis remains unclear. It should be noted that hemodynamic parameters other than wall shear stress and oscillatory flow may also be involved in the onset of atherosclerosis [42].

2.5.3. Valvular Pathology

Text for the following subsection taken from:

[18] C. Hsu, J. Hutcheson and S. Ramaswamy, "Oscillatory Fluid-Induced Mechanobiology in Heart Valves with Parallels to the Vasculature," *Vascular Biology*, vol. 2, no. 1, pp. R59-R71, 2020.

Heart valves are subject to various ranges of mechanical stresses. In response to cyclic changes in mechanical loading, the valves undergo continuous remodeling, which can lead to pathology [43]. Valve anomalies are generally associated with inflammation, osteogenesis, apoptosis, necrosis, leaflet thickening, or formation of calcium nodules [44]. Early calcific lesions are characterized by increase in expression of cell adhesion molecules as well as pro-inflammatory cytokines such as transforming growth factor- β 1 [45] and bone morphogenetic proteins [46]. These cytokines can then induce valve interstitial cells to switch to a fibrotic or osteoblastic phenotype [47] [48], which results in loss of valve tissue homeostasis, upregulation of cathepsins [49], and formation of calcific lesions.

2.5.4. Biomechanical Context in Heart Valves

Text for the following subsection taken from:

[18] C. Hsu, J. Hutcheson and S. Ramaswamy, "Oscillatory Fluid-Induced Mechanobiology in Heart Valves with Parallels to the Vasculature," *Vascular Biology*, vol. 2, no. 1, pp. R59-R71, 2020.

As valve formation involves mechanically dependent processes of extracellular matrix (ECM) maturation, it has been observed that valve maintenance relies heavily on mechanotransduction, which initiates from a healthy hemodynamic environment [50]. Valve injury, on the other hand, can also be caused by changes in the hemodynamic environment that induces wear-and-tear of the endothelial valve tissue [21]. Once endothelial injury occurs, numerous active mechanisms are triggered, such as inflammation,

lipid accumulation, and changes in growth factors and cytokines, resulting in valve degeneration and calcification [26] [51]. Studies have revealed that earliest calcium deposits form at the cusp attachments of the valve leaflets, which experience the maximum level of flexural stress. These stresses may induce tissue degeneration and ultimately calcification [27] [51].

The responses of the valvular endothelium are, in some respects, similar to the vascular endothelium. For example, in both cases, the transport of compounds depends on the direction of blood flow on the valve endothelial surface [52] and the alignment of VECs is dependent on the magnitude and direction of shear stress [53]. However, an important distinction is the fact that aortic VECs align perpendicular to the direction of blood flow, whereas their vascular counterparts align in the parallel direction [54].

2.6. Bioreactor Systems

Bioreactors are devices that provide an ideal, controlled, and physiologically relevant environment for growing organisms such as cells, bacteria, or yeasts, and they are commonly used in industrial processes to produce antibodies, pharmaceuticals, and other organic byproducts. Common types of bioreactors include spinner flasks, rotation wall vessels, and perfusion systems. Other more complex types of bioreactor systems can be custom-built, provided that the system feeds adequate air and nutrients into the organism components while minimizing contamination and gas bubbles during dynamic culture. Bioreactor culture can help increase biocompatibility of the engineered valve tissues, which involve seeding cells on a scaffold and exposing tissues under a dynamic environment of interest that is similar to physiological conditions.

A flow perfusion bioreactor system is a semi-open system that allows continuous dynamic culture of cell and tissue components in an environment that feeds cells with fresh media while removing spent media. The tissue samples are subject to continuous mechanical stimulation, fresh nutrients, and waste removal throughout the entire culture period. Traditional batch bioreactor, on the other hand, all nutrients are fed into the bioreactor at the start of the culture with nothing added to or removed from the system during the entire culture process. The nutrient and waste product concentration change over time; therefore, batch bioreactor culture is a closed but unsteady system.

2.7. Summary

Flow oscillations play an important role in the early onset of developing cardiovascular calcification. Previous studies and clinical observations have correlated disturbed flow with endothelial inflammation and tissue calcification [3] [23]. Using OSI to study the effects of a specific flow oscillation on cardiovascular calcification may provide new insights to early development of CAVD. In addition, designing and constructing a novel bioreactor platform that induces valve tissue calcification may assist with development of diagnostic tools for early detection and the assessment of drug interventions for the treatment of CAVD, thereby avoiding or delaying the need for a prosthetic valve replacement.

Chapter III: Aim 1 – Effect of OSI on vascular pathology at the cellular level

3.1. Introduction

The vascular endothelium is known to respond to hemodynamic stimuli during continuous remodeling, and atherosclerosis often occurs at sites of VasEC dysfunction, particularly in regions exposed to oscillatory flow compared to unidirectional flow. Studies have shown significant changes in cardiovascular cell phenotype under various dynamic environments such as flow, flexure, and stretch [55]. Loss of endothelial integrity has been found in regions exposed to disturbed flow patterns at low shear stress, leading to reduced production of nitric oxide and an increase in VasEC apoptosis, resulting in accumulation of low-density lipoprotein cholesterol [56]. The cholesterol build-up therefore promotes VasSMC proliferation, migration, and osteogenic differentiation, resulting in calcification within the atherosclerotic plaques [57]. In this regard, there may be a range of flow oscillations that maintains or compromises vascular tissue integrity. It has been widely accepted that biomechanical cues due to environmental forces are critical in the maintenance of cardiovascular tissue homeostasis, however, using OSI as a key regulator to determine cell communication and molecular regulation has not been thoroughly explored. In this specific aim, we investigated the paracrine regulation of biochemical end-products between VasECs and VasSMCs in response to exposure to physiologically relevant oscillations through transcriptomic analyses of gene expressions of the above two vascular cell types.

Flow of genetic information stored in a DNA template involves transcription into RNA, followed by protein translation [58]. Expression of genetic information can vary due to environmental factors that determine the phenotype of the cell or tissue [59]. Common

methods such as northern blots and quantitative polymerase chain reaction (qPCR) are limited to measuring a small set of transcripts. RNA sequencing, in contrast, enables genome-wide quantification of gene expression that elucidates deep profiling of potential phenotypic changes under different physiological or pathological settings.

3.2. Methods

HAECs and HASMCs were purchased from Cell Biologics, Inc. (Chicago, IL) and PromoCell GmbH (Heidelberg, Germany), respectively. Both cell types were expanded in culture flasks using Endo Cell Growth Medium (Cell Applications, Inc., San Diego, CA) and Smooth Muscle Cell Growth Medium 2 with supplements (PromoCell GmbH, Heidelberg, Germany) with an addition of 1% penicillin-streptomycin (PS) in the respective growth medium. HAECs were seeded using a gelatin matrix coating for 24 hours at 2.0×10^5 cells per channel in 24-well Bioflux plates consisting of 8 microfluidic channels per plate (Fluxion Biosciences, Inc. Alameda, CA). The HAECs were then conditioned for 48 hours in the Bioflux shear stress cell assay system at an average shear stress magnitude of 1 dyne/cm^2 under the following OSIs: static (0 OSI/no flow), steady flow (0 OSI/steady flow), 0.25 OSI (moderate oscillation), and 0.50 OSI (full oscillation). The conditioned media from HAEC groups were collected and subsequently used to culture HASMCs in T25 flasks for 48 hours. Three samples of each cell type per flow group were conducted, and RNA was extracted and quantified in all HAEC and HASMC samples using TRIzol reagent (Invitrogen, Waltham, MA). The extracted RNA was suspended in $15 \mu\text{L}$ of UltraPure DEPC-treated Water (Invitrogen, Waltham, MA) and delivered to the RNA sequencing facility in the Center for Genome Technology at University of Miami. A total of 24 samples were delivered to conduct RNA sequencing.

The RNA samples were sequenced via paired-end reading, which enabled both ends of the RNA sample to be sequenced, allowing alignment algorithms to map reads over repetitive regions more precisely. Upon termination of the reads, a database of FASTQ files consisting of base pairs were provided as raw data. The raw data was then transferred to the Department of Biostatistics at Florida International University for further alignment of base pairs, mapping base pairs with existing human gene cards, and calculating total number of raw counts for each specific gene. Initial FASTQ data processing was conducted by Ms. Zhenghua Gong from Dr. Changwon Yoo's team using Python and delivered to us as .csv files containing all detected genes from the reads with the respective counts for each cell type in all sample groups.

Further data processing was conducted using MATLAB 2022a (Mathworks, Natick, MA) by Asad Mirza, a PhD candidate from the CV-PEUTICS Laboratory using a built-in `rnaseqde` function. Read counts from the .csv file was normalized by dividing each sample's raw counts size factor, which was estimated by a pseudo-reference sample [60]. The reference sample was estimated by the geometric mean of each gene across all sample groups, and the median of the ratio of the counts to this reference was used as the size factor. The differences in the gene expressions between groups were determined by comparing the fold change for each gene. A logarithmic scale of base 2 (\log_2) of the fold change was reported to symmetrize the shifts of data points. The `rnaseqde` function uses an exact test to determine differences between each flow group [60] [61], and a significance with a threshold of p-value was set to less than 0.05. The genes that were deemed significant had a $\log_2 > 1$ and were reported into upregulated or downregulated genes with respect to each flow group.

3.3. Results

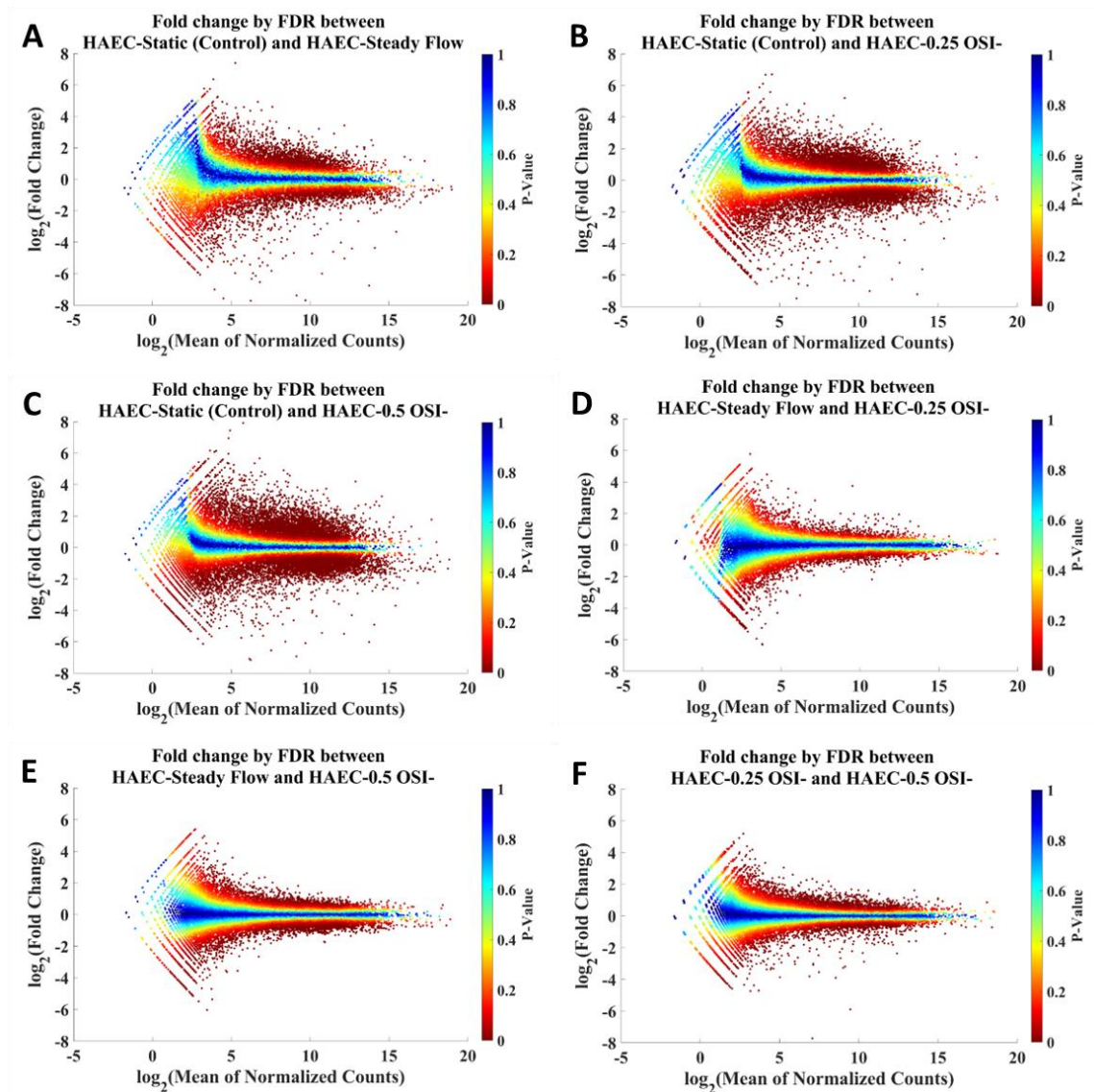


Figure 8. HAEC Log₂ fold change gene expression comparisons across all flow groups.

We examined the effect of OSIs on HAECs and paracrine communication with HASMCs via secretion of biomolecular cues. Following 48 hours of OSI conditioning on the HAECs and 48 hours of conditioning of HASMCs using spent media from HAECs, a total of 56,308 genes were found our raw RNA sequencing results. A database of upregulated and downregulated gene expressions was generated for each cell type and each flow group

(Figure 8 and Figure 9). The genes were arranged by heat map color spectrum with the highest significance in shown in red and lowest significance shown in blue. Table 1 and Table 2 summarize the top 15 genes in order of significance for HAEC and HASMC, respectively.

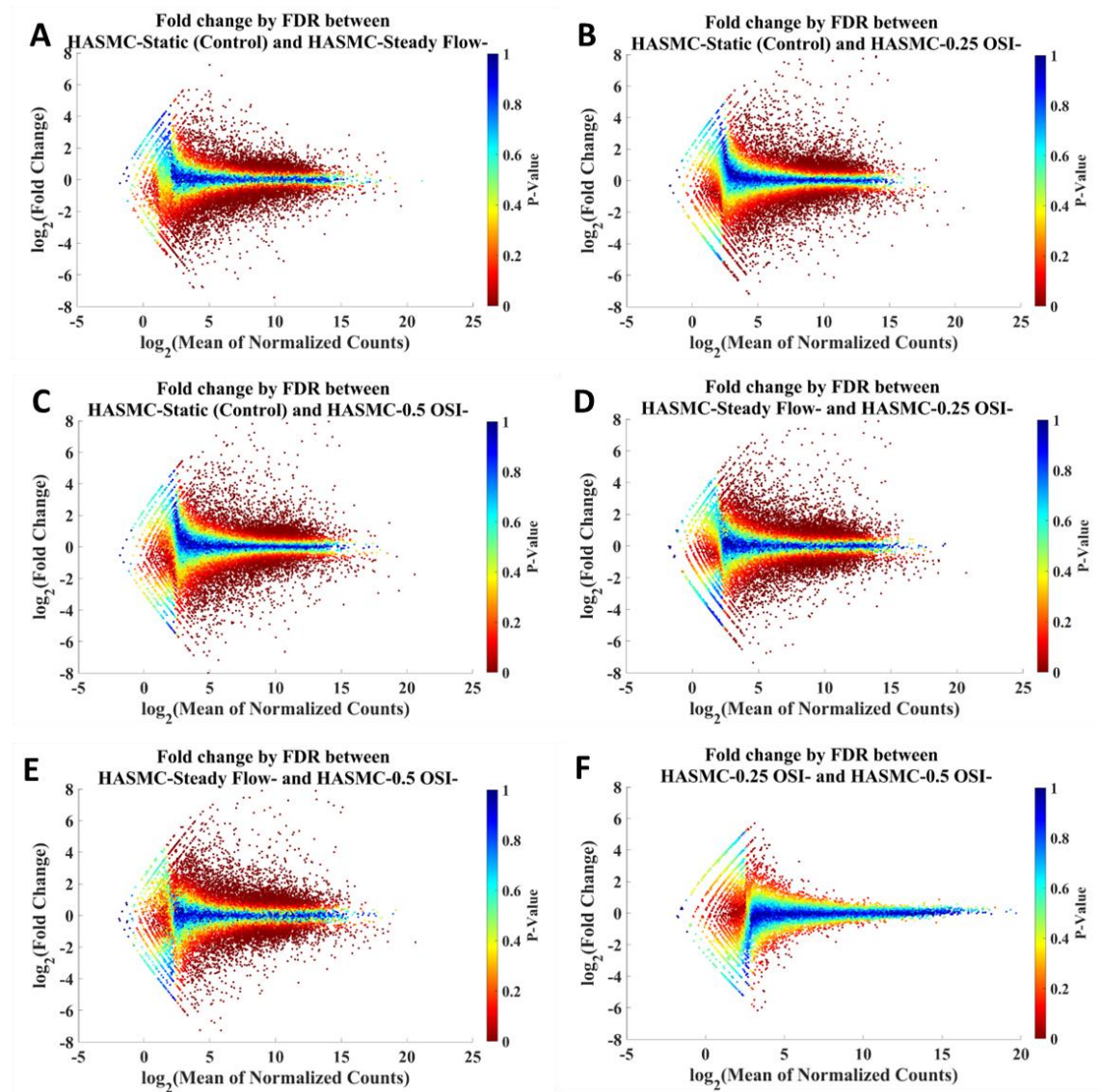


Figure 9. HASMC Log₂ fold change gene expression comparisons across all flow groups.

Future studies involve further mining of the RNA sequencing data to better understand relation between flow groups and gene expressions for each cell type. However, in the

scope of examining genes associated with cardiovascular remodeling, we further selected a few genes of interest to compare between the groups in HAEC (Figure 10) and HASMC (Figure 11), specifically CDH5 (VE-Cadherin), MMP10, and SELE (E-selectin) in the HAECs and ACTA2, MYH11, and TAGLN in the HASMCs.

Table 1. HAEC Top 15 Genes in Order of Significance between Flow Groups

Static (Control) vs Steady Flow						Static (Control) vs 0.25 OSI					
Up Regulated	Log 2 Fold Change	P-Value	Down Regulated	Log 2 Fold Change	P-Value	Up Regulated	Log 2 Fold Change	P-Value	Down Regulated	Log 2 Fold Change	P-Value
THBS1	1.161	0	TAGLN	-6.76	0	THBS1	1.45	0	TAGLN	-7.21	0
NEAT1	3.418	9.22E-17	KRT19	-4.36	0	PRSS35	5.2	4.82E-26	KRT19	-5.63	0
SEMA3G	3.21	6.73E-14	PLAT	-3.34	0	TM4SF18	3.56	7.91E-22	PLAT	-3.68	0
FABP4	2.9	6.33E-13	ALDOA	-1.79	0	LIPG	3.23	1.87E-20	HMGA1	-2.61	0
PRKY	3.05	2.96E-11	TGM2	-1.58	0	HMGCS1	3.22	4.69E-17	TGM2	-2.47	0
ITGA11	3.256	4.23E-11	GAPDH	-1.47	0	PTGS2	3.12	9.68E-17	ALDOA	-1.94	0
MMRN1	2.49	7.77E-11	PKM	-1.38	0	TBC1D4	2.88	9.27E-16	GAPDH	-1.78	0
NGFR	4.605	7.89E-11	ACTB	-1.12	0	ITGA11	3.47	2.04E-15	PTRF	-1.67	0
CSGALNACT1	2.597	1.50E-10	ACTG1	-1.05	0	LRRC4	3.36	2.55E-15	PKM	-1.61	0
TM4SF18	2.696	1.55E-10	GS1-600G8.5	-7.69	8.02E-39	RSRP1	3	2.62E-15	ACTB	-1.58	0
RSRP1	2.729	2.59E-10	CADM3	-6	1.01E-32	HMGCR	2.93	4.30E-15	ACTG1	-1.41	0
PILRB	4.393	9.06E-10	NEFL	-7.39	9.72E-32	PDGFD	2.92	7.57E-15	MT-CO3	-1.37	0
NPTX1	4.921	1.67E-09	CCND2	-4.61	1.03E-24	TLL1	4.08	8.00E-15	MT-CO2	-1.37	0
ZNF704	3.645	2.66E-09	SERPIND1	-5.04	1.92E-24	PIEZO2	2.76	1.07E-14	ANXA2	-1.32	0
HERC2P2	2.811	3.13E-09	KRT7	-4.72	3.04E-21	NEAT1	2.55	5.35E-14	MT-CYB	-1.27	0

Static (Control) vs 0.5 OSI						Steady Flow vs 0.25 OSI					
Regulated	Log 2 Fold Change	P-Value	Down Regulated	Log 2 Fold Change	P-Value	Up Regulated	Log 2 Fold Change	P-Value	Down Regulated	Log 2 Fold Change	P-Value
MMRN1	3.25	0	TAGLN	-6.01	0	PRSS35	3.75	2.77E-14	IFI6	-2.18	6.35E-14
THBS1	1.773	0	KRT19	-4.91	0	DHCR24	1.94	1.84E-07	LGALS9	-1.71	1.02E-08
SEMA3G	3.737	2.30E-27	PLAT	-3.7	0	MSMO1	1.92	2.49E-07	AC002075.4	-Inf	2.36E-08
NEAT1	4.195	8.18E-25	MT2A	-2.66	0	HMGCS1	1.96	4.29E-07	FAM101A	-1.58	5.13E-08
RSRP1	3.629	6.33E-24	ALDOA	-2.62	0	PSAT1	1.72	7.36E-07	MAGED4B	-3.19	2.06E-07
ZNF704	4.569	5.16E-23	HMGA1	-2.57	0	GEM	2.83	1.33E-06	MX1	-1.68	3.73E-06
HERC2P2	3.614	2.02E-22	LGALS1	-2.46	0	PHGDH	2	2.37E-06	RP11-497H16.5	-Inf	4.00E-06
RP11-159D12.2	4.682	2.62E-22	SH3BGRL3	-2.46	0	LDLR	1.66	2.86E-06	MYO15A	-4.3	4.28E-06
PIEZO2	3.376	1.23E-21	GAPDH	-2.25	0	ACAT2	1.85	3.22E-06	PDE2A	-1.34	7.46E-06
NKTR	3.131	1.24E-21	PKM	-2.09	0	TMEM97	1.98	3.69E-06	RP11-19P22.8	-6.32	1.08E-05
PRKY	3.546	1.50E-21	PFN1	-1.89	0	SQLE	1.7	4.92E-06	CST1	-6.28	1.14E-05
ITGA11	3.825	1.65E-21	ENO1	-1.86	0	PTGS2	1.65	6.29E-06	CTXN1	-1.35	1.62E-05
HERC2P3	4.902	4.12E-21	MT-CO2	-1.53	0	RP11-399J13.2	3.33	1.16E-05	HYI	-1.23	1.94E-05
LIPG	2.951	1.64E-20	ACTB	-1.5	0	FAM129A	1.64	3.14E-05	TRBC2	-1.52	2.25E-05
LPL	4.132	4.53E-20	PTRF	-1.5	0	HMGCR	1.53	4.13E-05	ZNRF3-AS1	-Inf	2.27E-05

Steady Flow vs 0.5 OSI						0.25 OSI vs 0.5 OSI					
Up Regulated	Log 2 Fold Change	P-Value	Down Regulated	Log 2 Fold Change	P-Value	Up Regulated	Log 2 Fold Change	P-Value	Down Regulated	Log 2 Fold Change	P-Value
LPL	1.817	3.44E-07	NGFR	-8.5	7.86E-62	ADAMTS18	1.6	2.45E-11	PRSS35	-5.89	7.21E-76
SLC7A14	2.352	4.13E-06	ISG15	-1.76	2.19E-12	ABCG2	1.62	5.05E-10	NGFR	-7.72	1.70E-39
CCDC144B	2.021	4.16E-06	IFI6	-1.7	8.08E-12	GJA5	2.19	1.07E-09	PHGDH	-3.89	8.68E-34
ADAMTS18	1.392	1.34E-05	ADM2	-2.66	9.51E-10	ITGB4	1.68	7.22E-09	FAM129A	-3.27	1.31E-31
NCAM2	2.305	1.91E-05	RP11-110G21.2	-Inf	1.06E-09	PDE2A	1.38	1.22E-08	ASNS	-3.19	1.38E-30
ANKRD36	1.626	2.47E-05	AC004556.1	-3.56	1.02E-08	NEAT1	1.62	5.46E-08	PSAT1	-2.89	3.33E-28
RP11-566E18.1	1.699	3.76E-05	RP11-338E21.2	-Inf	4.11E-08	MIR503HG	1.87	6.91E-08	ADM2	-3.55	1.40E-23
RP11-159D12.2	1.363	3.77E-05	IL32	-1.3	2.04E-07	PKHD1L1	2.14	8.85E-08	JDP2	-2.67	8.95E-21
ZNF117	1.331	4.36E-05	PGF	-1.28	3.25E-07	ART4	1.94	1.25E-07	DHCR24	-2.36	3.83E-19
HERC2P3	1.394	4.82E-05	RP11-497H16.5	-5.36	4.76E-07	SLC7A14	2.35	1.59E-07	ACAT2	-2.34	6.28E-19
CXCL12	3.598	6.48E-05	NUPR1	-1.81	5.26E-07	ACSM3	1.48	2.46E-07	SLC6A9	-3.81	2.11E-18
ANKRD36C	1.585	8.85E-05	NRGN	-1.27	6.15E-07	KCNN3	1.35	3.07E-07	CHAC1	-2.28	6.54E-16
ADRA2A	2.614	0.000108	ASNS	-1.64	7.38E-07	ABCA1	1.34	3.16E-07	TMEM97	-2.22	2.52E-15
GOLGA8A	1.525	0.000118	FAM129A	-1.62	1.01E-06	TNFSF10	1.67	3.98E-07	FDFT1	-1.74	1.73E-14
CXCL8	1.274	0.000124	ZNRF3-AS1	-6.04	1.04E-06	ABCA6	1.32	5.93E-07	GEM	-3.08	3.10E-14

Table 2. HASMC Top 15 Genes in Order of Significance between Flow Groups

Static (Control) vs Steady Flow						Static (Control) vs 0.25 OSI					
Up Regulated	Log 2 Fold Change	P-Value	Down Regulated	Log 2 Fold Change	P-Value	Up Regulated	Log 2 Fold Change	P-Value	Down Regulated	Log 2 Fold Change	P-Value
PDK4	2.82	0	CD248	-3.43	0	RSAD2	Inf	0	ACTA2	-4.12	0
SERPINE1	1.71	0	HSPB6	-2.21	0	OASL	13.72	0	COL3A1	-2.841	0
ITGA5	1.6	0	COL1A1	-1.66	0	CCL5	10.9	0	COL1A1	-2.79	0
TIMP1	1.56	0	COL6A1	-1.28	0	MX1	8.787	0	HSPB6	-2.101	0
FTH1	1.15	0	C7	-7.42	1.37E-68	OAS1	8.652	0	CALD1	-2.021	0
FOXS1	3.5	2.18E-28	APOE	-5.13	5.51E-49	IFIT2	7.895	0	COL1A2	-1.916	0
MFSD2A	4.73	2.80E-27	PPL	-4.96	3.16E-46	IFIT1	7.819	0	COL5A1	-1.887	0
CCL5	4.59	4.05E-25	CHRD1	-5.57	5.40E-42	OAS3	7.743	0	FN1	-1.738	0
DUSP4	3.3	1.47E-22	C3	-4.54	3.01E-40	OAS2	6.963	0	COL6A1	-1.736	0
MT1L	2.93	3.30E-22	OLFML1	-4.15	4.68E-34	ISG15	6.794	0	CCDC80	-1.732	0
KRT86	3.56	5.93E-21	SCG2	-3.92	4.26E-33	IFI6	6.375	0	TAGLN	-1.562	0
RASD1	3	1.17E-20	STEAP4	-3.9	8.45E-33	IFIT3	6.126	0	FBN1	-1.546	0
ALOX15B	4.32	2.74E-20	KIF26B	-3.73	1.14E-31	HMOX1	3.707	0	COL6A2	-1.538	0
PPP1R14C	3.17	6.84E-20	TMEM119	-3.86	3.32E-31	WARS	3.541	0	THBS1	-1.288	0
OLAH	3.23	9.07E-20	H19	-6.24	1.22E-30	MT2A	2.383	0	COL4A2	-1.243	0

Static (Control) vs 0.5 OSI						Steady Flow vs 0.25 OSI					
Up Regulated	Log 2 Fold Change	P-Value	Down Regulated	Log 2 Fold Change	P-Value	Up Regulated	Log 2 Fold Change	P-Value	Down Regulated	Log 2 Fold Change	P-Value
RSAD2	Inf	0	ACTA2	-3.66	0	OASL	Inf	0	TXNIP	-3.81	0
OASL	14.04	0	COL3A1	-2.92	0	RSAD2	Inf	0	ACTA2	-3	0
CCL5	11.46	0	COL1A1	-2.77	0	OAS1	11.1	0	CTGF	-2.15	0
MX1	8.923	0	COL1A2	-1.88	0	MX1	8.19	0	COL3A1	-1.99	0
IFIT2	8.272	0	COL5A1	-1.84	0	IFIT2	8.08	0	PDK4	-1.81	0
IFIT1	7.946	0	FN1	-1.75	0	IFIT1	7.87	0	COL4A1	-1.78	0
OAS3	7.768	0	COL6A1	-1.57	0	OAS3	7.84	0	POSTN	-1.74	0
OAS2	7.175	0	COL6A2	-1.5	0	OAS2	7.12	0	COL1A2	-1.7	0
ISG15	6.976	0	COL4A2	-1.26	0	IFIT3	6.85	0	FN1	-1.69	0
IFIT3	6.431	0	CARMN	-6.65	4.18E-27	ISG15	6.77	0	COL4A2	-1.59	0
IFI6	6.417	0	C7	-5.73	5.55E-26	IFI6	6.47	0	SPARC	-1.43	0
WARS	3.862	0	A2M	-5.21	8.33E-25	CCL5	6.28	0	THBS1	-1.34	0
HMOX1	3.625	0	FER1L4	-4.9	9.83E-21	HMOX1	4.08	0	COL1A1	-1.15	0
MT2A	2.638	0	APOE	-4.68	3.19E-19	WARS	4	0	GSDMB	-4.4	1.36E-18
FTH1	1.522	0	FMO2	-5.22	9.77E-19	CMPK2	Inf	4.70E-102	KRT86	-4.46	4.70E-17

Steady Flow vs 0.5 OSI						0.25 OSI vs 0.5 OSI					
Up Regulated	Log 2 Fold Change	P-Value	Down Regulated	Log 2 Fold Change	P-Value	Up Regulated	Log 2 Fold Change	P-Value	Down Regulated	Log 2 Fold Change	P-Value
OASL	Inf	0	TXNIP	-3.39	0	AC004556.1	3.266	5E-04	AC068580.5	-Inf	0.003
RSAD2	Inf	0	PAPPA	-2.66	0	ZP1	Inf	0.001	FREM3	-3.45	0.003
OAS1	11.1	0	PDK4	-2.4	0	RP11-111H13.1	Inf	0.001	RP11-872J21.3	-Inf	0.005
IFIT2	8.47	0	CTGF	-2.07	0	DMC1	Inf	0.001	EIF3CL	-1.82	0.006
MX1	8.34	0	COL3A1	-2.06	0	IFIT1B	Inf	0.002	RP11-367F23.2	-5.63	0.007
MX2	8.21	0	POSTN	-1.88	0	TEX22	4.328	0.004	RAET1L	-5.98	0.007
IFIT1	8.01	0	FN1	-1.69	0	RP11-214K3.24	5.295	0.005	CNR1	-1.51	0.013
OAS3	7.88	0	COL4A1	-1.67	0	AC011551.3	Inf	0.005	CXCR4	-2.6	0.014
OAS2	7.35	0	COL1A2	-1.66	0	CTD-2369P2.5	4.317	0.006	AC112198.1	-4.97	0.015
IFIT3	7.17	0	COL4A2	-1.6	0	METTL24	Inf	0.006	CARD8-AS1	-2.78	0.016
ISG15	6.96	0	SPARC	-1.26	0	RP11-38G5.4	Inf	0.006	PDGFB	-4.91	0.018
CCL5	6.85	0	COL1A1	-1.12	0	ABCG4	Inf	0.007	TMEM100	-2.65	0.019
IFI6	6.52	0	SERPINE1	-1.01	0	HRASLS2	4.73	0.007	DLG5-AS1	-3.28	0.02
WARS	4.33	0	SERPINA5	-Inf	3.96E-23	CTD-2619J13.27	4.102	0.008	SHH	-Inf	0.02
HMOX1	4.01	0	KRT86	-4.93	1.76E-19	EMCN	4.326	0.009	RP11-297N6.4	-2.81	0.025

Highest total number of significantly upregulated and downregulated gene expressions in HAEC is observed between the Static vs. 0.50 OSI groups, while lowest significant differences are found between Steady vs. 0.25 OSI. In HASMCs, on the other hand, highest total number of significantly upregulated and downregulated genes was observed between

Steady vs. 0.50 OSI groups, and the lowest significant differences were found between 0.25 OSI vs. 0.50 OSI.

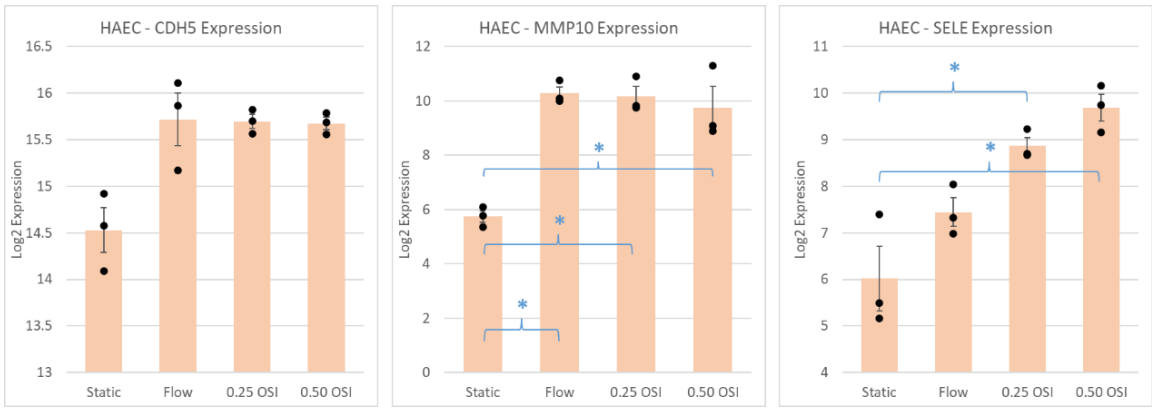


Figure 10. HAEC gene expression of CDH5, MMP10, and SELE in all flow groups

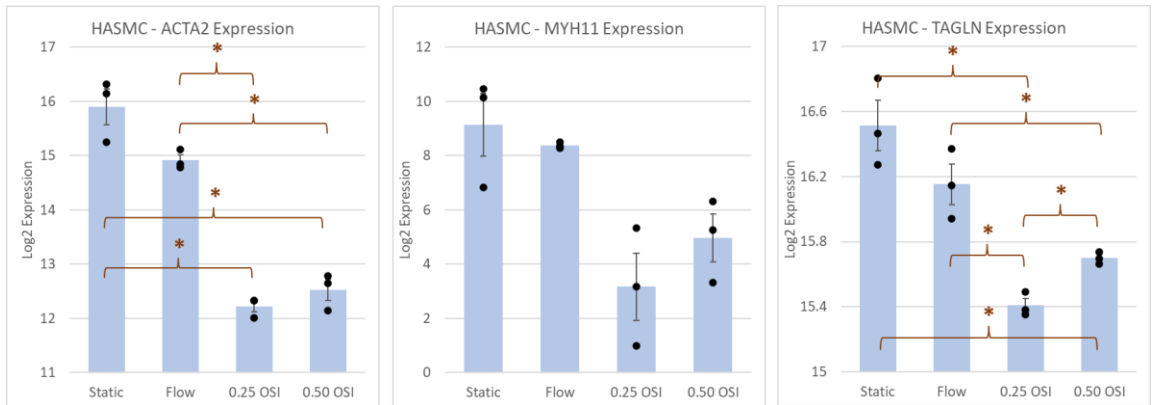


Figure 11. HASMC gene expression of ACTA2, MYH11, and TAGLN in all flow groups.

3.4. Discussion

A 48-hour conditioning time was applied to observe gene expression variations due to exposure to various OSIs in HAECs and paracrine signaling of biomolecular cues in HASMCs [62]. Highest total number of significantly upregulated and downregulated gene expressions in HAEC was observed between the Static vs. 0.50 OSI groups, suggesting that Static and 0.50 OSI groups result in most different cellular responses. Lowest total number of significantly upregulated and downregulated gene expressions in HAEC was

observed between Steady vs. 0.25 OSI groups, indicating that cellular responses to steady flow and 0.25 OSI, or moderate oscillation, are most similar compared to other static or other OSI groups.

Of the original 56,308 genes from the raw counts, we specifically examined the upregulation and downregulation of a few genes related to cardiovascular remodeling. Increased expression of CDH5 was observed in the steady flow, 0.25 OSI, and 0.50 OSI groups (Figure 10). This may suggest an increase in maintaining lateral endothelial junction due to loss of cell contact in the HAECs from exposure to flow [63]. We also observed a significant increase in expression of MMP10 in the steady flow, 0.25 OSI, and 0.50 OSI groups. This may be an indication of vascular remodeling promoted by inflammatory stimuli [64]. The SELE (E-selectin) marker exhibited a gradual increase in expression as the OSI increased, with a significant increase ($p < 0.05$) in 0.50 OSI compared to the Static group, indicating that high flow oscillations may have triggered potential endothelial activation which may be associated with endothelial dysfunction [65].

The HASMCs exhibited significant downregulation of ACTA2, MYH11, and TAGLN expressions in the 0.25 OSI and 0.50 OSI groups (Figure 11). These three genes are associated with maintaining smooth muscle cell spindle-like shape and cell contractility, therefore a downregulation of these genes may indicate loss of smooth muscle cell contractility [66].

3.5. Summary

RNA transcription is the process of synthesizing a segment of RNA based on a section of a DNA template. The RNA segments are then converted into amino acid sequences that later formulate into proteins, which ultimately establish the phenotypic expressions of a

cell. Dysregulated RNA transcription can cause diseases and cancers; therefore, RNA sequencing provides information on potential protein expressions and changes and regulation of cell phenotypes. We utilized the paired-end sequencing method to determine the amount of gene counts for each gene detected. Paired-end reads sequence both ends of the RNA fragment, providing reasonably robust estimates and improved accuracy. This method has therefore become a cost-effective alternative to traditional single-end strategy [67]. We found that the OSI flow groups exhibited changes in the pro-remodeling expressions of HAECs and loss of contractility expressions in the HASMCs. This suggests the possibility of increased immune responses from the endothelium due to increased OSI conditions. In the next chapter, we continue our investigation into the effects of OSI on valvular cell types with our focus specifically on genes of interest and calcification as endpoint responses beyond gene expression.

Chapter IV: Aim 2 – Effect of OSI on valvular calcification at the cellular level

4.1. Introduction

Text for the following subsection taken from:

[23] C.-P. Hsu, A. Tchir, A. Mirza, D. Chaparro, R. Herrera, J. Hutcheson and S. Ramaswamy, "Valve Endothelial Cell Exposure to High Levels of Flow Oscillations Exacerbates Valve Interstitial Cell Calcification," *Bioengineering*, vol. 9, no. 8, 2022.

Calcific aortic valve disease, one of the most prevalent chronic heart problems, involves hardening of aortic valve leaflets due to calcium phosphate deposition, resulting in stenosis, regurgitation, and reduced cardiac output. Clinical data have shown a global increase in over 100% of CAVD cases in the past 30 years [1]. Current treatment options for early CAVD intervention are not available, and the main factors associated with development of CAVD remain unclear. Heart valves are subject to various mechanical stresses from hemodynamic flow environments, and heart valve remodeling occurs in response to cyclic mechanical loading [18]. Healthy cardiac function requires the aortic heart valve to facilitate unidirectional flow from the left ventricle into the aorta to the systemic circulation during systole, with minimal blood flow resistance.

Most aortic valves consist of three equal-sized leaflets forming three lines of coaptation. Bicuspid aortic valve malformations are some of the most common congenital heart conditions that affect approximately 1–2% of the population [68]. Each valve leaflet contains a ventricularis layer, a spongiosa layer, and a fibrosa layer (Figure 5). The ventricularis consists of mainly elastin fibers and faces the left ventricle. The fibrosa layer is mainly composed of collagen and faces the aortic side of the heart. The spongiosa layer is sandwiched between the ventricularis and fibrosa layers and is mainly composed of glycosaminoglycans [69]. Due to the valve structure and direction of blood flow, laminar

flow with high shear stress is mainly observed on the ventricularis side, while the fibrosa layers are mainly dominated by low shear stress and oscillatory flow [21]. CAVD mineral deposition is most often clinically observed on the fibrosa layer.

Studies have shown that low shear stresses are commonly associated with vascular lesions and calcifications [19] [25]. Specifically, regions of valve tissues that experience low wall shear stress, coupled with blood flow oscillations, triggers inflammation [3]. This pathological mechanical environment is present on the heart valve's fibrosa layer [5]. To further specify and quantify flow disturbances to valve calcification, we utilized OSI as a parameter to correlate precise flow oscillation magnitudes with the development of CAVD. OSI is a measurement of flow disturbances that quantifies the ratio between the forward flow net temporal shear stress to the total temporal shear stress magnitude that is assumed to be always positive (Equation 1), and the OSI value ranges between zero (no oscillation, or steady flow) to 0.50 (full oscillation, or forward flow in half the temporal cycle and reversed flow in the other half) [6]. Using OSI as a quantitative description of flow oscillations to connect to valve calcification has not been previously investigated. If there is an association between OSI and heart valve calcification, this can subsequently be used to create a human calcific valve engineered tissue model system to assess emerging therapeutics to treat calcific valve disease. As a first step, we therefore examined VIC responses to the paracrine signaling of biochemical end-products from VECs that were exposed to varying OSI values.

The valve endothelium is known to respond to hemodynamic stimuli during continuous remodeling, and CAVD often initiates at sites of VEC dysfunction, particularly in regions exposed to oscillatory flow compared to unidirectional flow. In this aim, we utilized the

OSI parameter to quantify the level of flow oscillations on the valve endothelium, exposed the VECs under dynamic culture of different OSI values, and subsequently immersed the VICs in VEC-conditioned media with PC components to further investigate paracrine effects on VIC calcification. We found that VIC-induced calcification was augmented under maximum oscillatory flow conditions in valvular cell types from both human and rat species. These findings establish a basis to engineer *in vitro* calcific human valve tissues, which can later be applied to test the effectiveness of potential therapeutics to treat aortic valve calcification.

4.2. Methods

4.2.1. *In Vitro* Experiments and Calcification Assessments Using Rat Cells

Text for the following subsection taken from:

[23] C.-P. Hsu, A. Tchir, A. Mirza, D. Chaparro, R. Herrera, J. Hutcheson and S. Ramaswamy, "Valve Endothelial Cell Exposure to High Levels of Flow Oscillations Exacerbates Valve Interstitial Cell Calcification," *Bioengineering*, vol. 9, no. 8, 2022.

Rat (species: *Rattus norvegicus*) VECs and VICs were purchased from Celprogen, Inc. (Torrance, CA) and Innoprot (Bizkaia, Spain), respectively. The VECs were expanded in extracellular matrix coated T75 culture flasks (Celprogen, Inc., Torrance, CA) with rat valvular endothelial primary cell culture complete growth media with serum and antibiotics (Celprogen, Inc., Torrance, CA), and the VICs were expanded with Dulbecco's modified Eagle medium (DMEM) containing 10% FBS and 1% PS in non-coated T75 culture flasks. VECs were then seeded with gelatin at 2.0×10^5 cells per channel in a 24-well Bioflux plate consisting of 8 microfluidic channels per plate (Fluxion Biosciences, Inc., Alameda, CA) using DMEM containing 10% FBS and 1% PS. Upon 24 hours after seeding and confirmation of VEC attachment, the VECs were then conditioned for 48 hours in a shear

stress cell assay system (Bioflux, Fluxion Biosciences, Inc., Alameda, CA) at an average shear stress magnitude of 1 dyne/cm² to promote an atherogenic environment [24]. Each Bioflux well plate with the cells was conditioned under an OSI flow group for 48 hours, and a total of four flow groups was investigated: static (0 OSI/no flow), steady flow (0 OSI/steady flow), 0.25 OSI (moderate oscillation), and 0.50 OSI (full oscillation). Conditioned media from all four VEC flow groups were collected separately from each Bioflux plate, and an equal volume of pro-calcifying (PC) media was added to each of the collected VEC-conditioned media groups. The final VEC-conditioned PC media mixture consisted of 1.8 mM CaCl₂ (Sigma-Aldrich, St. Louis, MO), 3.8 mM NaH₂PO₄ (Sigma-Aldrich, St. Louis, MO), 0.4 units/mL of inorganic pyrophosphate (Sigma-Aldrich, St. Louis, MO) [70], and 5% FBS with 1% PS [71]. The VEC-conditioned PC media was then subsequently used to statically culture VICs in 12-well plates for 7 days, with one media change that was performed on day 4 for the respective VEC-conditioned flow groups. Upon termination of VIC exposure to media from various VEC-conditioned flow groups, VIC calcification was measured using alizarin red staining (ARS, Ricca Chemical Company, Arlington, TX). The alizarin red dye was then extracted and quantified with a microplate reader at 405 nm (Synergy HTX Multimode Reader, Biotek Agilent, Santa Clara, CA). Three replicates were conducted for each conditioning group, and data were evaluated using a one-way ANOVA in conjunction with Tukey's post hoc analysis in SPSS (IBM, Armonk, NY) with statistical significance identified when $p < 0.05$. Key phenotypic markers expressed by VICs conditioned in various VEC-paracrine communicated flow groups were also assessed using real time quantitative polymerase chain reaction (RT-qPCR) at three replicates per target gene per flow group. Data from RT-qPCR consisted of

cycle threshold, or C_T values, which were analyzed using the Livak method $\Delta\Delta C_T$ [72] to compute fold change with Fresh PC as the control group and Actb as the housekeeping gene [73]. The Fresh PC media consisted of only pro-calcifying ingredients with no paracrine signaling from VECs.

4.2.2. *In Vitro* Experiments and Calcification Assessments Using Human Cells

Human (Species: *Homo sapiens*) VECs and VICs were purchased from Lonza Bioscience (Basel, Switzerland) and Innoprot (Bizkaia, Spain), respectively. Both cell types were expanded in culture. VECs were seeded for 24 hours at 2.0×10^5 cells per channel in 24-well Bioflux plates (Fluxion Biosciences, Inc. Alameda, CA) consisting of 8 microfluidic channels per plate. The VECs were conditioned for 48 hours in the Bioflux shear stress cell assay system at an average shear stress magnitude of 1 dyne/cm^2 under the following OSI conditions: static (0 OSI/no flow), steady flow (0 OSI/steady flow), 0.25 OSI (moderate oscillation), and 0.50 OSI (full oscillation). The conditioned media from VEC groups were subsequently collected, and a portion were ultracentrifuged at 50,000 RPM ($\sim 100,000g$) for 70 minutes. After ultracentrifugation, the non-exosomal (NonEX) supernatants were transferred into separate tubes while the exosome (EX) pellets were re-suspended in fresh PC media. Both groups were subsequently used to culture VICs in 24-well plates with equal concentration of PC ingredients consisting of 1.8 mM CaCl_2 , 3.8 mM NaH_2PO_4 , and 0.4 units/mL of inorganic pyrophosphate [70] at 5% FBS and 1% PS [71]. VIC culture duration lasted for 7 days with no media change. The Fresh PC positive control group consisted of only PC ingredients with no VEC-conditioned media. The negative control groups were VICs exposed to VEC-conditioned media but with no PC components. VIC calcification was quantified using ARS at absorbance wavelength of 405 nm after dye

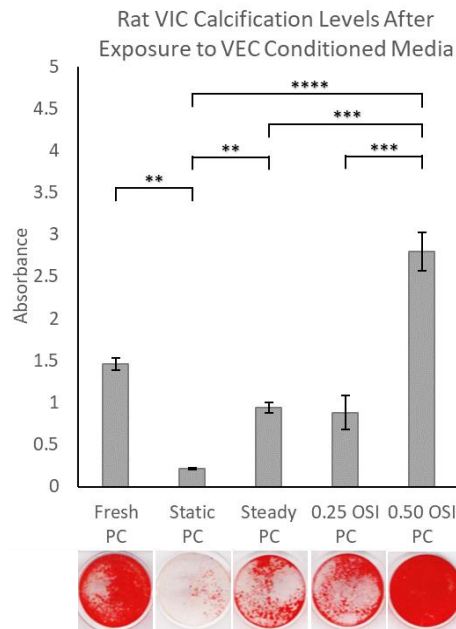
extraction with 10% (v/v) CH₃COOH. ARS quantification was normalized to the amount of protein secreted in each respective well. Protein quantification was conducted using the Pierce BCA Protein Assay Kit (Thermo Fisher Scientific, Waltham, MA) with a microplate reader at wavelength 562 nm. Three replicates were conducted for each control and experimental group, and statistical analysis was performed using a one-way ANOVA in conjunction with Tukey's post hoc analysis in SPSS (IBM, Armonk, NY). Statistical significance was identified when $p < 0.05$.

4.3. Results

4.3.1. Rat Valvular Cell Assessments

Text and images for the following subsection taken from:

[23] C.-P. Hsu, A. Tchir, A. Mirza, D. Chaparro, R. Herrera, J. Hutcheson and S. Ramaswamy, "Valve Endothelial Cell Exposure to High Levels of Flow Oscillations Exacerbates Valve Interstitial Cell Calcification," *Bioengineering*, vol. 9, no. 8, 2022.



*Figure 12. Rat VIC calcification in oscillatory flow conditioned VEC media with PC components with respective ARS stains. Plot data are expressed as means with $n = 3$ samples with error bars representing standard error of the means (SEM) [23], Statistical significance: **** $p < 0.001$, *** $p < 0.005$, ** $p < 0.05$.*

The ARS results revealed the highest VIC calcification in the 0.50 OSI group (Figure 12). Specifically, statistical assessments showed significantly increased calcification in the 0.50 OSI group compared to the 0 OSI Static ($p < 0.05$), 0 OSI Steady ($p < 0.05$), and 0.25 OSI ($p < 0.05$) groups. Comparisons of VIC calcification between Fresh PC vs. 0 OSI Static and 0 OSI Steady vs. 0 OSI Static were also significantly different ($p < 0.05$), while VIC calcification between 0.25 OSI vs. 0 OSI Static and 0.25 OSI vs. 0 OSI Steady groups were not significantly different ($p > 0.05$). VIC calcification between Fresh PC and 0.50 OSI groups were also not statistically significant ($p > 0.05$).

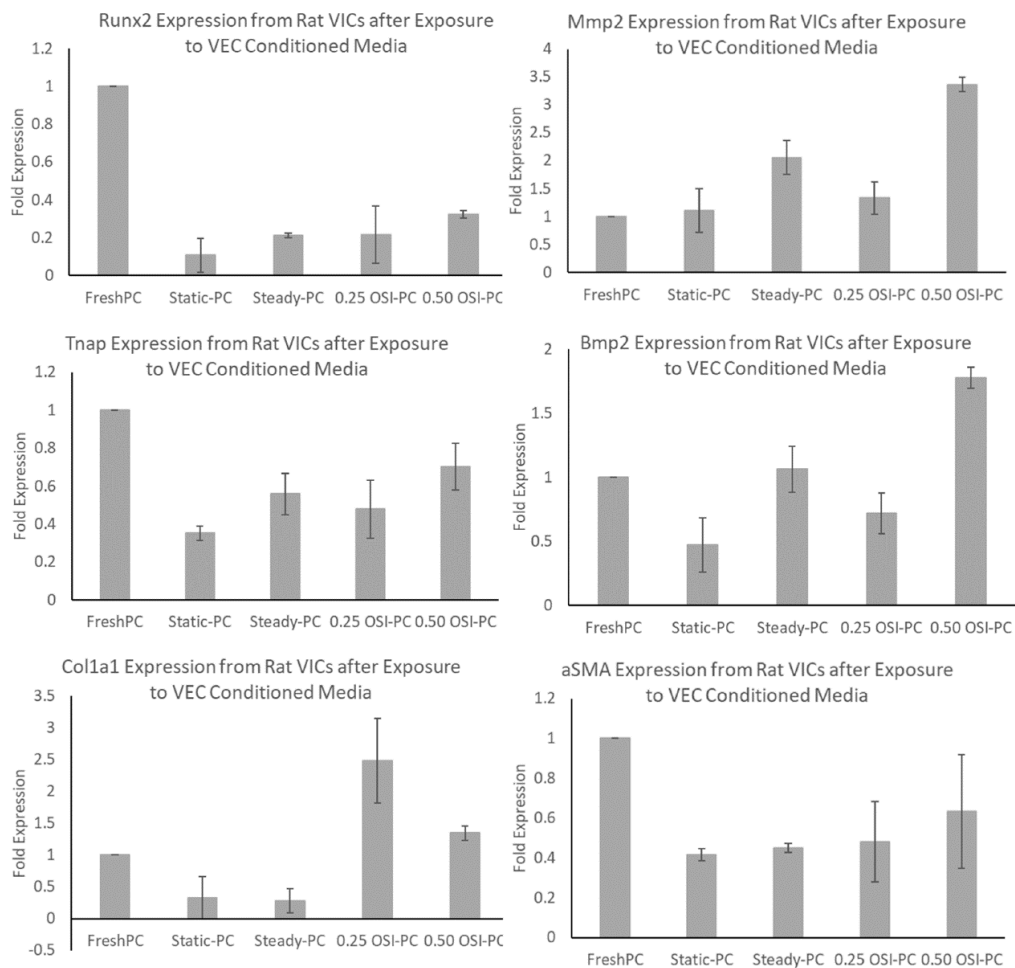


Figure 13. Rat VIC gene expression after 7-day exposure to pro-calcifying VEC-conditioned media [23].

Gene expression results (Figure 13) indicated upregulation in calcific genes in the Fresh PC and 0.50 OSI groups, specifically Runx2, Mmp2, Tnap, and Bmp2. The highest alpha-SMA expression was also observed in the Fresh PC group, and the highest expression of type I collagen ($p = 0.0503$) was observed in the 0.25 OSI group. However, the fold changes were not statistically significant ($p > 0.05$) across the groups.

4.3.2. Human Valvular Cell Assessments

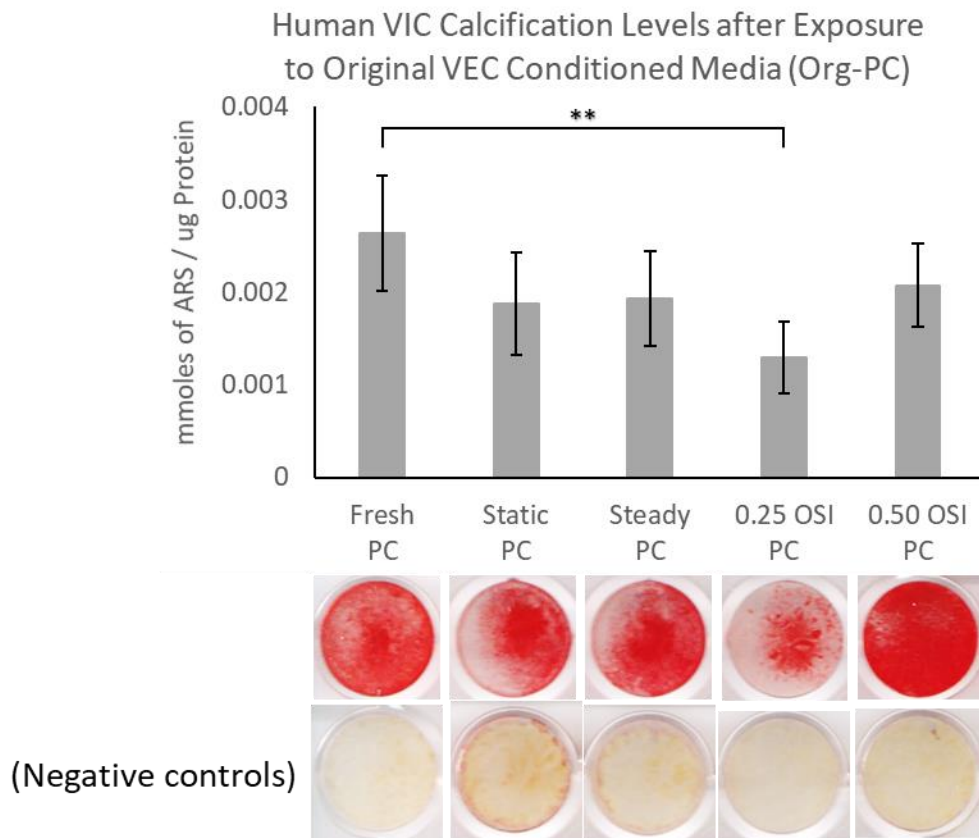


Figure 14. Human VIC calcification after 7-day exposure to oscillatory flow conditioned VEC media with added PC components. Statistical significance: $**p < 0.05$.

VIC calcification after exposure to the original, not ultracentrifuged VEC-conditioned media (Figure 14) showed no significant calcification differences between all flow groups ($p > 0.05$) except for Fresh PC vs. 0.25 OSI ($p < 0.05$). VIC calcification after exposure to

ultracentrifuged EX-PC VEC-conditioned media (Figure 15) showed no significant differences between all flow groups ($p > 0.05$). VIC calcification after exposure to ultracentrifuged NonEX-PC VEC-conditioned media (Figure 16) showed a significantly lower calcification in all groups compared to the Fresh PC control, except for 0.50 OSI. Significant calcification is observed between the 0.50 OSI vs. Steady flow ($p < 0.05$) and the 0.50 OSI vs. 0.25 OSI ($p < 0.005$).

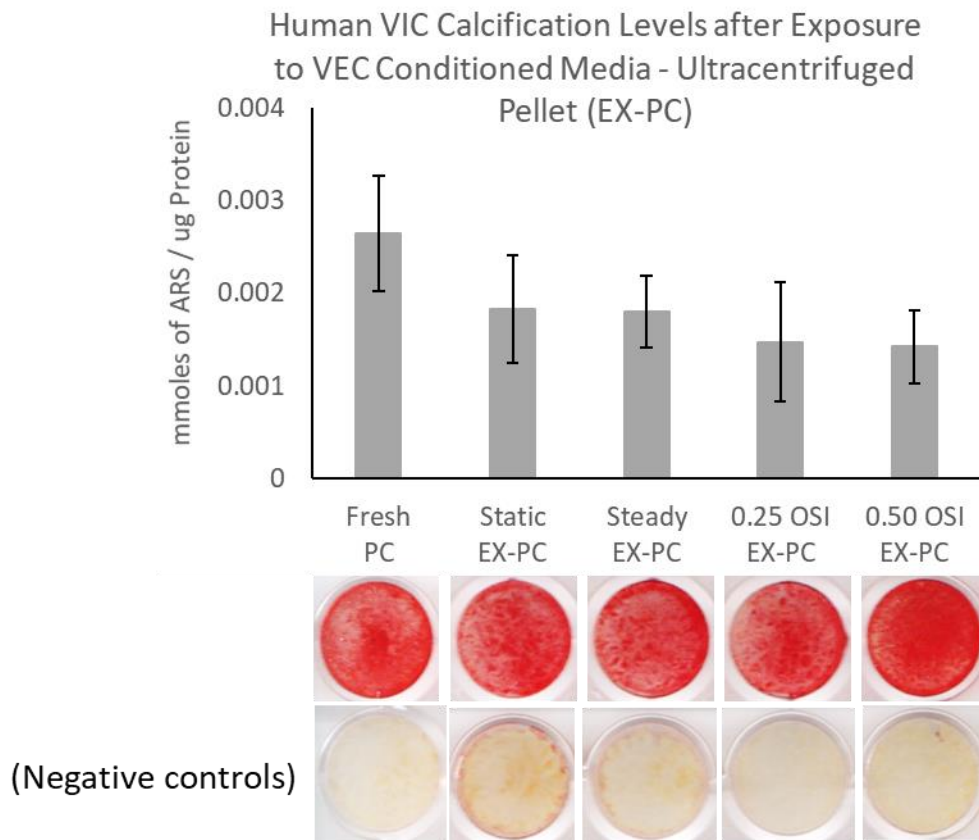


Figure 15. Human VIC calcification after 7-day exposure to ultracentrifuged oscillatory flow conditioned VEC media's exosomal pellet with added PC components. No statistical significance was observed between the groups.

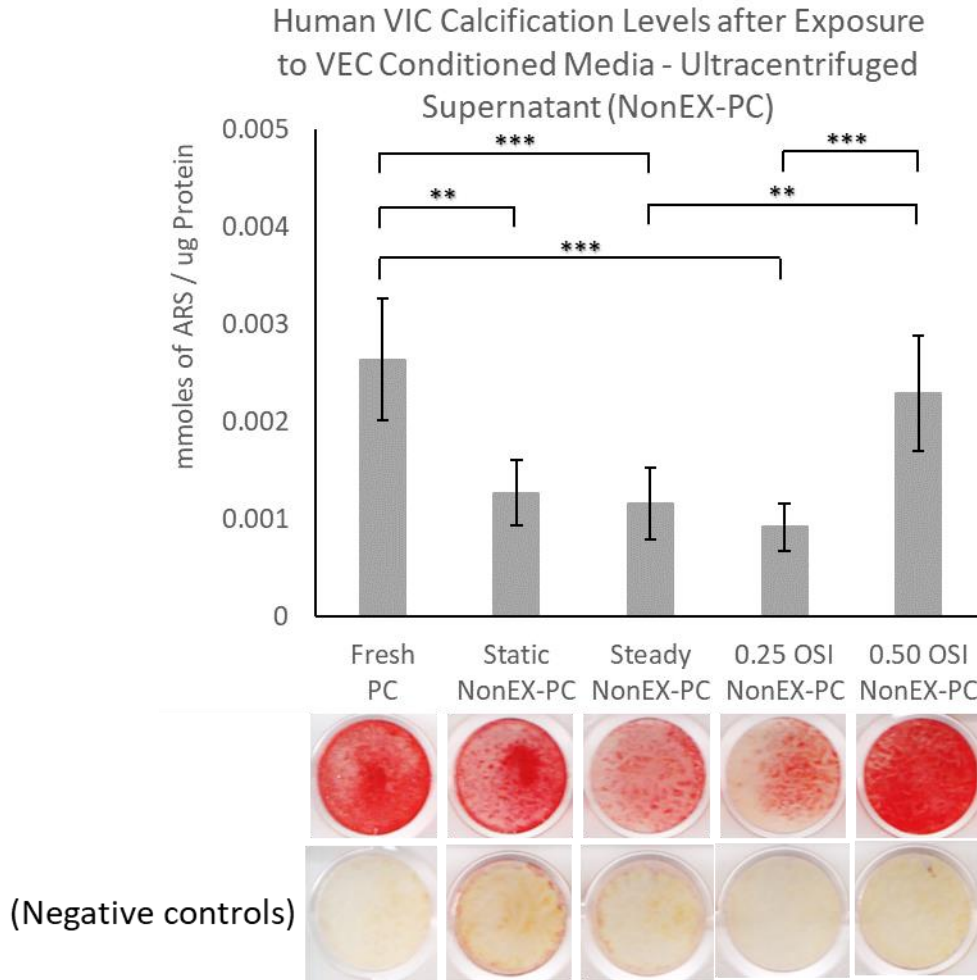


Figure 16. Human VIC calcification after 7-day exposure to ultracentrifuged oscillatory flow conditioned VEC media's non-exosomal supernatant with added PC components. Statistical significance: *** $p < 0.005$, ** $p < 0.05$.

4.4. Discussion

In the rat valvular cell studies, highest VIC calcification was observed in the 0.50 OSI group. Specifically, statistical assessment showed significantly increased calcification in the 0.50 OSI group compared to the Static ($p < 0.001$), Steady flow ($p < 0.005$), and 0.25 OSI ($p < 0.005$) groups. Comparisons of VIC calcification between 0.25 OSI vs. Static and 0.25 OSI vs. 0 OSI (steady flow) were found to be not significant ($p > 0.05$). This finding suggests that VECs exposed to low-to-moderate levels of flow oscillations maintain a

quiescent VIC phenotype via paracrine signaling. On the other hand, augmented calcific conditions coupled with high oscillatory flow regions (OSI = 0.50) on VECs leads to substantial risk of increasing VIC calcification. This corroborates current theories of increased VIC calcification under disturbed flow [5] and the fact that calcification occurs on the fibrosa layer of valve leaflets where flow oscillations are mainly observed [23]. However, whether molecular targets in this VEC-to-VIC paracrine regulated pathway can be targeted to reduce valve calcification needs to be further investigated.

Presence of paracrine regulation from VECs also seem to generally lower gene expressions associated with osteogenic differentiation of VICs, specifically Tnap and Runx2, which exhibited highest expression in the Fresh PC group. In the OSI groups, an increase in Mmp2 and Bmp2 expressions was observed in VICs exposed to the 0.50 OSI conditioned media, in which may be associated with remodeling.

In the human valvular cell studies, significant VIC calcification was observed in 0.50 OSI NonEx-PC group. This suggests that non-exosome signaling such as cytokines released by the VECs are primarily responsible for inducing calcification in the VICs when cultured under biomechanically induced high OSIs in combination with PC environments.

4.5. Summary

Valve remodeling involves paracrine regulation between VECs and VICs, and improper communication between these two cell types can lead to valve calcification. As VECs are known to respond to hemodynamic stimuli, specifically previous studies have shown pro-inflammatory phenotypic changes in VECs when exposed to substantial disturbed flow [22], the relay of these pro-inflammatory biomolecular cues resulted in phenotypic switching of quiescent VICs to an osteogenic phenotype. We studied the role of OSI as a

regulator for valve calcification on 2D cellular level from two species, and we observed that high flow oscillations promote pro-inflammatory VEC phenotypes that leads to substantial risks for valve calcification. In the next chapter, we further investigate high oscillatory flow effects on valve tissue calcification and valve hydrodynamic performance using a co-culture VEC-VIC system under PC environments.

Chapter V: Aim 3 – An *in vitro* engineered tissue model system to recreate the etiology of valve calcification

5.1. Introduction

A major obstacle in developing therapeutic targets for CAVD is an absence of human tissue model systems that can recreate the etiology of valve calcification and reliably assess responses to a potential treatment. In this study, a bioreactor was developed to deliver flow oscillations in an *in vitro* environment to further study the relation between OSI and valve calcification. The bioreactor system provided a controlled flow environment for valvular tissue growth, which consisted of seeding and co-culturing of VECs and VICs on a bio-scaffold. One of the goals of this bioreactor system is to produce *de novo* calcified human valve tissues that mimic the morphology of CAVD at early stages. The system enables longitudinal mechanistic studies with evolving levels of calcification in engineered valve tissues exposed to dynamic flow culture and can also potentially serve as a platform for discovery and assessment of future potential therapeutics that is needed for the long-term care of patients with CAVD.

5.1.1. Bio-scaffolds vs. Synthetic Scaffolds

Previous studies conducted by Brittany Gonzalez, PhD (FIU 2020) from CV-PEUTICS laboratory involved seeding of HBMSCs (RoosterBio, Inc., Frederick, MD) in both porcine small intestinal submucosa (PSIS, CorMatrix Cardiovascular Inc., Roswell, GA) bio-scaffolds and poly glycolic acid-poly L-lactic acid (PGA-PLLA, Biofelt, Biomedical Structures, Warwick, RI) synthetic scaffolds, followed by conditioning in a perfusion bioreactor system under a physiologically relevant pulsatile aortic flow environment for 14 days to observe changes in HBMSC differentiation into cardiovascular phenotypes. We

utilized the extra samples generated from previous studies to determine the choice of scaffold for the current aim. Conditioned PSIS and PGA-PLLA samples were fixed in 10% (w/v) formalin (Fisher Scientific, Waltham, MA) and embedded in optimal cutting temperature (OCT) compound (Fisher Scientific, Waltham, MA) prior to sectioning at 16 μm using a cryostat. Sectioned samples were then stained with elastin mouse monoclonal primary antibody (Novus Biologicals, Littleton, CO) and goat anti-mouse polyclonal secondary antibody (Thermo Fisher, Waltham, MA), as well as 4',6-diamidino-2-phenylindole (DAPI, 0.2 $\mu\text{g}/\text{mL}$, Cayman Chemical, Ann Arbor, MI). Stained samples were then imaged using a confocal microscope (Nikon Eclipse Ti, Minato, Tokyo, Japan), shown in Figure 17.

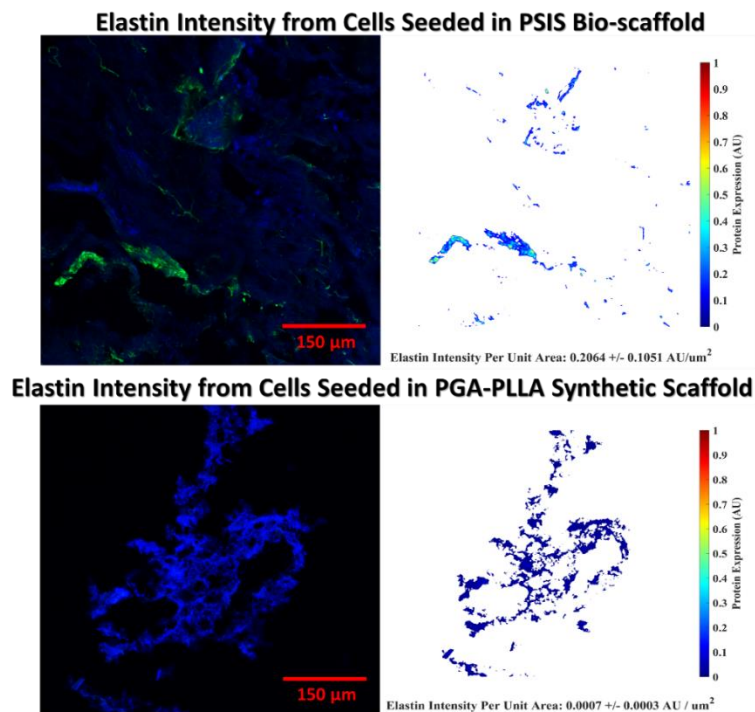


Figure 17. Elastin (green) deposition in PSIS (top) vs. in PGA-PLLA (bottom) [74]

The images showed that HBMSCs seeded on PSIS bio-scaffold facilitated higher production of elastin ECM under flow mechanical conditions compared to PGA-PLLA

synthetic scaffolds. This suggests that ECM on PSIS bio-scaffolds allowed valvular cells to communicate and further secrete engineered matrices such as elastin that will be useful for enhancing cardiovascular regeneration. Therefore, PSIS bio-scaffold was selected to continue with our co-culture of VECs and VICs.

5.1.2. Cardiac Output, GOA, and EOA

Average normal adult resting cardiac output (CO) is approximately 5 liters per minute at a heart rate (HR) of 70 beats per minute (BPM). The amount of blood pumped by the heart is dependent on the demand for oxygen, therefore regulation of cardiac output is heavily determined by the nervous system, endocrine system, and paracrine signaling [75]. To determine stroke volume (SV) for a normal resting CO, we used the following Equation 3:

$$CO = HR \times SV$$

Equation 3. Cardiac output is the product of heart rate, measured in beats per minute, and the stroke volume, measured in liters per minute

$$SV = \frac{CO}{HR} = \frac{5 \text{ l/min}}{70 \text{ bpm}} = 0.0714 \frac{\text{l}}{\text{beat}} = 71.4 \text{ mL/beat}$$

Equation 4. Using Equation 3 to determine nominal adult resting heart stroke volume

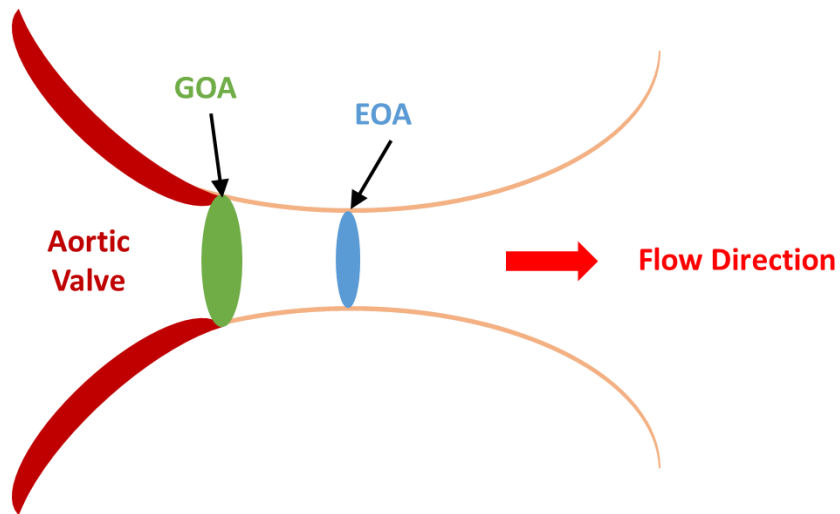


Figure 18. GOA vs. EOA

While atrium and ventricular chamber sizes can remain constant, the SV can be affected by the inflow shape of the valve leaflet and the cross-sectional area of the aorta. During ventricular ejection, a jet stream from blood acceleration is produced and the momentum from this acceleration continues downstream beyond the aortic valve to a point where the cross-sectional area is minimal, forming the effective orifice area (EOA), or the narrowest flow cross-sectional area in the flow stream (Figure 18). The geometric orifice area (GOA), conversely, is measured at the anatomic valve opening that is upstream of the EOA [76].

5.1.3. Bernoulli's Principle and Modified Bernoulli's Equation

Bernoulli's principle relates the speed of a fluid to the pressure gradient of the fluid. Within a horizontal flow, points of higher fluid velocity will have less pressure than points of slower velocity.

$$P_1 + \frac{1}{2}\rho v_1^2 + \rho g h_1 = P_2 + \frac{1}{2}\rho v_2^2 + \rho g h_2$$

Equation 5. Bernoulli's equation, consisting of pressure (P), density (ρ), flow velocity (v), and elevation (h)

Assuming a horizontal flow, $h_1 = h_2$, and that $v_2 \gg v_1$ under valvular stenosis or high regurgitation conditions, the equation can be re-written as:

$$\Delta P = \frac{1}{2}\rho v_2^2$$

Blood density is equal to 1060 kg/m³ and pressure in the original Bernoulli's equation is measured in mmHg. Given that 1 mmHg = 133 Pascals, or 133 kg/ms², we can re-write the above equation as:

$$\Delta P = \frac{1}{2} * \frac{1060}{133} * v_2^2$$

$$\Delta P = 3.985 * v_2^2$$

$$\Delta P = 4v_2^2$$

Equation 6. Modified Bernoulli's Equation

The modified Bernoulli's equation (Equation 6) was first introduced to determine the EOA of valves based on flow rate through the valve [77]. When transvalvular pressure is measured, the Bernoulli's equation can be used to convert pressure gradient into velocity through the valve opening. An increased flow velocity across the valve is associated with stenosis or narrowing of the valve [78].

5.1.4. Elastic Modulus (Young's Modulus) and Hertzian Theory

The elastic modulus, or Young's modulus, is used to characterize stiffness of materials and is defined as the ratio between stress and strain within the elastic regime. The stress and strain parameters are governed by Equation 7 and Equation 8, respectively. In biological samples, differences in stiffness are found between various cell phenotypes, as well as between normal and diseased conditions [79] [80].

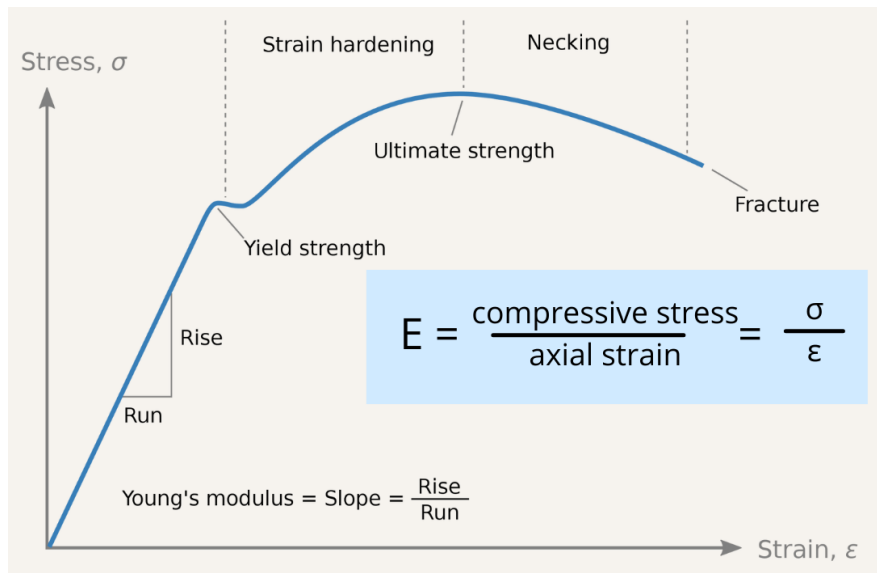


Figure 19. Young's modulus is determined by the linear region before yield strength from a stress-strain curve [81]

$$\sigma = \frac{F}{A}$$

Equation 7. Stress is defined by force divided area

$$\epsilon = \frac{\Delta L}{L}$$

Equation 8. Axial strain is the ratio between change in length over the original length

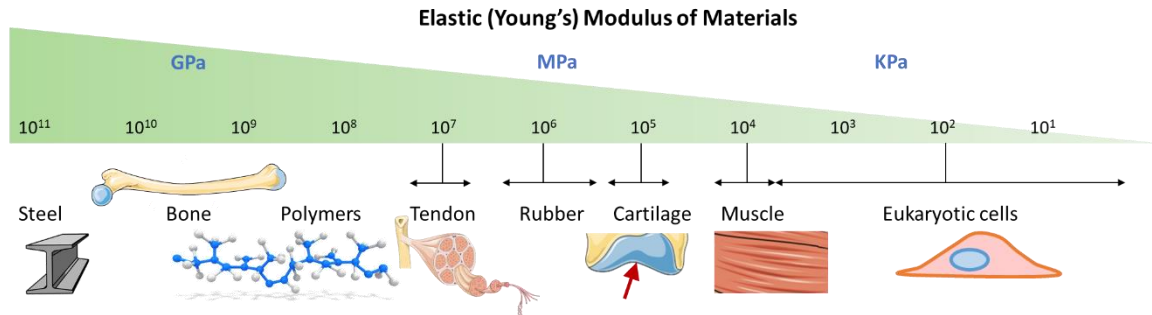


Figure 20. Overview of the Young's Modulus of different materials [82]

The Hertz model is commonly used to approximate nanoindentation experiments of biological samples [83]. The model assumes an isotropic and linear elastic material that occupies an infinitely extending space. In addition, the indenter is also assumed to be undeformable with no additional external interaction between the indenter and the sample.

5.2. Methods

5.2.1. Bioreactor Design and CFD

A novel pulsatile flow bioreactor system that facilitates oscillatory flow conditions was designed and manufactured with acrylic material at FIU's machine shop facility. The exterior of the bioreactor was cylindrical shaped, and the interior consisted of three separate concentric compartments at 43 mm in diameter and 39 mm in length to house three valves Figure 23. Prior to fabrication, SolidWorks (Dassault Systemes, Waltham, MA, USA) assemblies (Figure 23) consisting of three 1-mm thick hollow cylindrical scaffolds were

placed inside the three-valve bioreactor chamber to simulate aortic valves in a controlled flow environment. The assemblies were saved in .step files and imported into ANSYS (Ansys, Inc., Canonsburg, PA) for CFD simulations within Windows 10, 64-bit operating system (Microsoft, Inc., Redmond, WA, USA), where mesh processing was carried out with Fluid Meshing software. The meshed geometry consisted of 1157524 elements and 225850 nodes (Figure 21). An inlet square velocity waveform (Figure 22) was identified to produce an OSI of ~ 0.50 and a time-averaged wall shear stress (TAWSS) in the order of $0.1 - 0.4 \text{ Pa}$ ($1 - 4 \text{ dyne/cm}^2$) on the scaffold's outer wall surfaces. The fluid was assumed to be incompressible with a density of 1.01 g/cm^3 and a dynamic viscosity of 1.27 cP [84]. A no-slip condition on the bioreactor wall was assumed in the simulation and a convergence criterion of 1×10^{-6} was set for the residuals.

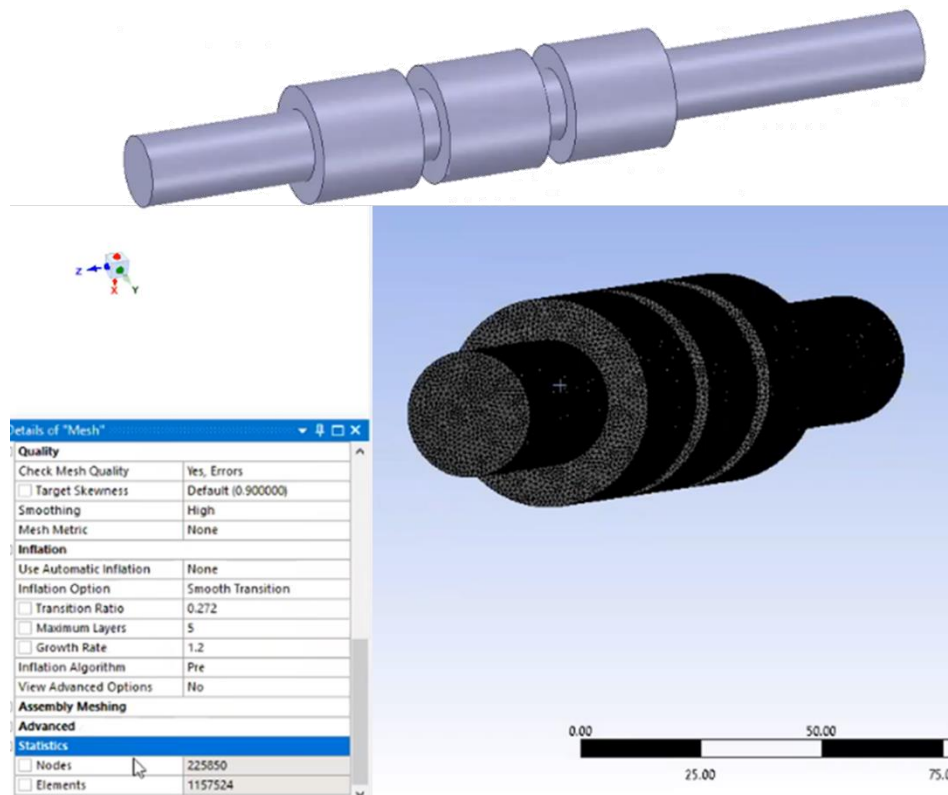


Figure 21. Bioreactor flow domain (top) and meshed elements (bottom)

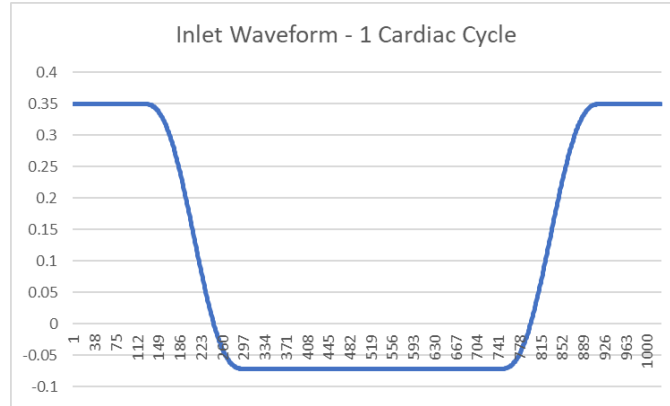


Figure 22. Input square waveform of 1 cardiac cycle. Waveform was used to generate the desired TAWSS and OSI in our bioreactor using the Vivitro Superpump (Vivitro Labs, Victoria, BC, Canada).

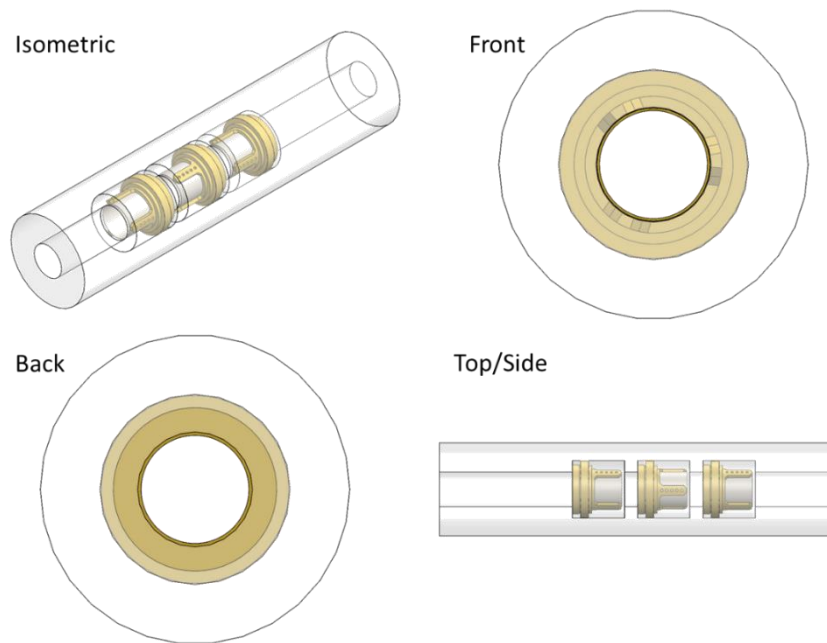


Figure 23. Bioreactor schematic. Detailed mechanical drawings in Appendix I.

Design verification was conducted with a magnetic volumetric flow probe from the Vivitro Pulse Duplicator System (Vivitro Labs, Victoria, BC, Canada) shown in Appendix II.

5.2.2. Valvular Cell Seeding and Valve Tissue Conditioning in Bioreactor

Human VECs and VICs from Aim 2 were expanded in respective flasks and culture media.

Prior to cell seeding, three cylindrical PSIS bio-scaffolds with 26 mm in diameter, 1 mm

in thickness, and 36 mm in length were sutured to custom, 3D-printed valve holders of polylactic acid (PLA) material along its annulus and three posts (Figure 24 and Figure 25), forming a tri-leaflet configuration mimicking the native aortic valve under flow conditions. All bioreactor components and sutured bio-scaffolds were sterilized with ethylene oxide (EtO, AN 306, Anprolene, Andersen Products Inc., HawRiver, NC) for 12 hours.

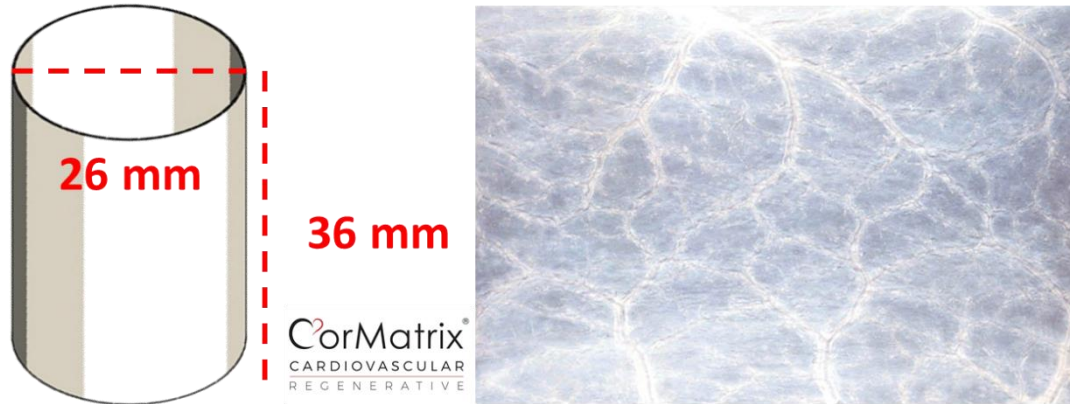


Figure 24. PSIS geometry and material texture



Figure 25. 3D printed valve holders in aortic tri-leaflet configuration with three posts

Cell seeding consisted of a co-culture arrangement that included both VECs and VICs, with a VEC to VIC ratio set to 34:27 [85]. The VICs were seeded first for 96 hours in rotisserie, followed by seeding of VECs for an additional 72 hours [85]. Total cell seeding density was set to ~ 1.2 million cells/cm² [55] [86]. Seeding media consisted of DMEM

(Fisher Scientific, Waltham, MA) with 10% FBS (Atlanta Biologics, Atlanta, GA), 1% PS (HyClone, Fisher Scientific, Waltham, MA), 82 $\mu\text{g}/\text{mL}$ L-ascorbic acid 2-phosphate (AA2P) (Sigma-Aldrich, St. Louis, MO), and 2 ng/mL basic fibroblast growth factor (bFGF) (Corning, Fisher Scientific, Waltham, MA) [86].

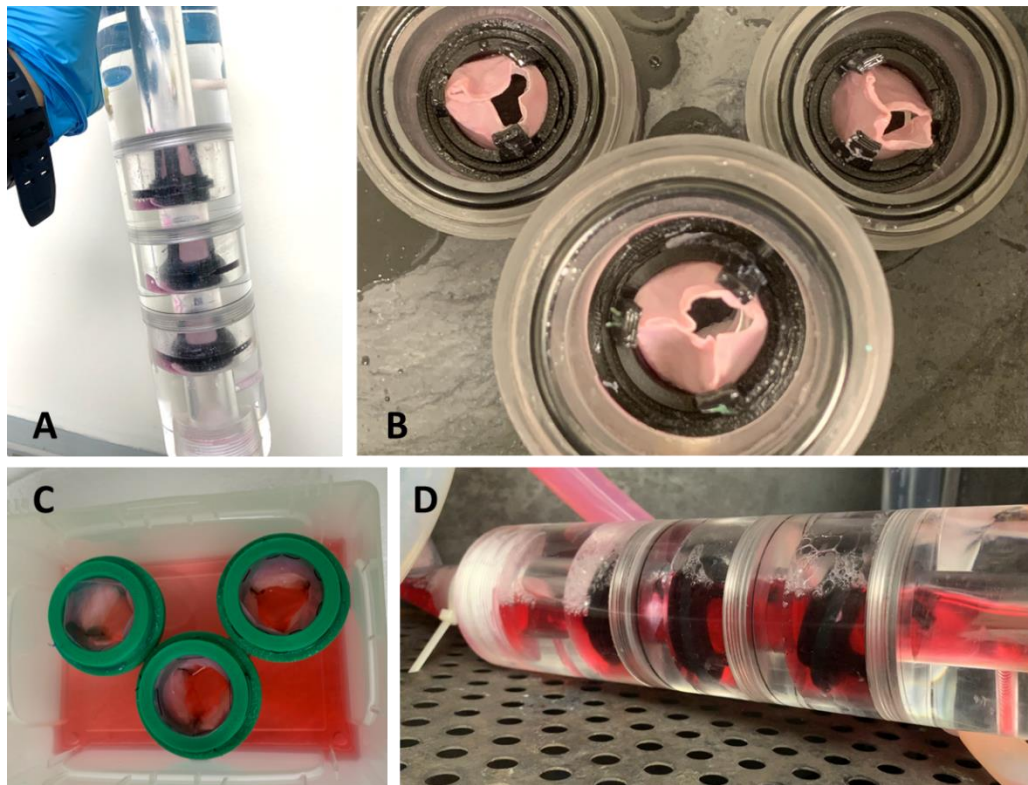


Figure 26. (A) Drained bioreactor with three conditioned PSIS valves. Each valve was seeded with VECs and VICs and conditioned in PC media under 0.50 OSI flow environment. (B) Removal of conditioned valves from bioreactor chambers. (C) Three PSIS valves, each seeded with VECs and VICs and conditioned in static PC media. (D) Bioreactor conditioning of PSIS valves with PC media.

Seeded valve tissues were subject to static conditioning (0 OSI) and 0.50 OSI in the bioreactor system (Figure 26) in DMEM with 5% FBS, 1% PS, 82 $\mu\text{g}/\text{mL}$ AA2P, 2 ng/mL bFGF, 1.8 mM CaCl_2 , 3.8 mM NaH_2PO_4 , and 0.4 units/mL of inorganic pyrophosphate for 7 days with no media change (PC components same as Aim 2). Conditioned samples were then fixed in 10% w/v histological grade formalin (Fisher Scientific, Waltham, MA) at 4°C

overnight. The samples were placed in the Vivitro Pulse Duplicator (Vivitro Labs Inc., Victoria, BC, Canada) for hydrodynamic testing and then embedded in OCT compound (Figure 27) and stored in -80°C for sectioning, staining, and histological assessments.

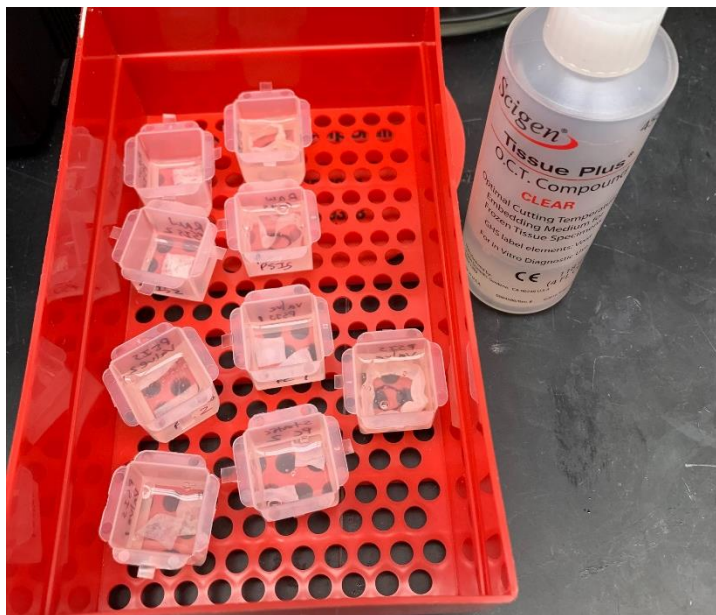


Figure 27. Embedding of samples in OCT compound after hydrodynamic testing

Embedded samples were later sectioned at $16\ \mu\text{m}$ using a cryostat. To observe co-culture seeding of VECs and VICs, sectioned samples were subsequently stained with rabbit anti-CD31 primary antibody (PA5-14372, Thermo Fisher, Waltham, MA) and mouse anti- αSMA (REF 14-9760-82, Invitrogen eBioscience, Thermo Fisher), followed by donkey anti-mouse and anti-rabbit polyclonal secondary antibodies (ab150108 and ab150073, Abcam, Cambridge, UK). Stained samples were imaged using a confocal microscope (Nikon, Eclipse Ti, Minato, Tokyo, Japan). To observe the level of calcification in the conditioned samples, sectioned samples were stained with ARS (Ricca Chemical Company, Arlington, TX) and imaged with AmScope (United Scope, LLC, Irvine, CA).

5.2.3. Valve Hydrodynamic Assessments

Hydrodynamic testing was performed using a pulse duplicator system (Vivitro Labs Inc., Victoria, BC, Canada) filled with 0.9% saline solution with the PSIS valve mounted in the aortic position (Figure 28). A flow probe was affixed between the aortic and ventricular chambers and pressure transducers were inserted in the atrial, ventricular, and aortic locations (AMpack, Vivitro Labs Inc., Victoria, BC, Canada). Tests utilized a stroke volume of 71.4 mL, a heart rate of 70 BPM, and an input flow waveform comprising of a 35% systolic-65% diastolic configuration (S35 Waveform, Vivitest software, Vivitro Laboratories).

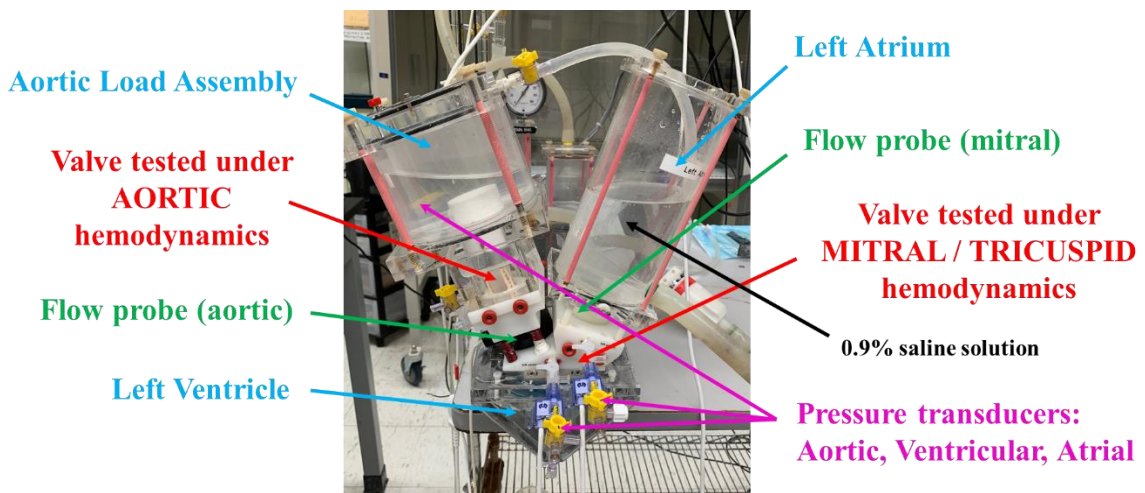

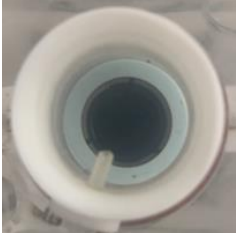






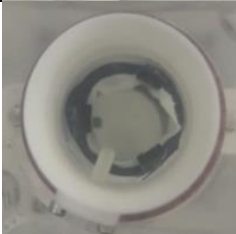



Figure 28. Schematic of the Vivitro pulse duplicator for valve hydrodynamic testing

The experimental groups included three bioreactor 0.50 OSI-conditioned valves and three statically conditioned PSIS valves. A bi-leaflet mechanical valve, a bioprosthetic tri-leaflet valve, and three raw PSIS tri-leaflet valves were used as controls (Table 3). Data consisted of transvalvular pressure (ΔP) and volumetric flowrate (Q_{rms}) in the valve's open configuration, in addition to regurgitation factor (RF%), and valve EOA. Statistical analysis was performed for each parameter using a one-way ANOVA and SEM in

conjunction with Tukey's post hoc analysis in SPSS (IBM, Armonk, NY). Significance was identified when $p < 0.05$.

Table 3. Valve in open and closed configurations during hydrodynamic testing

Valve Type	Open Configuration	Closed Configuration	Diameter (mm)
Mechanical			26
Bioprosthetic			27
Raw PSIS			26
Static (0 OSI) Conditioned PSIS with VECs and VICs			26
Bioreactor (0.50 OSI) Conditioned PSIS with VECs and VICs			26

5.2.4. Mechanical Properties of Conditioned Valves

Nanoindentation was performed with assistance from Dr. Lihua Lou using Dr. Arvind Agarwal's laboratory equipment in the Department of Mechanical and Materials Engineering. Conditioned PSIS valves were cut into three rectangular strips from each sample group for nanoindentation. A flat-end indenter probe with a diameter of $500\ \mu\text{m}$ was used, and a 10% indentation depth of the sample's thickness was applied at a loading of $2\ \mu\text{m/s}$ for $40\ \mu\text{m}$ at the center of the samples shown in Figure 29. Raw data consisted of load and displacement, and the Hertz model was used to approximate the Young's modulus of the samples [87].

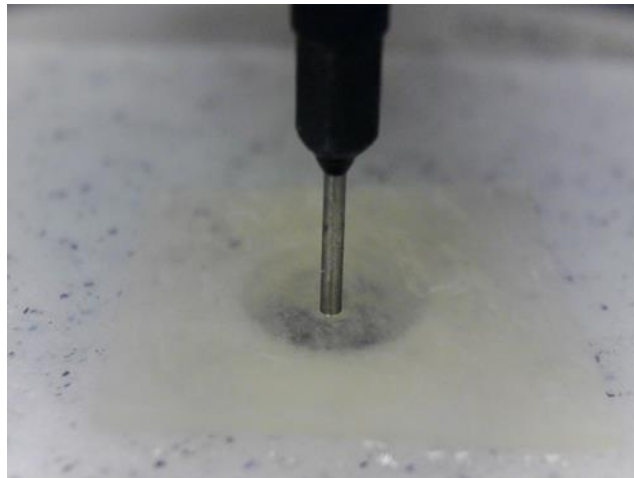


Figure 29. Flat-end circular indenter over a PSIS sample

5.3. Results

5.3.1. CFD Results and Cell Seeding Verification

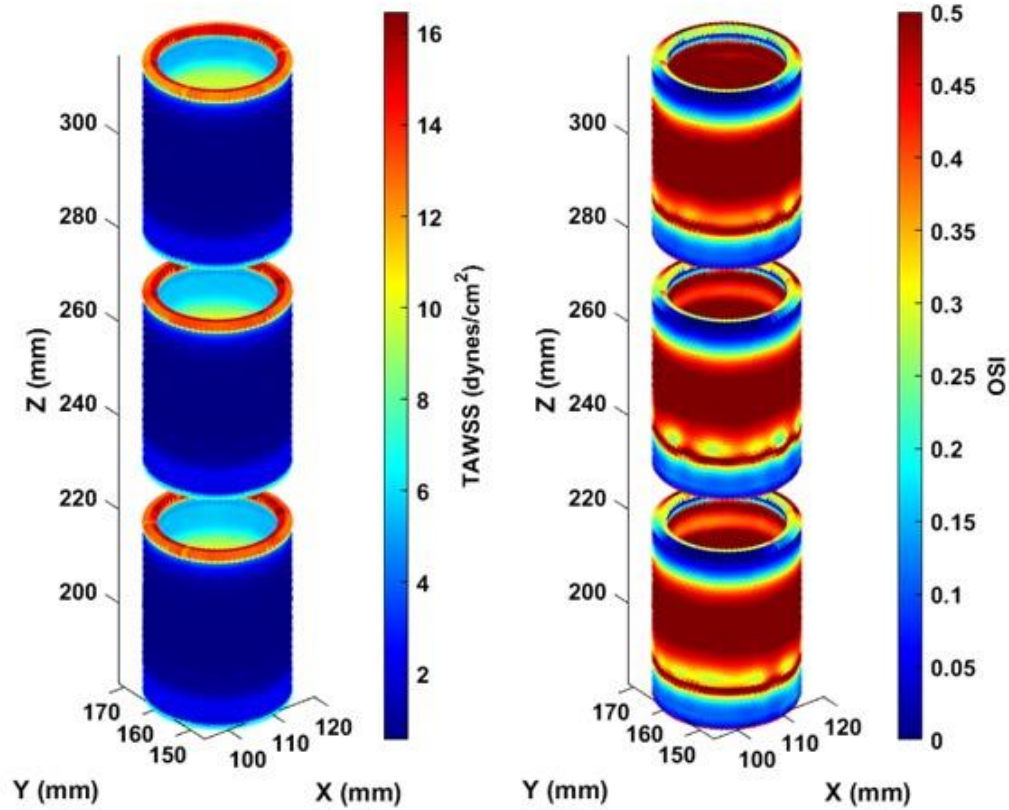


Figure 30. CFD simulation results of wall shear stress and OSI ranges on conditioned valve surfaces

The CFD simulation was an effective way to identify a bioreactor setup and an inlet flow waveform that produces a flow environment of our interest, specifically high OSI in combination with low TAWSS (Figure 30). Majority of the valve surfaces away from the scaffold edges were subject to high OSIs accompanied by low TAWSS.

Immunofluorescent images showed distribution of CD31 (green) and α SMA (red) from our co-culture system consisting of VECs and VICs in bioreactor and static conditions (Figure 31).

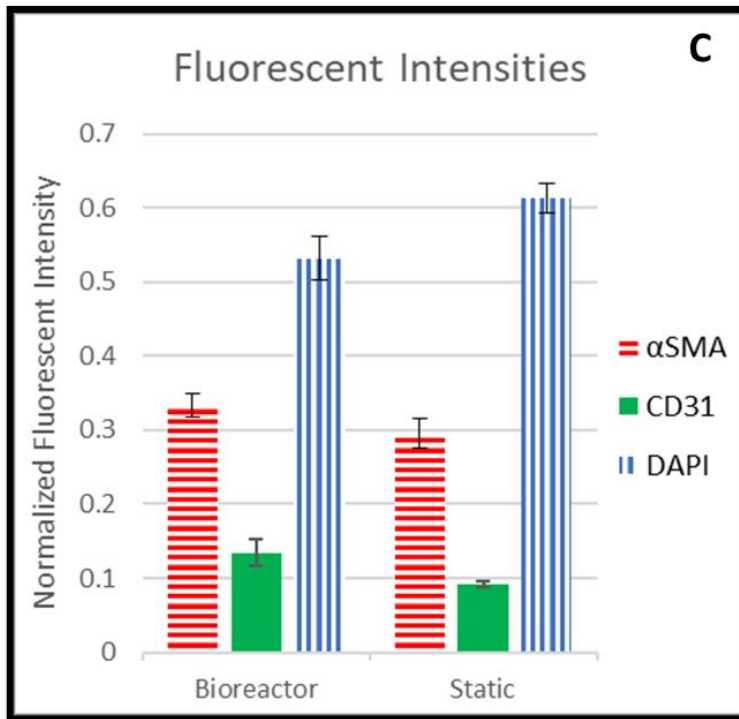
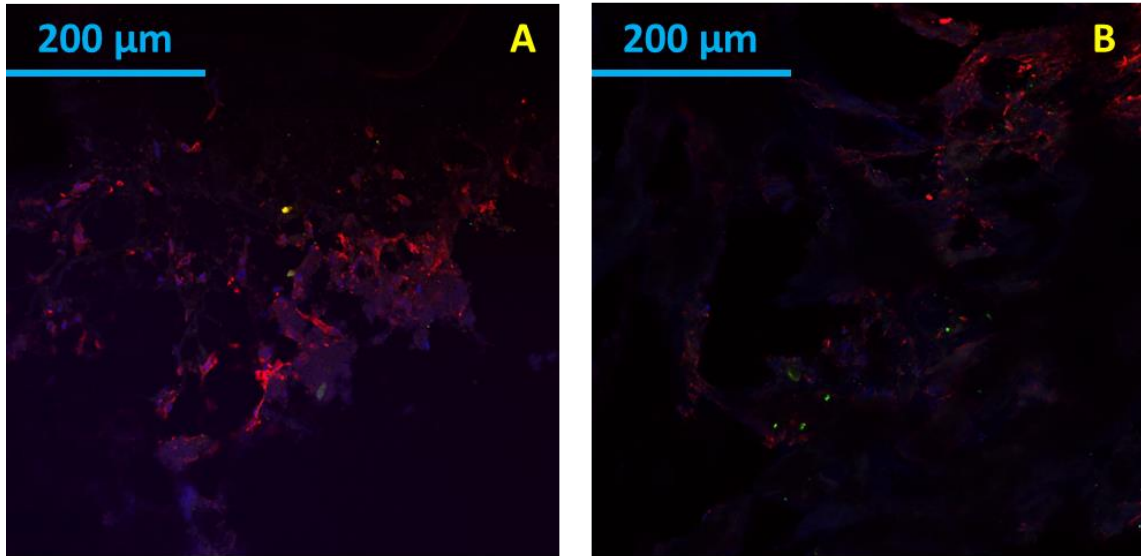


Figure 31. Immunofluorescent staining of bioreactor (A) and static (B) samples. Quantified intensities of α SMA in red ($p = 0.17$), CD31 in green ($p = 0.061$), and DAPI in blue (C).

5.3.2. Valve Hydrodynamic Assessments

Valve hydrodynamic test results included valve regurgitation factor (%), transvalvular pressure (mmHg), volumetric flowrate (mL/s), and EOA (cm²). Lowest regurgitation was found in the mechanical valve (Figure 32), and the unconditioned raw PSIS valve had the highest regurgitation factor. While the static PSIS and bioreactor PSIS valves have a significantly lower regurgitation factor compared to bioprosthetic and raw PSIS, there is no significant difference observed between the static and the bioreactor PSIS valves. All other groups, apart from static PSIS vs. bioreactor PSIS, were statistically different.

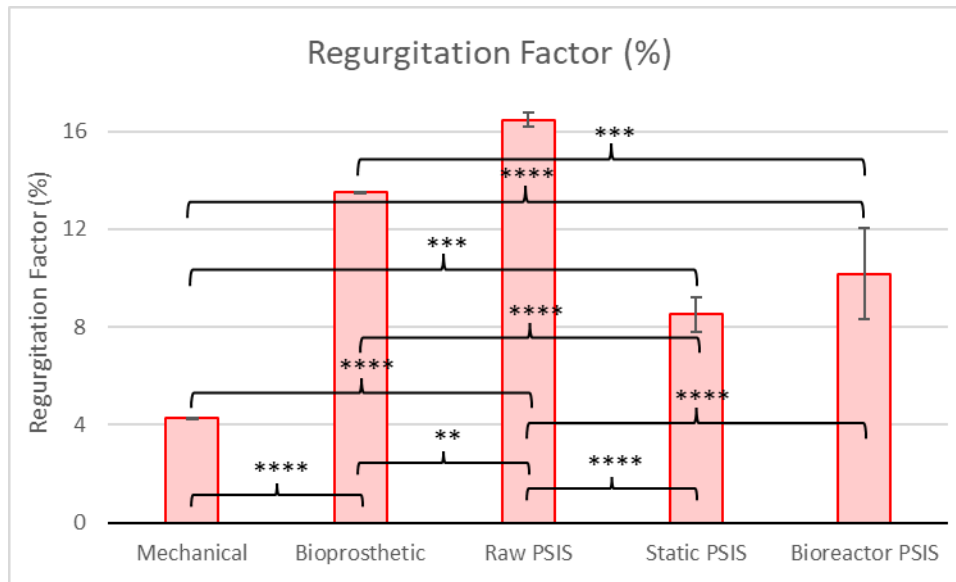


Figure 32. Regurgitation factor comparison between experimental and control groups

Transvalvular pressure in the aortic position measures the difference between aortic and ventricular pressures. Our results show that the raw PSIS and bioreactor PSIS valves had the lowest transvalvular pressures, while the mechanical, bioprosthetic, and static PSIS valves were relatively higher. Statistical significance was observed between all groups except for mechanical vs. bioprosthetic and raw PSIS vs. bioreactor PSIS, as shown in Figure 33.

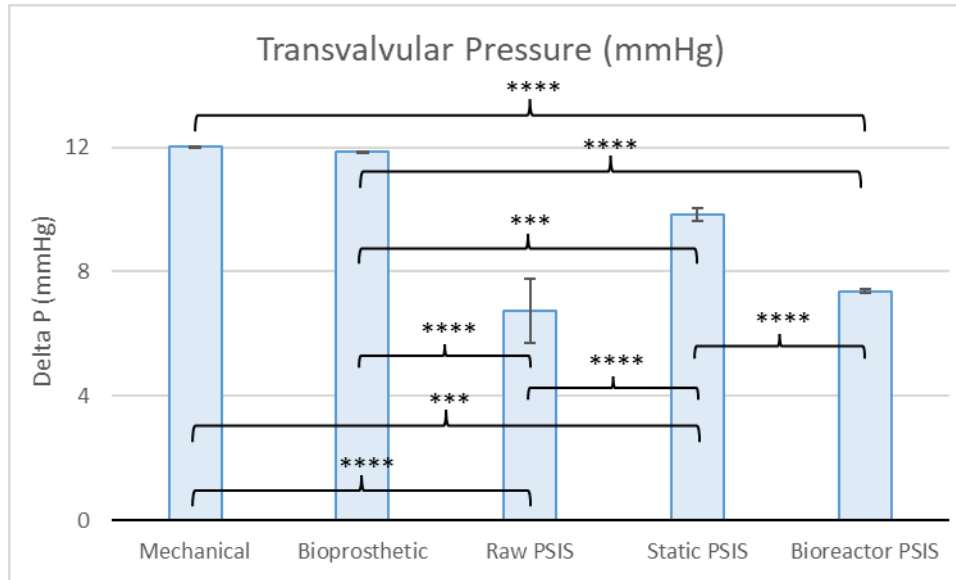


Figure 33. Transvalvular pressure comparison between experimental and control groups. Highest EOAs were observed in the raw PSIS and bioreactor PSIS valves (Figure 34). Statistical significance was not observed between raw PSIS vs. bioreactor PSIS. In contrast, the EOAs of mechanical valve, bioprosthetic, and static PSIS valves were significantly smaller than raw PSIS and bioreactor PSIS valves.

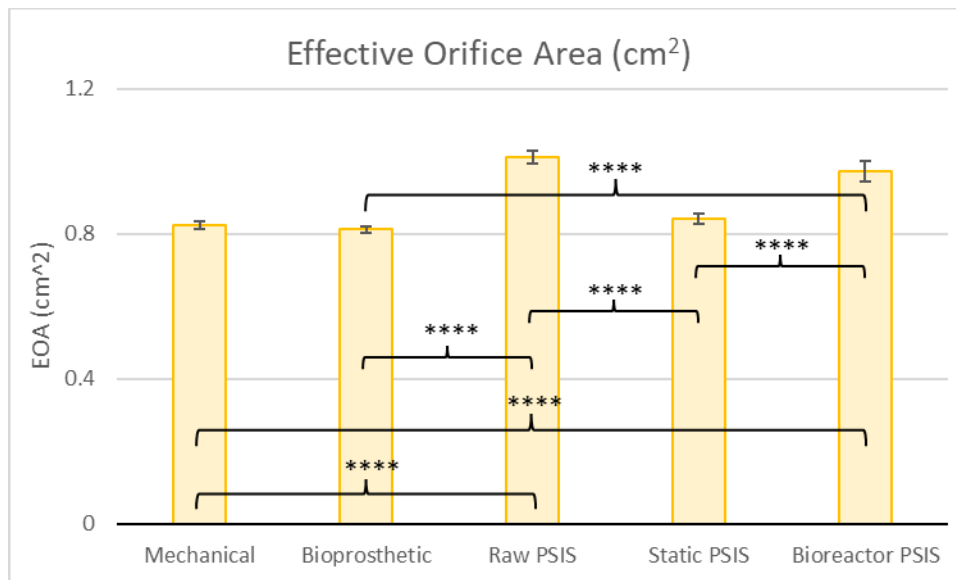


Figure 34. EOA comparison between experimental and control groups

Lowest volumetric flow rate was found in the raw PSIS valve, in which is also significantly lower than mechanical and bioprosthesis valves (Figure 35). However, there is no statistical difference between raw PSIS vs. static PSIS, raw PSIS vs. bioreactor PSIS valves, and static PSIS vs. bioreactor PSIS.

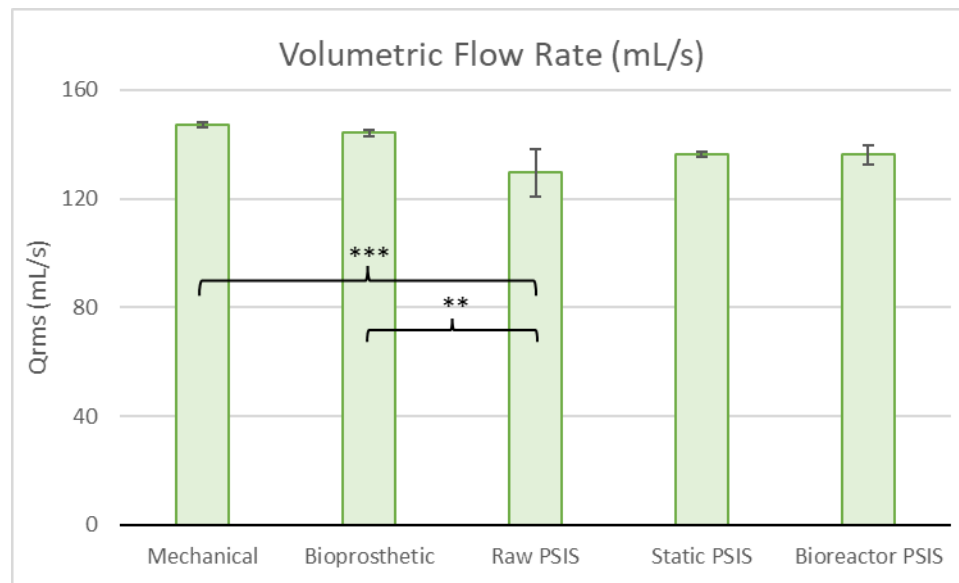


Figure 35. Volumetric flowrate comparison between experimental and control groups

5.3.3. Mechanical Properties of Conditioned Valves

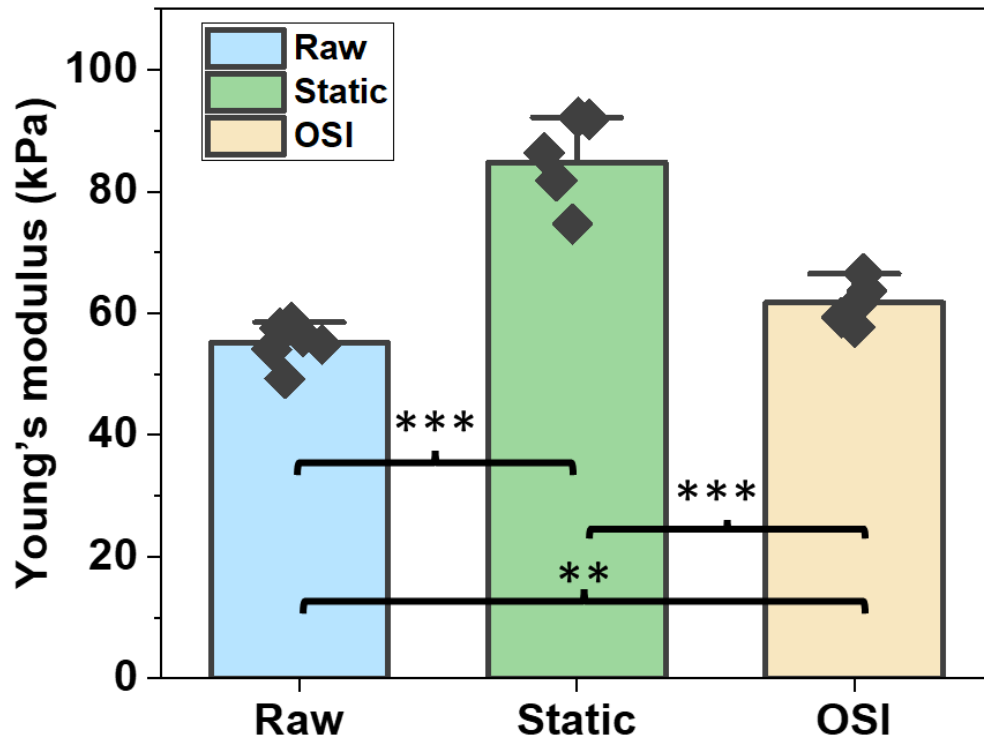


Figure 36. Young's moduli of raw PSIS, statically calcified PSIS, and bioreactor (OSI) calcified PSIS samples. Statistical significance: ** $p < 0.01$, *** $p < 0.001$

The OSI group in Figure 36 represents PSIS valves conditioned in high OSI in a bioreactor. Highest Young's modulus was observed in the static PSIS valves, and the lowest in the raw PSIS valves. Significant differences were also found between raw PSIS vs. static PSIS, static PSIS vs. bioreactor PSIS, and raw PSIS vs. bioreactor PSIS.

5.3.4. Calcification Assessments of Conditioned Valves

ARS was conducted on sectioned bioreactor PSIS valves, raw PSIS valves, and static PSIS valves to show calcification levels in each group (Figure 37). The ARS images show small areas of calcification in the static PSIS valves and the bioreactor PSIS valves. The raw PSIS valves were not calcified. Significant differences ($p < 0.05$) were observed between bioreactor PSIS vs. raw PSIS and static PSIS vs. raw PSIS. Marginally significant

differences ($p = 0.07$) [88] [89] were observed between bioreactor PSIS vs. static PSIS, with calcification in the bioreactor PSIS valve being relatively higher than calcification in static PSIS valve.

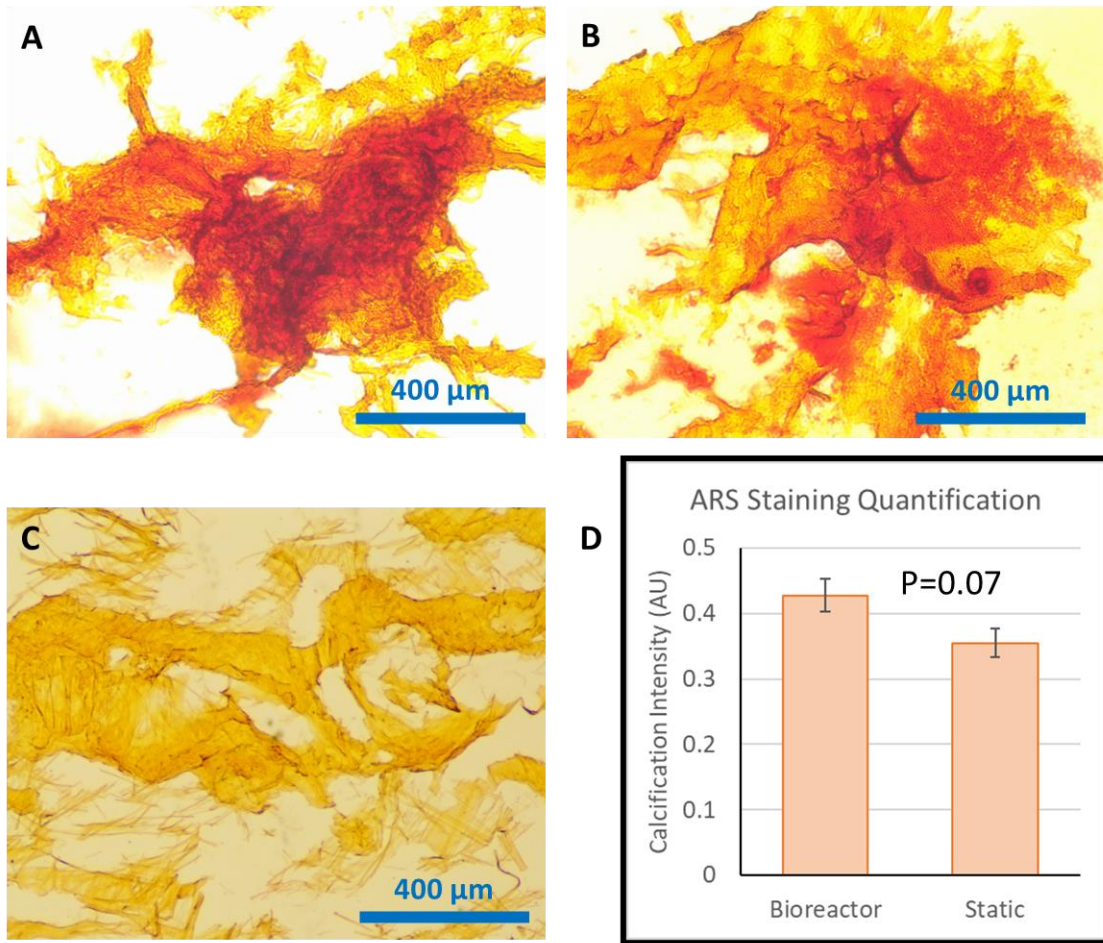


Figure 37. ARS images of bioreactor PSIS valve (A), static PSIS valve (B), raw PSIS valve (C), and quantified level of calcification (D).

5.4. Discussion

The bioreactor system was an effective setup to generate a desired flow environment for valve tissue engineering. It can serve as a platform to recreate the etiology of human tissue remodeling, as well as to study the mechanisms associated with these cellular activities and potentially intervene with the processes. In this aim, we designed and fabricated a

bioreactor that delivered low shear stress ($1 - 4 \text{ dynes/cm}^2$) and high OSI (0.50 OSI) while allowing valve tissues to maintain its original leaflet movement during conditioning. The goal of this aim was to create calcific valve tissues in the bioreactor using human VECs and VICs seeded on scaffolds, and our ARS images showed calcified regions in the bioreactor-conditioned valves. A separate static group using the same VECs and VICs seeded in PSIS and a negative control group consisting of raw PSIS valve with no cells were also conducted for comparison. ARS images (Figure 37, Figure 41, and Figure 43) showed similar calcification regions between bioreactor PSIS valves and static PSIS valves, respectively. However, the calcification intensity in the bioreactor PSIS valves was marginally significantly higher than the static PSIS valves ($p=0.07$) [88] [89]. The raw PSIS valves, on the other hand, had no ARS stains. The ARS stains in both static PSIS and bioreactor PSIS valves indicate early onset of valve calcification. The ARS stains between static (0 OSI) and bioreactor (0.50 OSI) PSIS valves were also similar to our findings in aim 2's 2D cellular studies shown in Figure 14. A higher ARS stain in the bioreactor PSIS valves may indicate increased VIC activation, leading to increased α SMA expression as shown in our immunofluorescent stains (Figure 31). The immunofluorescent images also showed aggregation of both CD31 and α SMA proteins interspersed across the scaffolds, despite VICs being seeded 96 hours prior to seeding VECs in the co-culture to mimic VEC on the outer layer exposed to fluid shear stress. Expression of α SMA was also observed to be higher in the bioreactor (0.50 OSI) valves compared to the static samples. Though not statistically significant, this observation concurs with our 2D gene expression findings shown in Figure 13 [23].

The static PSIS valves exhibited the highest Young's modulus compared to the raw PSIS and bioreactor PSIS samples. The raw PSIS had a significantly lower Young's modulus than both static PSIS and bioreactor PSIS groups, indicating that the VEC-VIC co-culture conditioning generated a layer of tissue on the PSIS scaffold therefore increasing the elastic modulus of the scaffold. The static PSIS valve, however, had a significantly higher Young's modulus than the bioreactor PSIS valve, and this may be due to compromised valve tissue under the 0.50 OSI environment. Alternatively, the high OSI may be protecting the valve under dynamic culture by redistributing calcified deposits in a way that maintains the EOA and transvalvular pressures, thereby delaying valve failure.



Figure 38. Hydrodynamic results of Raw PSIS valve, Static PSIS valve, and Bioreactor PSIS valve. (A) Regurgitation factor, (B) Transvalvular pressure, ΔP , (C) Effective orifice area, EOA, and (D) Volumetric flowrate, Q_{rms} .

Using parameters obtained by the Vivitro pulse duplicator, an ideal healthy valve should have low RF, low transvalvular pressure, high EOA, and high flowrate. Hydrodynamic

data showed significant differences in individual parameters between each group (Figure 38). The bioreactor PSIS valve exhibited a relatively higher RF than the static PSIS valve, but the differences were not statistically significant. The raw PSIS and bioprosthetic valves, on the other hand, exhibited a significantly higher RF than both static PSIS and bioreactor PSIS valves. A high RF can be an indicator of valve stenosis. Based on literature, mild regurgitation is observed between 0 – 15%, and severe regurgitation is when RF is greater than 50% [90]. Apart from the raw PSIS valve, all other valves tested in this aim exhibited mild regurgitation characteristics. The raw PSIS valve showed grade II intermediate regurgitation (15 – 30%) [90], and this may be due to a thinner valve leaflet with higher curve flexibility, therefore more prone to leakage from the static head pressure in the closed configuration.

Transvalvular pressures of the bioreactor PSIS valve was significantly lower than the static PSIS valve. Interestingly, both the mechanical and bioprosthetic valves exhibited the highest transvalvular pressures while the raw PSIS showed the lowest pressure gradient. According to the modified Bernoulli's equation (Equation 6), a high transvalvular pressure indicates a high jet velocity across the valve. A transvalvular pressure of 30 mmHg or more is considered high gradient and may be an indication of valve stenosis [91], and our results showed that all valves were not stenotic based on transvalvular pressure values.

The volumetric flowrate of all tested valves showed the least variation between groups. No significant differences were found between volumetric flowrate of static PSIS and bioreactor PSIS valves when compared to the clinically available bioprosthetic and mechanical valves. As echocardiograms (ECHO) detect movement of blood through the heart based on flow volume, this may be one of the main reasons why current ECHO

machines are unable to differentiate minor differences between early onset of valve calcification from healthy valves, and that CAVD becomes only detectable after intermediate to late stages of calcification, where flowrate is significantly lower, and RF becomes significantly visible. Despite the lack of differences between both calcific valves and clinically available valves, the raw PSIS valves showed significantly lower volumetric flowrate when compared to both mechanical and bioprosthetic. This also corresponds to the raw PSIS valve having the lowest transvalvular pressure gradient, in which slows down the flow of fluid.

Hydrodynamic assessments showed highest EOA in the raw PSIS and bioreactor PSIS valves, while lowest EOAs were observed in the clinically available mechanical and bioprosthetic valves. Between static PSIS vs. bioreactor PSIS, the EOA was also significantly lower in the statically conditioned group. Since small EOA corresponds to higher jet velocity, and that high jet velocity indicates higher transvalvular pressure based on Bernoulli's principle, naturally the bioprosthetic and mechanical valves with the highest transvalvular pressures exhibited significantly smaller EOAs, and that the raw PSIS group with the lowest transvalvular pressure showed highest EOA.

According to our nanoindentation results combined with hydrodynamic data, we observed that an increase in valve stiffness leads to potential loss of leaflet flexibility and poor coaptation. This was reflected in our hydrodynamic assessments, where smallest EOA was observed in the static PSIS valve which exhibited the highest Young's modulus. A small EOA leads to high jet velocity and high transvalvular pressure based on modified Bernoulli's principle. This theory was also reflected in static PSIS valve showing highest

transvalvular pressure. In summary, we observed a trend that correlates stiffness and transvalvular pressure, where the higher the stiffness, the higher the transvalvular pressure. Overall, our aim 3 showed that bioreactor can be an effective device for valve tissue engineering. The ARS images showed early onset of calcification with bioreactor slightly more calcified than static valves. Even though the bioreactor conditioned valves had a higher level of calcification, the hydrodynamic assessments showed better performances in the bioreactor PSIS valves compared to static PSIS valves with a significantly higher EOA and significantly lower transvalvular pressure. This suggests that the concomitant high OSI and calcification ingredients present on the bioreactor PSIS valve delayed valve failure by maintaining a larger EOA and smaller transvalvular pressure via distribution of calcification that high OSI induces, which was not possible in the statically cultured valve. Through dynamic tissue culture, the bioreactor was able to better maintain the functionality of valve leaflets compared to statically calcified valves. However, to confirm that the bioreactor recapitulates early onset of human valve calcification, further protein assessments will need to be conducted in comparison to the statically calcified valves. Some of the study limitations include choice of pro-calcific media may alter specific mechanisms, in which certain ingredients may result in varied gene expressions. Other limitations include an absence of significant correlation between bioreactor and statically conditioned level of calcification, α SMA, and CD31 expressions. In addition, during bioreactor conditioning, the valve holder closest to the bioreactor outlet was not always fully secured in place.

5.5. Summary

Calcific aortic valve disease is one of the most prevalent chronic heart problems, and the risk of mortality is associated with valve stenosis from increased mineralization, leading to eventual heart failure. Due to a lack of an early diagnostic tool and proper CAVD treatment, development of a platform for therapeutic discovery would present a breakthrough in the management of CAVD. Our data suggests that valve tissues exposed to high flow oscillations present a similar level of calcification compared to statically conditioned valves, though the bioreactor generated a shear-dependent mechanotransduction environment that is more similar to the physiological development of CAVD compared to static conditions. In addition, the high OSI condition seem to redistribute calcified deposits in a manner that maintains valve function and delays valve failure. By generating early CAVD tissues using the bioreactor, the system also allows further studies on progressive deterioration of valve hydrodynamic functions due to changes in mechanical properties in tissue integrity.

Impact and Future Studies

Our results showed the bioreactor PSIS valves had higher level of calcification, however they also exhibited better valve hydrodynamic performance compared to the static PSIS valves. Additional immunostaining for glycosaminoglycans (GAG) can be conducted to confirm if the bioreactor recapitulates early onset calcification pathology [92]. Other future studies include conducting protein analysis of conditioned media from the bioreactor system and static conditioning via methods like mass spectroscopy to determine calcification pathways for potential drug development. The bioreactor system could then be used as a testbed for therapeutic treatment or intervention for early onset of CAVD.

Visual inspection of high-speed camera videos shows a possible delay in valve closing in the bioreactor PSIS valve compared to the control raw PSIS valve. Assessments of GOA of the valve across one cardiac cycle can be conducted to determine GOA as a function of time (Figure 39).

Integration of such function would reveal the total valve open area cross the cardiac cycle, and differentiation of the function would provide the rate (cm^2/s) at which the valve opens and closes in that cardiac cycle. While current clinical echocardiograms evaluate valve functions in a similar manner as the Vivitro system and may be unable to detect early valve calcification, development of new instruments that can detect the closing time of aortic valves may be able to assess early valve calcification, such as relative closing time between S1 and S2 sounds which occur before systole and diastole, respectively.

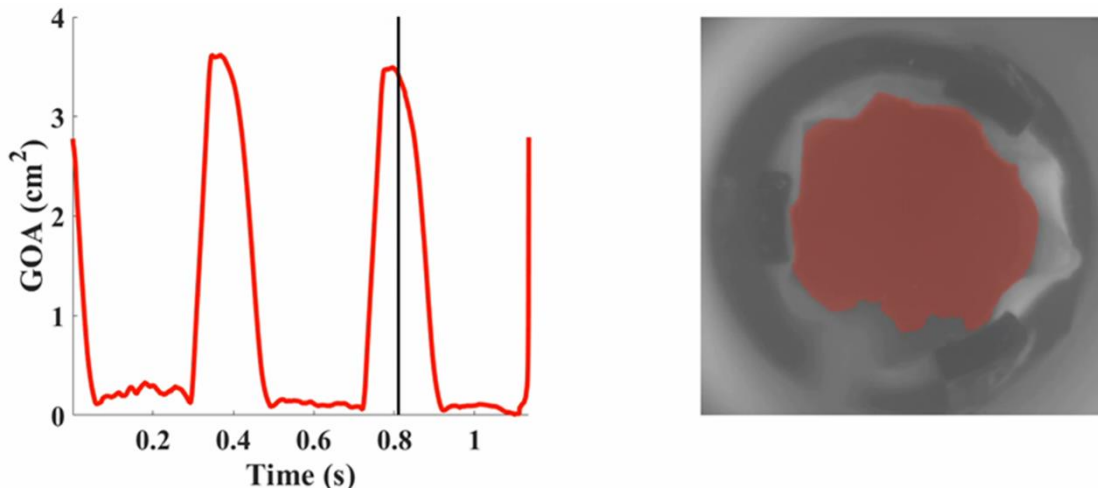


Figure 39. GOA of bioreactor PSIS valve in the open configuration

To determine optimal valve performance based on transvalvular pressure, EOA, RF, and volumetric flow rate, the values of these parameters from a set of healthy valves can be collected. This generates a database for all four parameters that defines healthy valve performance. The parameters can then be plotted on individual axes, and regions with the

densest dataset can be found to determine a function that calculates the most optimal valve performance. The same approach can also be applied to determine a function of diseased valve performance.

REFERENCES

- [1] S. Yadgir, C. Johnson, V. Aboyans, O. Adebayo, R. Adedoyin, M. Afarideh, F. Alahdab, A. Alashi, V. Alipour, J. Arabloo, S. Azari, C. Barthelemy, C. Benziger, A. Berman, A. Bijani, J. Carrero, C. F, A. Daryani, A. Durães and G. Roth, "Global, Regional, and National Burden of Calcific Aortic Valve and Degenerative Mitral Valve Diseases, 1990-2017," *Circulation*, vol. 141, no. 21, pp. 1670-1680, 2020.
- [2] K. Sider, M. Blaser and C. Simmons, "Animal models of calcific aortic valve disease," *Int J Inflam*, 2011.
- [3] S. Rathan, C. Ankeny, S. Arjunon, Z. Ferdous, S. Kumar, J. Esmerats, J. Heath, R. Nerem, A. Yoganathan and H. Jo, "Identification of side- and shear-dependent microRNAs regulating porcine aortic valve pathogenesis," *Scientific Reports*, vol. 6, 2016.
- [4] C. Simmons, G. Grant, E. Manduchi and P. Davies, "Spatial Heterogeneity of Endothelial Phenotypes Correlates With Side-Specific Vulnerability to Calcification in Normal Porcine Aortic Valves," *Circulation Research*, vol. 96, no. 7, pp. 792-799, 2005.
- [5] J. Esmerats, N. Villa-Roel, S. Kumar, L. Gu, M. Salim, M. Ohh, W. Taylor, R. Nerem, A. Yoganathan and H. Jo, "Disturbed Flow Increases UBE2C (Ubiquitin E2 Ligase C) via Loss of miR-483-3p, Inducing Aortic Valve Calcification by the pVHL (von Hippel-Lindau Protein) and HIF-1 α (Hypoxia-Inducible Factor-1 α) Pathway in Endothelial Cells," *Arterioscler Thromb Vasc Biol*, vol. 39, no. 3, pp. 467-481, 2019.
- [6] X. He and D. Ku, "Pulsatile flow in the human left coronary artery bifurcation: average conditions," *J Biomech Eng*, vol. 118, no. 1, pp. 74-82, 1996.
- [7] J. Wang, P. Paritala, J. Mendieta, Y. Gu, O. Raffel, T. McGahan, T. Lloyd and Z. Li, "Carotid Bifurcation With Tandem Stenosis—A Patient-Specific Case Study Combined in vivo Imaging, in vitro Histology and in silico Simulation," *Front. Bioeng. Biotechnol.*, vol. 20, 2019.
- [8] D. Ku, "Blood Flow In Arteries," *Annual Review of Fluid Mechanics*, vol. 29, pp. 399-434, 1997.
- [9] J. Butcher and R. Nerem, "Valvular endothelial cells regulate the phenotype of interstitial cells in co-culture: effects of steady shear stress," *Tissue Engineering*, vol. 12, no. 4, pp. 905-915, 2006.

- [10] M. Patel, "On Laminary Boundary Layers in Oscillatory Flow," *Proceedings of the Royal Society of London. Series A, Mathematical and Physical Sciences*, vol. 347, no. 1648, pp. 99-123, 1975.
- [11] K. Ahn and M. Ibrahim, "Laminar/turbulent oscillating flow in circular pipes," *International Journal of Heat and Fluid Flow*, vol. 13, no. 4, pp. 340-346, 1992.
- [12] K. Gersten, H. Schlichting, C. Mayes, H. Oertel, E. Krause and K. Mayes, *Boundary-Layer Theory*, Berlin Heidelberg: Springer-Verlag, 2000.
- [13] IBIDI GMBH, "The Different Types of Flow," 2021.
- [14] J. Sundin, M. Bustamante, T. Ebbers, P. Dyverfeldt and C. Carlhall, "Turbulent Intensity of Blood Flow in the Healthy Aorta Increases With Dobutamine Stress and is Related to Cardiac Output," *Front. Physiol.*, 2022.
- [15] A. Mahalingam, U. Gawandalkar, G. Kini, A. Buradi, T. Araki, N. Ikeda, A. Nicolaidis, J. Laird, L. Saba and J. Suri, "Numerical analysis of the effect of turbulence transition on the hemodynamic parameters in human coronary arteries," *Cardiovasc Diagn Ther*, vol. 6, no. 3, pp. 208-220, 2016.
- [16] N. WW, M. O'Rourke and C. Vlachopoulos, *McDonald's Blood Flow in Arteries*, Boca Raton: CRC Press, 2011.
- [17] K. Witter, Z. Tonar and H. Schopper, "How many Layers has the Adventitia? - Structure of the Arterial Tunica Externa Revisited," *Anat Histol Embryol*, vol. 46, no. 2, pp. 110-120, 2017.
- [18] C. Hsu, J. Hutcheson and S. Ramaswamy, "Oscillatory Fluid-Induced Mechanobiology in Heart Valves with Parallels to the Vasculature," *Vascular Biology*, vol. 2, no. 1, pp. R59-R71, 2020.
- [19] M. Gomel, R. Lee and K. Grande-Allen, "Comparing the Role of Mechanical Forces in Vascular and Valvular Calcification Progression," *Front. Cardiovasc. Med.*, 2019.
- [20] O. Arjmandi-Tash, S. Razavi and R. Zambouri, "Possibility of Atherosclerosis in an Arterial Bifurcation Model," *Bioimpacts*, vol. 1, no. 4, pp. 225-228, 2011.
- [21] K. Balachandran, P. Sucusky and A. Yoganathan, "Hemodynamics and mechanobiology of aortic valve inflammation and calcification," *Int J Inflamm*, 2011.
- [22] J. Esmerats, J. Heath and H. Jo, "Shear-Sensitive Genes in Aortic Vallve Endothelium," *Antioxidants & Redox Signaling*, vol. 25, pp. 401-414, 2016.

- [23] C.-P. Hsu, A. Tchir, A. Mirza, D. Chaparro, R. Herrera, J. Hutcheson and S. Ramaswamy, "Valve Endothelial Cell Exposure to High Levels of Flow Oscillations Exacerbates Valve Interstitial Cell Calcification," *Bioengineering*, vol. 9, no. 8, 2022.
- [24] A. Malek, S. Alper and S. Izumo, "Hemodynamic Shear Stress and Its Role in Atherosclerosis," *JAMA*, vol. 282, pp. 2035-2042, 1999.
- [25] Y. Chatzizisis, A. Coskun, M. Jonas, E. Edelman, C. Feldman and P. Stone, "Role of Endothelial Shear Stress in the Natural History of Coronary Atherosclerosis and Vascular Remodeling: Molecular, Cellular, and Vascular Behavior," *Journal of the American College of Cardiology*, vol. 49, no. 25, pp. 2379-2393, 2007.
- [26] J. Veinot, "Pathology of inflammatory native valvular heart disease," *Cardiovascular Pathology*, vol. 15, no. 5, pp. 243-251, 2006.
- [27] M. Thubrikar, J. Aouad and S. Nolan, "Patterns of calcific deposits in operatively excised stenotic or purely regurgitant aortic valves and their relation to mechanical stress," *The American Journal of Cardiology*, vol. 58, no. 3, pp. 304-308, 1986.
- [28] A. Gupta and S. Bhatnagar, "Vasoregression: a shared vascular pathology underlying macrovascular and microvascular pathologies?," *Journal of Integrative Biology*, vol. 19, pp. 733-753, 2015.
- [29] P. Rajendran, T. Rengarajan, J. Thangavel, Y. Nishigaki, D. Sakthisekaran, G. Sethi and I. Nishigaki, "The Vascular Endothelium and Human Diseases," *Int J Biol Sci*, vol. 9, no. 10, pp. 1057-1069, 2013.
- [30] R. Finsterwalder, M. Ganesan, H. Leb, A. Habberthuer, J. Basilio, I. Lang, M. Krunic, D. Wiedermann and P. Petzelbauer, "Hypoxia/reperfusion predisposes to atherosclerosis," *PLOS ONE*, vol. 13, 2018.
- [31] G. Owens, M. Kumar and B. Wamhoff, "Molecular regulation of vascular smooth muscle cell differentiation in development and disease," *Physiological Reviews*, vol. 84, pp. 767-801, 2004.
- [32] P. Fransen, C. Van Hove, A. Leloup, W. Martinet, G. De Meyer, K. Lemmens, H. Bult and D. Schrijvers, "Dissecting out the complex Ca²⁺ – mediated phenylephrine-induced contractions of mouse aortic segments," *PLOS ONE*, vol. 10, 2015.
- [33] A. Leloup, C. Van Hove, S. Moundt, G. De Meyer, G. De Keulenaer and F. P., "Vascular smooth muscle cell contraction and relaxation in the isolated aorta: a critical regulator of large artery compliance.," *Physiological Reports*, vol. 7, 2019.

- [34] Q. Liu, B. Yan, C. Yu, Y. Zhang and P. CC, "Attenuation of systolic blood pressure and pulse transit time hysteresis during exercise and recovery in cardiovascular patients," *IEEE Transactions on Bio-Medical Engineering*, vol. 61, pp. 346-352, 2014.
- [35] C. Stefanadis, C. Vlachopoulos, E. Tsiamis, L. Diamantopoulos, K. Toutouzas, N. Giatrakos, S. Vaina, D. Tsekoura and T. P, "Unfavorable effects of passive smoking on aortic function in men," *Annals of Internal Medicine*, vol. 128, no. 6, pp. 426-434, 1998.
- [36] D. Bia, R. Armentano, F. Pessana, Y. Zocalo, S. Lluberas and A. Avolio, "Non-symmetrical double-logistic analysis of 24 hour arterial stiffness profile in normotensive and hypertensive subjects," *IEEE Engineering in Medicine and Biology Society*, pp. 809-812, 2008.
- [37] L. Timmins, D. Molony, P. Eshtehardi, M. McDaniel, J. Oshinski, D. Giddens and H. Samady, "Oscillatory wall shear stress is a dominant flow characteristic affecting lesion progression patterns and plaque vulnerability in patients with coronary artery disease," *Journal of the Royal Society, Interface*, vol. 14, 2017.
- [38] B. Kwak, M. Back, M. Bochaton-Piallat, G. Caligiuri, M. Daemen, P. Davies, I. Hofer, P. Holvoet, H. Jo, R. Krams, S. Lehoux, C. Monaco, S. Steffens, R. Virmani, C. Weber, J. Wentzel and P. Evans, "Biomechanical factors in atherosclerosis: mechanisms and clinical implications," *European Heart Journal*, vol. 35, no. 43, pp. 3013-3020, 2014.
- [39] D. Nam, C. Hi, A. Rezvan, J. Sui, K. Budzyn, A. Llanos, D. Harrison, D. Giddens and H. Jo, "Partial carotid ligation is a model of acutely induced disturbed flow, leading to rapid endothelial dysfunction and atherosclerosis," *American Journal of Physiology: Heart and Circulatory Physiology*, pp. 1535-1543, 2009.
- [40] A. Joshi, R. Leask, J. Myers, M. Ojha, J. Butany and C. Ethier, "Intimal thickness is not associated with wall shear stress patterns in the human right coronary artery," *Arteriosclerosis, Thrombosis, and Vascular Biology*, vol. 24, pp. 2408-2413, 2004.
- [41] H. Jo, R. Dull, T. Hollis and J. Tarbell, "Endothelial albumin permeability is shear dependent, time dependent, and reversible," *American Journal of Physiology*, vol. 260, pp. H1992-H1996, 1991.
- [42] R. Amaya, L. Cancel and J. Tarbell, "Interaction between the stress phase angle (SPA) and the oscillatory shear index (OSI) affects endothelial cell gene expression," *PLOS ONE*, vol. 11, 2016.

- [43] M. Izquierdo-Gomez, I. Hernandez-Betancor, J. Garcia-Niebla, B. Mari-Lopez, I. Laynez-Cerdena and J. Lacalzada-Almeida, "Valve calcification in aortic stenosis: etiology and diagnostic imaging techniques," *BioMed Research International*, 2017.
- [44] L. Sun, S. Chandra and P. Sucosky, "Ex vivo evidence for the contribution of hemodynamic shear stress abnormalities to the early pathogenesis of calcific bicuspid aortic valve disease.," *PLOS ONE*, vol. 7, 2012.
- [45] B. Jian, N. Narula, Q. Li, E. Mohler and R. Levy, "Progression of aortic valve stenosis: TGF-beta1 is present in calcified aortic valve cusps and promotes aortic valve interstitial cell calcification via apoptosis," *Annals of Thoracic Surgery*, vol. 75, no. 2, pp. 457-465, 2003.
- [46] J. Kaden, S. Bickelhaupt, R. Grobholz, C. Vahl, S. Hagl, M. Brueckmann, K. Haase, C. Dempfle and M. Borggrefe, "Expression of bone sialoprotein and bone morphogenetic protein-2 in calcific aortic stenosis," *Journal of Heart Valve Disease*, vol. 13, no. 4, pp. 560-566, 2004.
- [47] A. Liu, V. Joag and A. Gotlieb, "The emerging role of valve interstitial cell phenotypes in regulating heart valve pathobiology," *American Journal of Pathology*, vol. 171, pp. 1407-1418, 2007.
- [48] E. Monzack and K. Masters, "Can valvular interstitial cells become true osteoblasts? A side-by-side comparison," *Journal of Heart Valve Disease*, vol. 20, no. 4, pp. 449-463, 2011.
- [49] M. Platt and W. Shockey, "Endothelial cells and cathepsins: biochemical and biomechanical regulation," *Biochimie*, vol. 122, pp. 314-232, 2016.
- [50] T. Neri, E. Hiriart, P. Vliet, E. Faure, R. Norris, B. Farhat, B. Jagla, J. Lefrancois, Y. Sugi, T. Moore-Morris, S. Zaffran, R. Faustino, A. Zambon, J. Desvignes, D. Salgado, R. Levine, J. Luis de la Pompa, A. Terzic, S. Evans, R. Markwald and M. Puceat, "Human pre-valvular endocardial cells derived from pluripotent stem cells recapitulate cardiac pathophysiological valvulogenesis," *Nature Communications*, vol. 10, 2019.
- [51] E. Mohler, "Mechanisms of aortic valve calcification," *American Journal of Cardiology*, vol. 94, no. 11, pp. 1396-1402, 2004.
- [52] Z. Zeng, Y. Yin, K. Jan and D. Rumschitzki, "Macromolecular transport in heart valves. II. Theoretical models," *American Journal of Physiology: Heart and Circulatory Physiology*, pp. H2671-H2686, 2007.

- [53] G. Mahler, C. Frenzl, Q. Cao and J. Butcher, "Effects of shear stress pattern and magnitude on mesenchymal transformation and invasion of aortic valve endothelial cells," *Biotechnology and Bioengineering*, vol. 111, pp. 2326-2337, 2014.
- [54] P. Davies, A. Passerini and C. Simmons, "Aortic valve turning over a new leaf(let) in endothelial phenotypic heterogeneity," *Arteriosclerosis, Thrombosis, and Vascular Biology*, vol. 24, no. 8, pp. 1331-1333, 2004.
- [55] S. Rath, M. Salinas, A. Villegas and S. Ramaswamy, "Differentiation and Distribution of Marrow Stem Cells in Flex-Flow Environments Demonstrate Support of the Valvular Phenotype," *PLOS ONE*, vol. 10, no. 11, 2015.
- [56] J. Wentzel, Y. Chatzizisis, F. Gijzen, G. Giannoglou, C. Feldman and P. Stone, "Endothelial shear stress in the evolution of coronary atherosclerotic plaque and vascular remodelling: current understanding and remaining questions," *Cardiovascular Research*, vol. 96, no. 2, pp. 234-243, 2012.
- [57] J. Bentzon, F. Otsuka, R. Virmani and E. Falk, "Mechanisms of Plaque Formation and Rupture," *Circulation Research*, vol. 114, no. 12, pp. 1852-1866, 2014.
- [58] F. Crick, "On Protein Synthesis," *Symp Soc Exp Biol.*, vol. 12, pp. 138-163, 1958.
- [59] K. Kukurba and S. Montgomery, "RNA Sequencing and Analysis," *Cold Spring Harb Protoc*, vol. 11, pp. 951-969, 2015.
- [60] S. Anders and W. Huber, "Differential expression analysis for sequence count data," *Genome Biology*, vol. 11, 2010.
- [61] J. Du Prel, B. Rohrig, G. Hommel and M. Blettner, "Choosing statistical tests: part 12 of a series on evaluation of scientific publications," *Dtsch Arztebl Int*, vol. 107, no. 19, pp. 343-348, 2010.
- [62] J. Uzarski, E. Scott and P. McFetridge, "Adaptation of endothelial cells to physiologically-modeled, variable shear stress," *PLOS ONE*, vol. 8, no. 2, 2013.
- [63] L. Sauter, A. Krudewig, L. Herwig, N. Ehrenfeuchter, A. Lenard, M. Affolter and H. Belting, "Cdh5/VE-cadherin Promotes Endothelial Cell Interface Elongation via Cortical Actin Polymerization during Angiogenic Sprouting," *Cell Reports*, vol. 9, no. 2, pp. 504-513, 2014.
- [64] J. Rodriguez, J. Orbe, S. Martinez de Lizarrondo, O. Calvayrac, C. Rodriguez, J. Martinez-Gonzalez and J. Paramo, "Metalloproteinases and atherothrombosis: MMP-10 mediates vascular remodeling promoted by inflammatory stimuli," *Frontiers In Bioscience-Landmark*, vol. 13, no. 8, pp. 2916-2921, 2008.

- [65] M. Silva, P. Videira and R. Sackstein, "E-Selectin Ligands in the Human Mononuclear Phagocyte System: Implications for Infection, Inflammation, and Immunotherapy," *Frontiers in Immunology*, 2018.
- [66] M. Grootaert and M. Bennett, "Vascular smooth muscle cells in atherosclerosis: time for a re-assessment," *Cardiovascular Research*, vol. 117, no. 11, pp. 2326-2339, 2021.
- [67] A. Freedman, J. Gaspar and T. Sackton, "Short paired-end reads trump long single-end reads for expression analysis," *BMC Bioinformatics*, vol. 21, no. 149, 2020.
- [68] L. Ait-Ali, I. Foffa, P. Festa and M. Graziaandrea, "Bicuspid aortic valve: epidemiology, genetics and clinics," *Recenti Prog Med*, vol. 103, no. 12, pp. 589-595, 2012.
- [69] J. Leopold, "Cellular mechanisms of aortic valve calcification," *Circ Cardiovasc Interv.*, vol. 5, no. 4, pp. 605-614, 2012.
- [70] S. Rathan, A. Yoganathan and C. O'Neill, "The role of inorganic pyrophosphate in aortic valve calcification," *J Heart Valve Dis*, vol. 23, no. 4, pp. 387-394, 2014.
- [71] S. Goto, M. Rogers, M. Blaser, H. Higashi, L. Lee, F. Schlotter, S. Body, M. Aikawa, S. Singh and E. Aikawa, "Standardization of Human Calcific Aortic Valve Disease In Vitro Modeling Reveals Passage-Dependent Calcification," *Front Cardiovasc Med*, vol. 6, no. 49, 2019.
- [72] K. Livak and T. Schmittgen, "Analysis of Relative Gene Expression Data Using Real-Time Quantitative PCR and the $2^{-\Delta\Delta CT}$ Method," *Methods*, vol. 25, no. 4, pp. 402-408, 2001.
- [73] V. Valente, S. Teixeira, L. Neder, O. Okamoto, S. Oba-Shinjo, S. Marie, C. Scrideli, M. Paco-Larson and C. Carlotti, "Selection of suitable housekeeping genes for expression analysis in glioblastoma using quantitative RT-PCR," *BMC Molecular Biology*, vol. 10, no. 17, 2009.
- [74] B. Gonzalez, A. Herrera, C. Ponce, M. Gonzalez Perez, C. Hsu, A. Mirza, M. Perez and S. Ramaswamy, "Stem Cell-Secreted Allogeneic Elastin-Rich Matrix with Subsequent Decellularization for the Treatment of Critical Valve Diseases in the Young," *bioengineering*, vol. 9, no. 10, 2022.
- [75] J. King and D. Lowery, *Physiology, Cardiac Output*, Treasure Island, FL: StatPearls Publishing, 2022.

- [76] D. Garcia, "What do you mean by aortic valve area: geometric orifice area, effective orifice area, or gorlin area?," *J Heart Valve Dis*, vol. 15, no. 5, pp. 601-608, 2006.
- [77] J. Holen, R. Aaslid, K. Landmark, S. Simonsen and T. Ostrem, "Determination of effective orifice area in mitral stenosis from non-invasive ultrasound Doppler data and mitral flow rate," *Acta Med Scand*, vol. 201, no. 1-2, pp. 83-88, 1977.
- [78] H. Baumgartner, J. Hung, J. Bermejo, J. Chambers, A. Evangelista, B. Griffin, B. Iung, C. Otto, P. Pellikka and M. Quinones, "Echocardiographic assessment of valve stenosis: EAE/ASE recommendations for clinical practice," *European Journal of Echocardiography*, vol. 10, pp. 1-25, 2009.
- [79] D. Docheva, D. Padula, C. Popov, W. Mutschler, H. Clausen-Schaumann and M. Schieker, "Researching into the cellular shape, volume and elasticity of mesenchymal stem cells, osteoblasts and osteosarcoma cells by atomic force microscopy," *Journal of Cellular and Molecular Medicine*, vol. 12, no. 2, pp. 537-552, 2007.
- [80] S. Cross, Y. Jin, J. Rao and J. Gimzewski, "Nanomechanical analysis of cells from cancer patients," *Nat Nanotechnol*, vol. 2, no. 12, pp. 780-783, 2007.
- [81] A. Helmenstine, "Young's Modulus Formula and Example," Science Notes and Projects, 20 March 2022. [Online]. Available: <https://sciencenotes.org/youngs-modulus-formula-and-example/>. [Accessed 18 September 2022].
- [82] E. Moeendarbary and A. Harris, "Cell mechanics: principles, practices, and prospects," *Wiley Interdiscip Rev Syst Biol Med*, vol. 6, no. 5, pp. 371-388, 2014.
- [83] S. Kontomaris, A. Malamou and A. Stylianou, "The Hertzian theory in AFM nanoindentation experiments regarding biological samples: Overcoming limitations in data processing," *Micron*, vol. 155, p. 103228, 2022.
- [84] S. Ramaswamy, S. Boronyak, L. T. A. Holmes, F. Sotiropoulos and M. Sacks, "A Novel Bioreactor for Mechanobiological Studies of Engineered Heart Valve Tissue Formation Under Pulmonary Arterial Physiological Flow Conditions," *J Biomech Eng*, vol. 136, no. 12, p. 121009, 2014.
- [85] X. Wang, M. Ali and C. Lacerda, "A Three-Dimensional Collagen-Elastin Scaffold for Heart Valve Tissue Engineering," *Bioengineering (Basel)*, vol. 5, no. 3, 2018.
- [86] B. Gonzalez, M. Perez-Nevarez, A. Mirza, M. Gonzalez Perez, Y. Lin, C. Hsu, A. Caobi, A. Raymond, M. Gomez Hernandez, F. Fernandez-Lima, F. George and S. Ramaswamy, "Physiologically Relevant Fluid-Induced Oscillatory Shear Stress

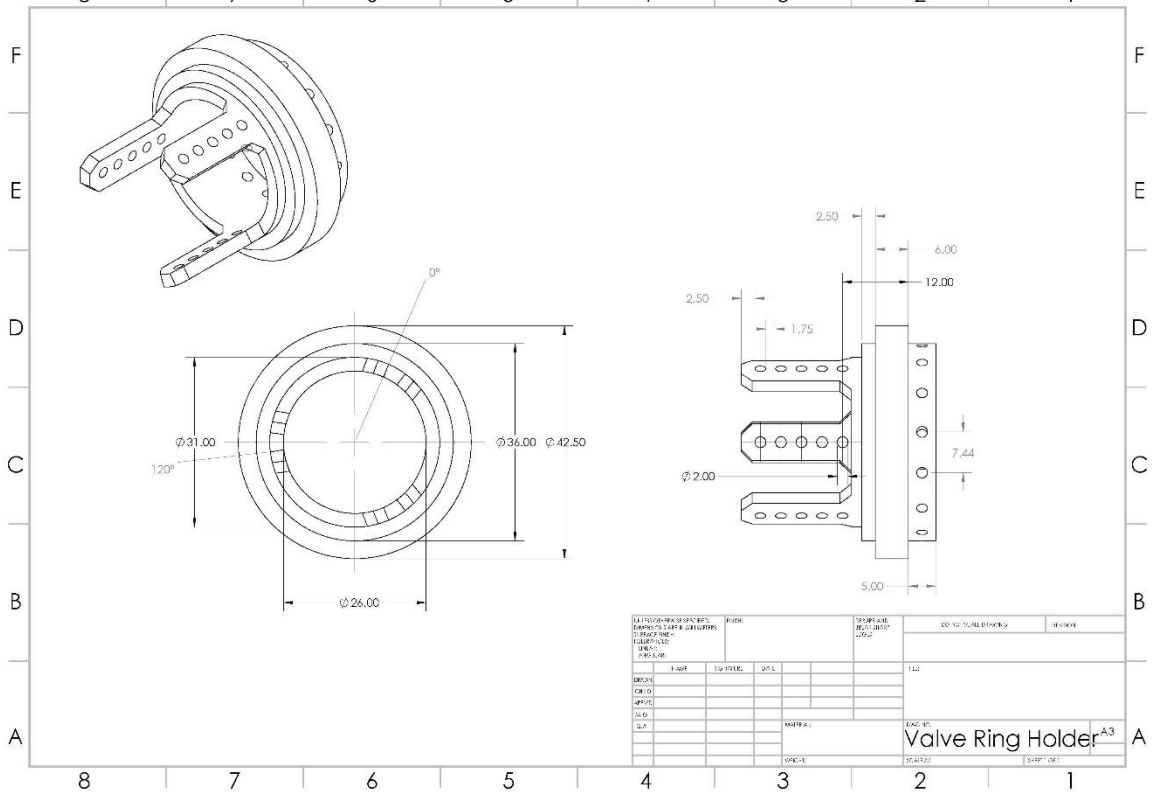
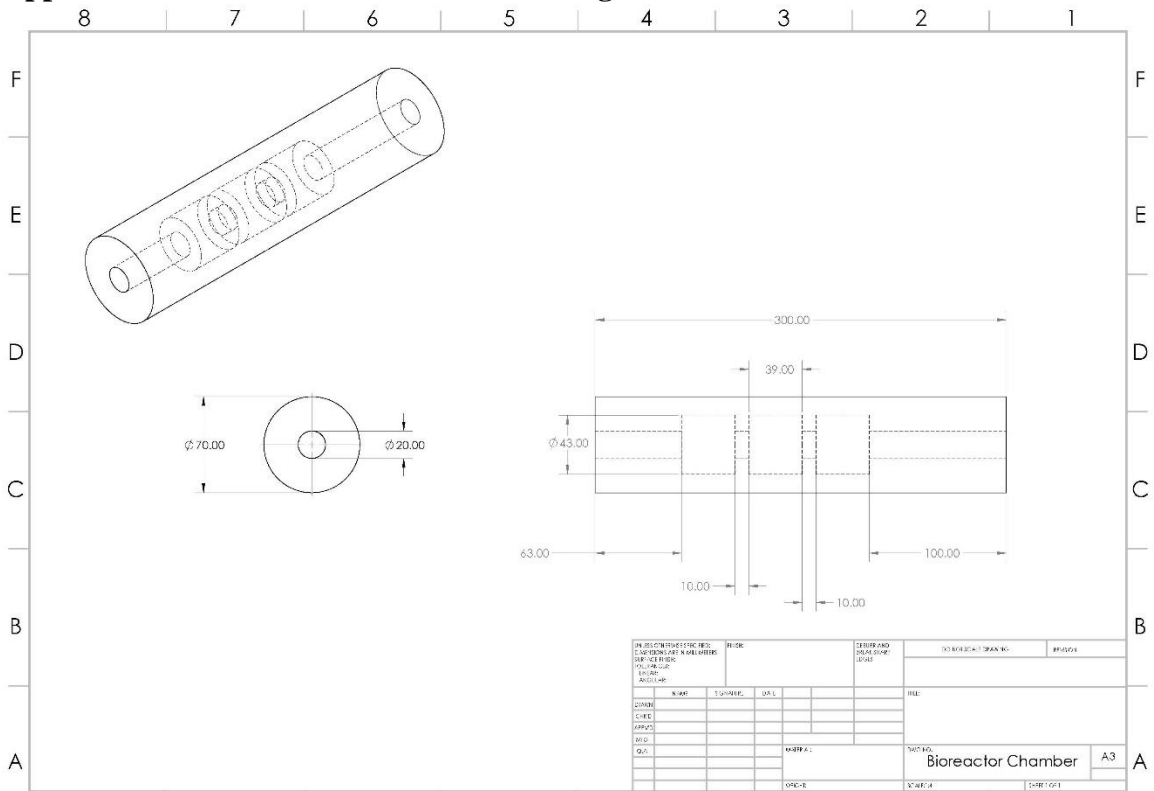
Stimulation of Mesenchymal Stem Cells Enhances the Engineered Valve Matrix Phenotype," *Front. Cardiovasc. Med.*, vol. 7, 2020.

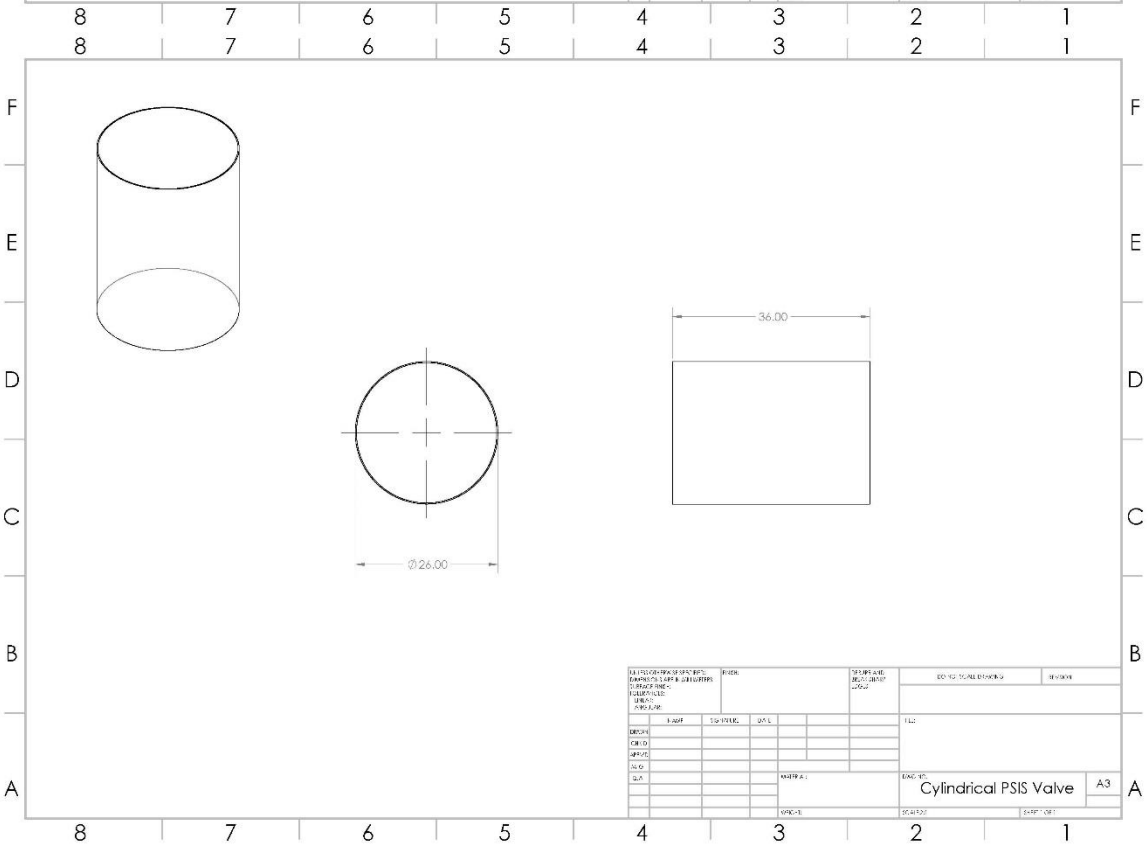
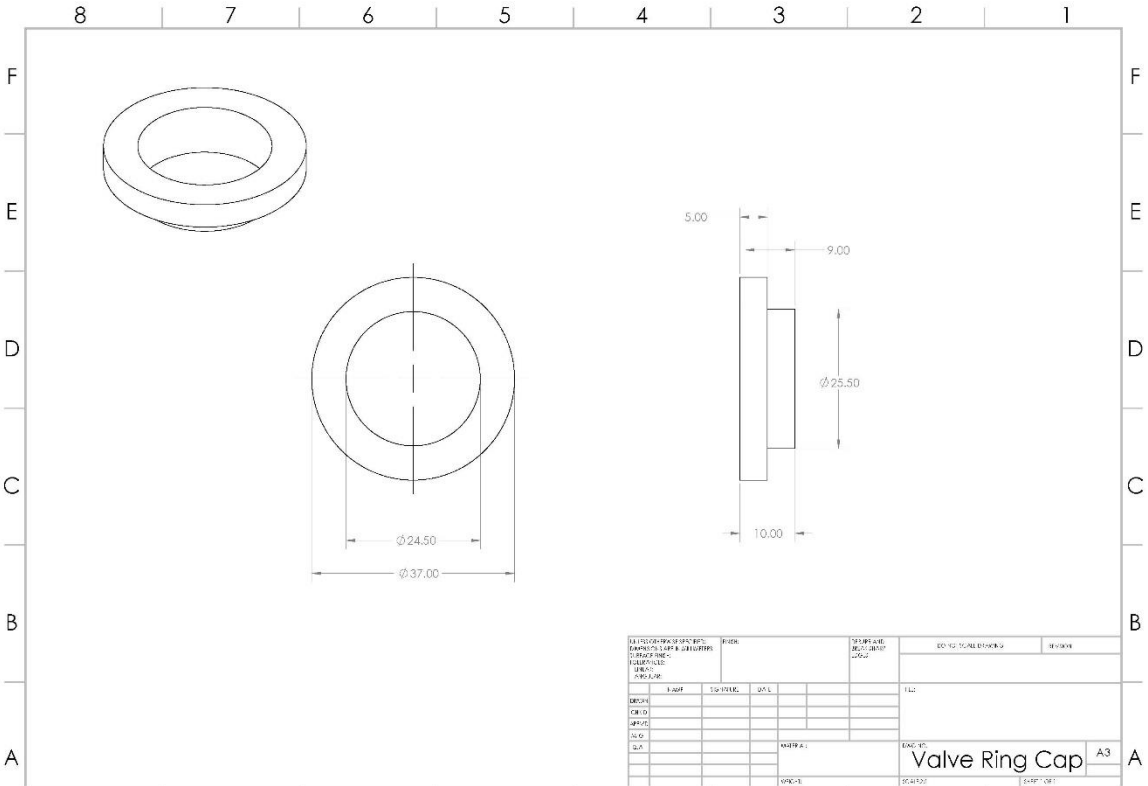
- [87] S. Kontomaris, "The Hertz Model in AFM Nanoindentation Experiments: Applications in Biological Samples and Biomaterials," *Micro and Nanosystems*, vol. 10, no. 1, pp. 11-22, 2018.
- [88] L. Pritschet, D. Powell and Z. Horne, "Marginally Significant Effects as Evidence for Hypothesis: Changing Attitudes Over Four Decades," *Psychological Science*, vol. 27, no. 7, 2016.
- [89] A. Olsson-Collentine, M. ALM Van Assen and C. Hartgerink, "The Prevalence of Marginally Significant Results in Psychology Over Time," *Psychol Sci*, vol. 30, no. 4, pp. 576-586, 2019.
- [90] E. Apostolakis and N. Baikoussis, "Methods of estimation of mitral valve regurgitation for the cardiac surgeon," *J Cardiothorac Surg*, vol. 4, no. 34, 2009.
- [91] A. Parnell and J. Swanevelder, "High transvalvular pressure gradients on intraoperative transesophageal echocardiography after aortic valve replacement: what does it mean?," *HSR Proc Intensive Care Cardiovasc Anesth*, vol. 1, no. 4, pp. 7-18, 2009.
- [92] A. Scott, L. Simon, H. Hutson, A. Porras and K. Masters, "Engineering the Aortic Valve Extracellular Matrix Through Stages of Development, Aging, and Disease," *J Mol Cell Cardiol.*, vol. 161, pp. 1-8, 2021.
- [93] S. Rathan and A. O. C. Yoganathan, "The role of inorganic pyrophosphate in aortic valve calcification," *The Journal of Heart Valve Disease*, vol. 23, no. 4, pp. 387-394, 2014.
- [94] A. Justiz Vaillant and A. Qurie, *Interleukin*, Treasure Island, FL: StatPearls Publishing, 2021.

APPENDICES

Digital copy of laboratory notebooks can be found here:
<https://www.denisehsu.com/PROJECTS/labnotebooks.html>
Dissertation video:
<https://youtu.be/Cl4DJN5Hwpc>

Appendix I: Bioreactor Mechanical Drawings





Appendix II: Bioreactor CFD Verification

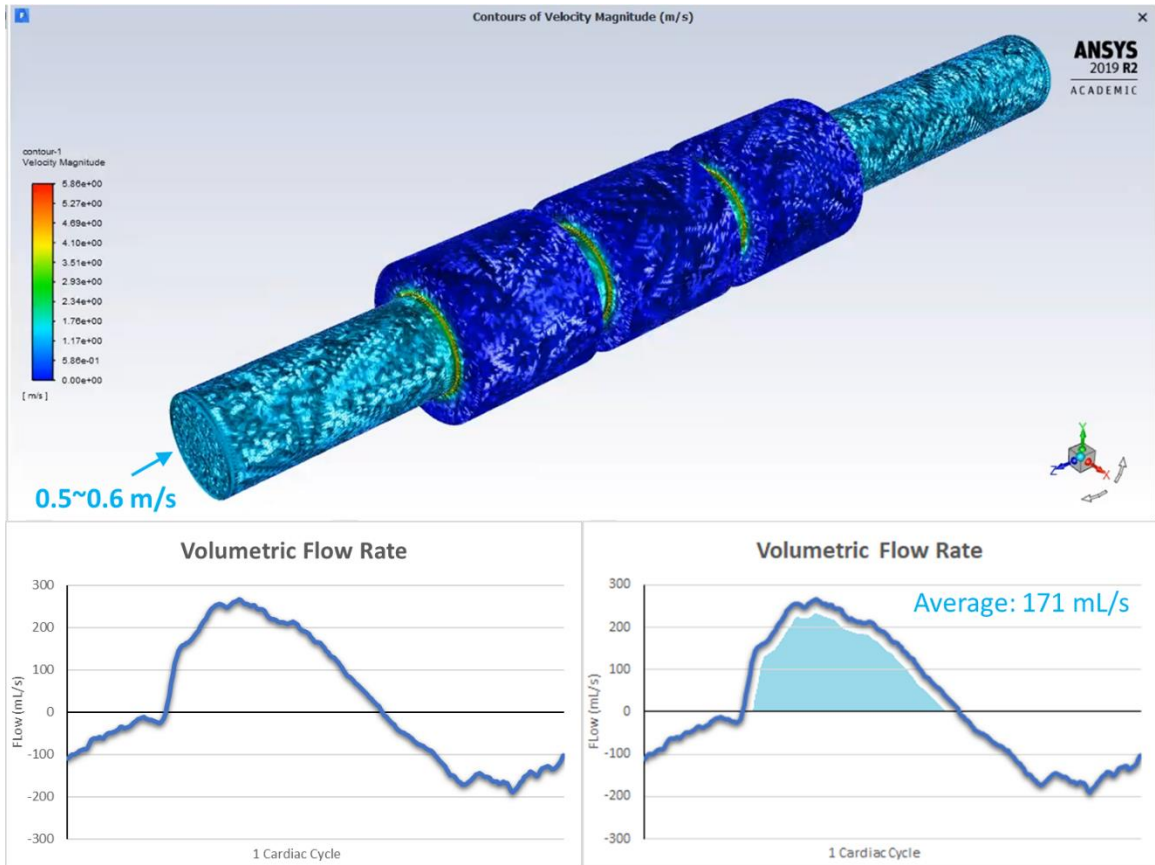


Figure 40. CFD velocity profile (top) and measured volumetric flow rate using Vivitro's magnetic flow probe (bottom)

Using the continuity and area equations,

$$Q = VA$$

$$A = \frac{\pi d^2}{4}$$

Where Q is volumetric flow rate in mL/s, V is flow velocity in m/s, and A is the outlet cross-sectional area (Appendix I) perpendicular to flow direction in m^2 , we estimated V to be approximately 0.5 ~ 0.6 m/s from the CFD diagram.

At 0.5 m/s,

$$\begin{aligned} Q &= VA = V * \frac{\pi d^2}{4} \\ &= 0.5 \frac{m}{s} * \frac{\pi * 0.02^2}{4} m^2 \\ &= 1.57 * 10^{-4} \frac{m^3}{s} = 157 \text{ mL/s} \end{aligned}$$

At 0.6 m/s,

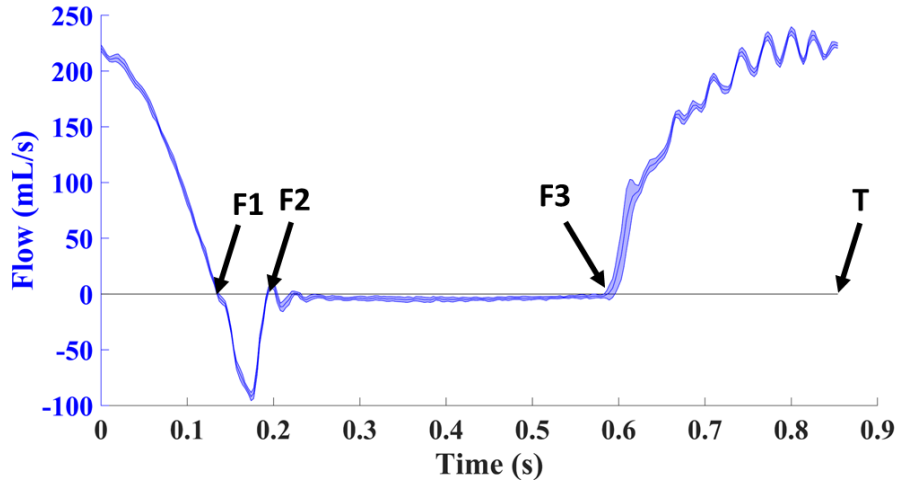
$$\begin{aligned} Q &= VA = V * \frac{\pi d^2}{4} \\ &= 0.6 \frac{m}{s} * \frac{\pi * 0.02^2}{4} m^2 \\ &= 1.88 * 10^{-4} \frac{m^3}{s} = 188 \text{ mL/s} \end{aligned}$$

CFD volumetric flow ranges between 157 mL/s and 188 mL/s. Measured result from flow probe was 171 mL/s, which lies within the CFD range.

Appendix III: Vivitro Pulse Duplicator Pressure/Flow Data and Statistical Analyses

Equations used to calculate hydrodynamic functionality:

Flow of One Cardiac Cycle



$$\text{Total Regurgitation} = 100 * \frac{\text{Closing Volume} + \text{Leakage Volume}}{\text{Forward Volume}}$$

$$\text{Closing Volume} = \int_{F1}^{F2} |\text{Flow}| dt$$

$$\text{Leakage Volume} = \int_{F2}^{F1} |\text{Flow}| dt$$

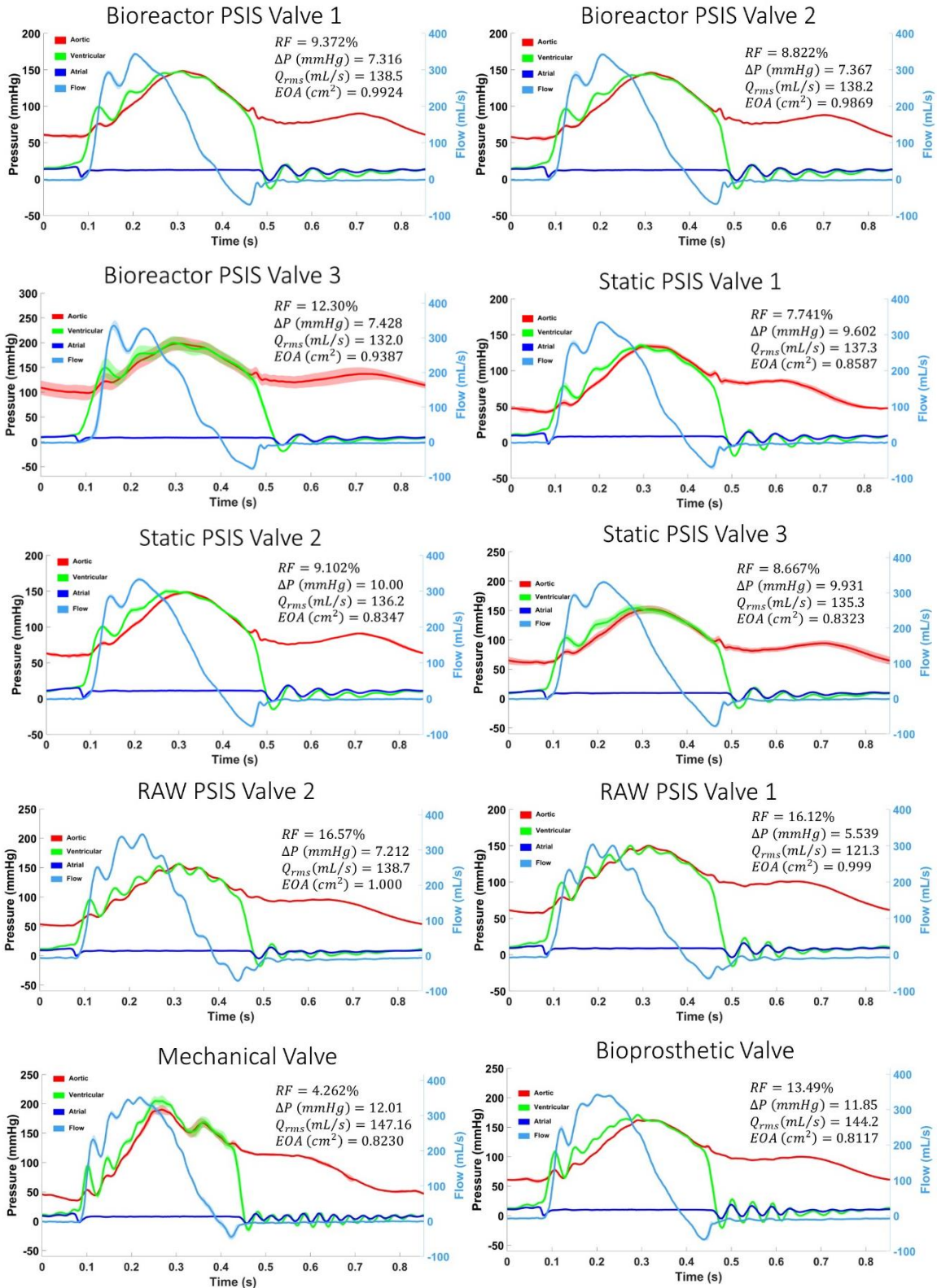
$$\text{Forward Volume} = \int_0^{F1} \text{Flow} dt + \int_{F3}^T \text{Flow} dt$$

$$\Delta P(\text{mmHg}) = \frac{1}{N} \left(\sum_{n=0}^{F1} \text{Pressure} + \sum_{n=F3}^T \text{Pressure} \right)$$

$$Q_{RMS} \left(\frac{\text{mL}}{\text{s}} \right) = \sqrt{\frac{\int_0^{F1} Q(t)^2 dt}{F1 - 0}} + \sqrt{\frac{\int_{F3}^T Q(t)^2 dt}{T - F3}}$$

$$E. O. A(\text{cm}^2) = \frac{Q_{RMS}}{51.6\sqrt{\Delta P}}$$

Pressure and flow curves per cardiac cycle:



Multiple Comparisons

Dependent Variable: Regurgitation_Factor

Tukey HSD

(I) Groups	(J) Groups	Mean Difference (I-J)	Std. Error	Sig.	95% Confidence Interval	
					Lower Bound	Upper Bound
Mechanical	Bioprosthetic	-9.228000*	.736563	.00000152	-11.65209	-6.80391
	RawPSIS	-12.198000*	.736563	.00000011	-14.62209	-9.77391
	StaticPSIS	-4.241333*	.736563	.00133100	-6.66542	-1.81725
	BioreactorPSIS	-5.902667*	.736563	.00008811	-8.32675	-3.47858
Bioprosthetic	Mechanical	9.228000*	.736563	.00000152	6.80391	11.65209
	RawPSIS	-2.970000*	.736563	.01590712	-5.39409	-.54591
	StaticPSIS	4.986667*	.736563	.00036656	2.56258	7.41075
	BioreactorPSIS	3.325333*	.736563	.00769383	.90125	5.74942
RawPSIS	Mechanical	12.198000*	.736563	.00000011	9.77391	14.62209
	Bioprosthetic	2.970000*	.736563	.01590712	.54591	5.39409
	StaticPSIS	7.956667*	.736563	.00000606	5.53258	10.38075
	BioreactorPSIS	6.295333*	.736563	.00005018	3.87125	8.71942
StaticPSIS	Mechanical	4.241333*	.736563	.00133100	1.81725	6.66542
	Bioprosthetic	-4.986667*	.736563	.00036656	-7.41075	-2.56258
	RawPSIS	-7.956667*	.736563	.00000606	-10.38075	-5.53258
	BioreactorPSIS	-1.661333	.736563	.23575179	-4.08542	.76275
BioreactorPSIS	Mechanical	5.902667*	.736563	.00008811	3.47858	8.32675
	Bioprosthetic	-3.325333*	.736563	.00769383	-5.74942	-.90125
	RawPSIS	-6.295333*	.736563	.00005018	-8.71942	-3.87125
	StaticPSIS	1.661333	.736563	.23575179	-.76275	4.08542

*. The mean difference is significant at the 0.05 level.

Multiple Comparisons

Dependent Variable: DeltaP

Tukey HSD

(I) Groups	(J) Groups	Mean Difference (I-J)	Std. Error	Sig.	95% Confidence Interval	
					Lower Bound	Upper Bound
Mechanical	Bioprosthetic	.160000	.389069	.99302428	-1.12046	1.44046
	RawPSIS	5.275333*	.389069	.00000072	3.99487	6.55579
	StaticPSIS	2.165667*	.389069	.00172399	.88521	3.44613
	BioreactorPSIS	4.639667*	.389069	.00000242	3.35921	5.92013
Bioprosthetic	Mechanical	-.160000	.389069	.99302428	-1.44046	1.12046
	RawPSIS	5.115333*	.389069	.00000096	3.83487	6.39579
	StaticPSIS	2.005667*	.389069	.00304639	.72521	3.28613
	BioreactorPSIS	4.479667*	.389069	.00000335	3.19921	5.76013
RawPSIS	Mechanical	-5.275333*	.389069	.00000072	-6.55579	-3.99487
	Bioprosthetic	-5.115333*	.389069	.00000096	-6.39579	-3.83487
	StaticPSIS	-3.109667*	.389069	.00009016	-4.39013	-1.82921
	BioreactorPSIS	-.635667	.389069	.51041802	-1.91613	.64479
StaticPSIS	Mechanical	-2.165667*	.389069	.00172399	-3.44613	-.88521
	Bioprosthetic	-2.005667*	.389069	.00304639	-3.28613	-.72521
	RawPSIS	3.109667*	.389069	.00009016	1.82921	4.39013
	BioreactorPSIS	2.474000*	.389069	.00061014	1.19354	3.75446
BioreactorPSIS	Mechanical	-4.639667*	.389069	.00000242	-5.92013	-3.35921
	Bioprosthetic	-4.479667*	.389069	.00000335	-5.76013	-3.19921
	RawPSIS	.635667	.389069	.51041802	-.64479	1.91613
	StaticPSIS	-2.474000*	.389069	.00061014	-3.75446	-1.19354

*. The mean difference is significant at the 0.05 level.

Multiple Comparisons

Dependent Variable: Qrms

Tukey HSD

(I) Groups	(J) Groups	Mean Difference (I-J)	Std. Error	Sig.	95% Confidence Interval	
					Lower Bound	Upper Bound
Mechanical	Bioprosthetic	2.96000	3.51690	.91135616	-8.6144	14.5344
	RawPSIS	17.61000*	3.51690	.00375673	6.0356	29.1844
	StaticPSIS	10.89333	3.51690	.06749163	-.6811	22.4677
	BioreactorPSIS	10.92667	3.51690	.06651058	-.6477	22.5011
Bioprosthetic	Mechanical	-2.96000	3.51690	.91135616	-14.5344	8.6144
	RawPSIS	14.65000*	3.51690	.01298618	3.0756	26.2244
	StaticPSIS	7.93333	3.51690	.23566856	-3.6411	19.5077
	BioreactorPSIS	7.96667	3.51690	.23258931	-3.6077	19.5411
RawPSIS	Mechanical	-17.61000*	3.51690	.00375673	-29.1844	-6.0356
	Bioprosthetic	-14.65000*	3.51690	.01298618	-26.2244	-3.0756
	StaticPSIS	-6.71667	3.51690	.37142019	-18.2911	4.8577
	BioreactorPSIS	-6.68333	3.51690	.37577817	-18.2577	4.8911
StaticPSIS	Mechanical	-10.89333	3.51690	.06749163	-22.4677	.6811
	Bioprosthetic	-7.93333	3.51690	.23566856	-19.5077	3.6411
	RawPSIS	6.71667	3.51690	.37142019	-4.8577	18.2911
	BioreactorPSIS	.03333	3.51690	1.00000000	-11.5411	11.6077
BioreactorPSIS	Mechanical	-10.92667	3.51690	.06651058	-22.5011	.6477
	Bioprosthetic	-7.96667	3.51690	.23258931	-19.5411	3.6077
	RawPSIS	6.68333	3.51690	.37577817	-4.8911	18.2577
	StaticPSIS	-.03333	3.51690	1.00000000	-11.6077	11.5411

*. The mean difference is significant at the 0.05 level.

Multiple Comparisons

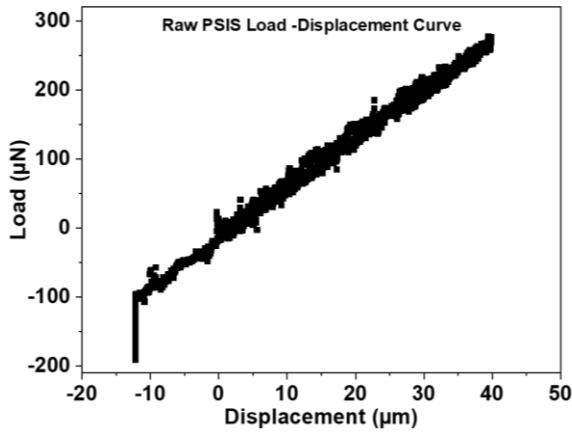
Dependent Variable: EOA

Tukey HSD

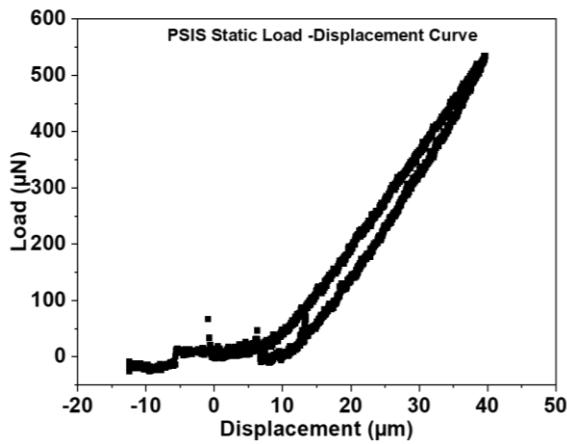
(I) Groups	(J) Groups	Mean Difference (I-J)	Std. Error	Sig.	95% Confidence Interval	
					Lower Bound	Upper Bound
Mechanical	Bioprosthetic	.0113000	.0145891	.93234068	-.036714	.059314
	RawPSIS	-.1866667*	.0145891	.00000125	-.234681	-.138653
	StaticPSIS	-.0189000	.0145891	.69980191	-.066914	.029114
	BioreactorPSIS	-.1496667*	.0145891	.00000973	-.197681	-.101653
Bioprosthetic	Mechanical	-.0113000	.0145891	.93234068	-.059314	.036714
	RawPSIS	-.1979667*	.0145891	.00000072	-.245981	-.149953
	StaticPSIS	-.0302000	.0145891	.30285581	-.078214	.017814
	BioreactorPSIS	-.1609667*	.0145891	.00000498	-.208981	-.112953
RawPSIS	Mechanical	.1866667*	.0145891	.00000125	.138653	.234681
	Bioprosthetic	.1979667*	.0145891	.00000072	.149953	.245981
	StaticPSIS	.1677667*	.0145891	.00000339	.119753	.215781
	BioreactorPSIS	.0370000	.0145891	.15785681	-.011014	.085014
StaticPSIS	Mechanical	.0189000	.0145891	.69980191	-.029114	.066914
	Bioprosthetic	.0302000	.0145891	.30285581	-.017814	.078214
	RawPSIS	-.1677667*	.0145891	.00000339	-.215781	-.119753
	BioreactorPSIS	-.1307667*	.0145891	.00003293	-.178781	-.082753
BioreactorPSIS	Mechanical	.1496667*	.0145891	.00000973	.101653	.197681
	Bioprosthetic	.1609667*	.0145891	.00000498	.112953	.208981
	RawPSIS	-.0370000	.0145891	.15785681	-.085014	.011014
	StaticPSIS	.1307667*	.0145891	.00003293	.082753	.178781

*. The mean difference is significant at the 0.05 level.

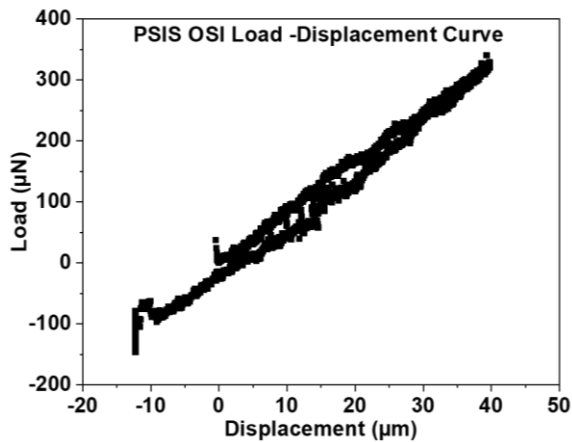
Appendix IV: Mechanical Nanoindentation



Sample A	Young's modulus (kPa)
1	57.57
	58.52
2	49.27
	54.87
3	54.08
	56.28
Average	55.10 ± 3.29



Sample A	Young's modulus (kPa)
1	74.63
	81.86
2	92.21
	91.9
3	81.79
	86.33
Average	84.79 ± 6.76



Sample A	Young's modulus (kPa)
1	66.51
	63.69
2	61.56
	59.3
3	57.68
	61.56
Average	61.72 ± 3.13

Appendix V: ARS Images and Quantification

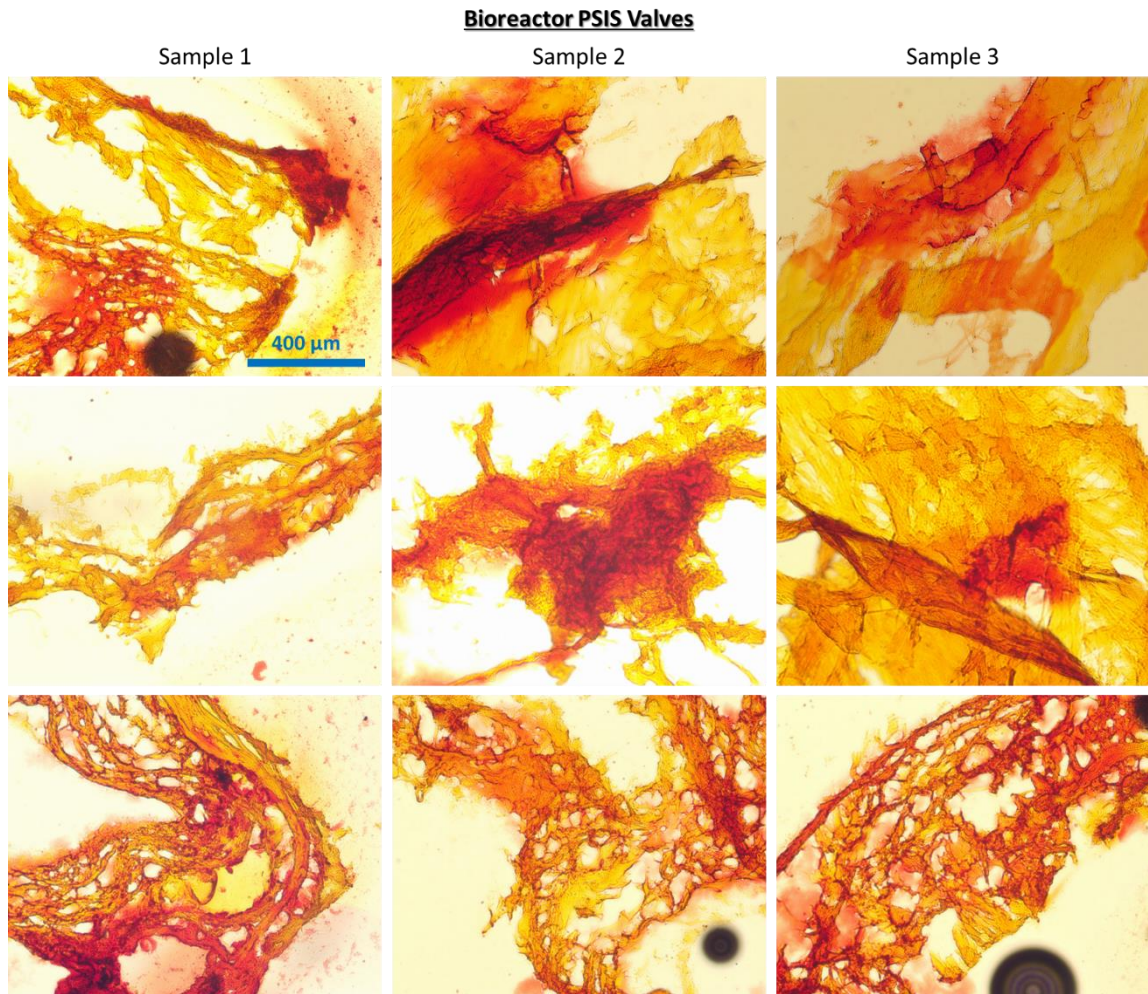


Figure 41. ARS images of bioreactor-conditioned valves. VECs and VICs were seeded in PSIS and conditioned at 0.50 OSI with PC media for 7 days.

Table 4. ARS Quantification - Bioreactor Conditioned Samples

Bioreactor Calcification Quantification (AU)		
Sample 1	Sample 2	Sample 3
0.4243	0.3118	0.4071
0.5694	0.4455	0.4169
0.4163	0.4526	0.3836

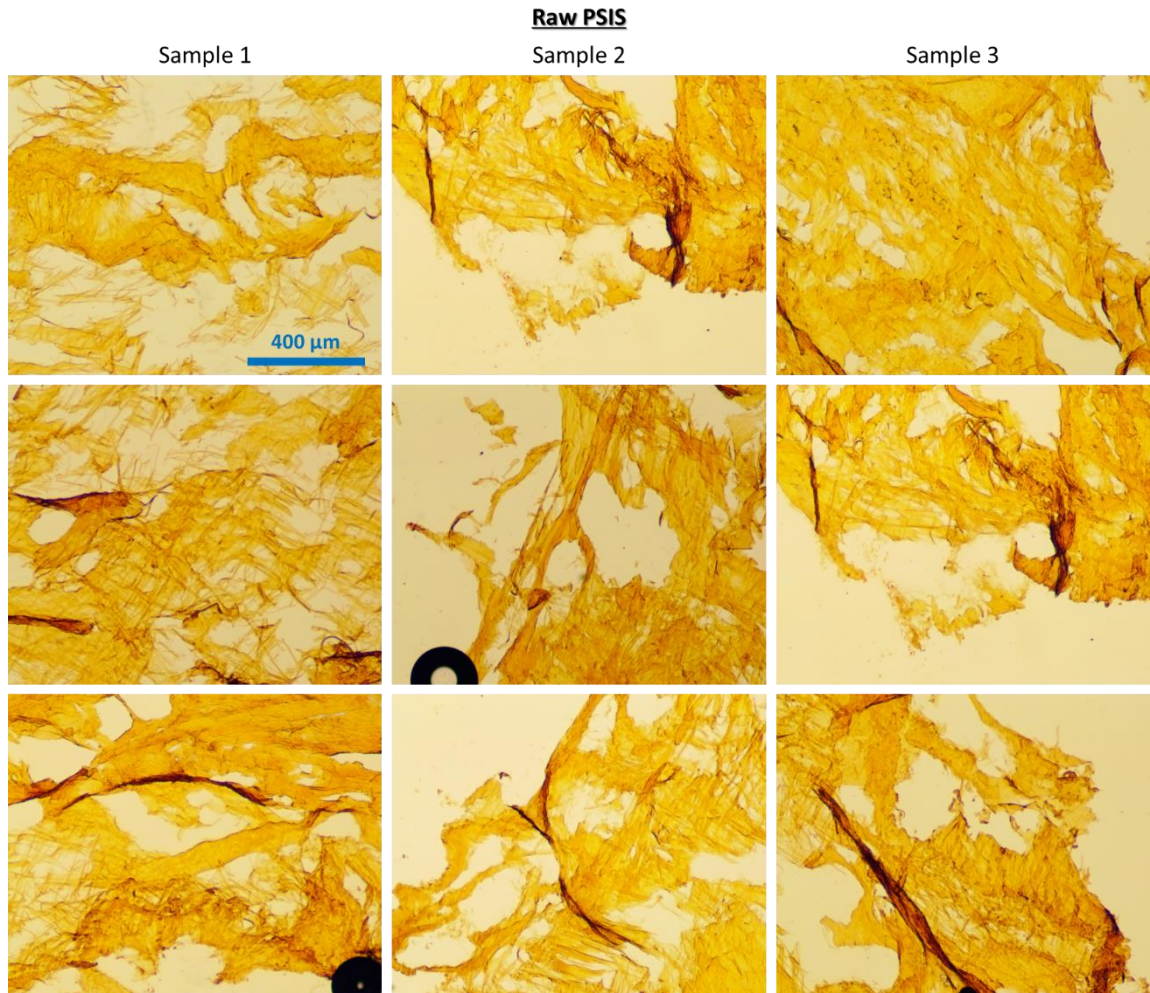


Figure 42. ARS images of raw PSIS.

Table 5. ARS Quantification - Raw PSIS Samples

Raw PSIS Calcification Quantification (AU)		
Sample 1	Sample 2	Sample 3
0	0	0
0	0	0
0	0	0

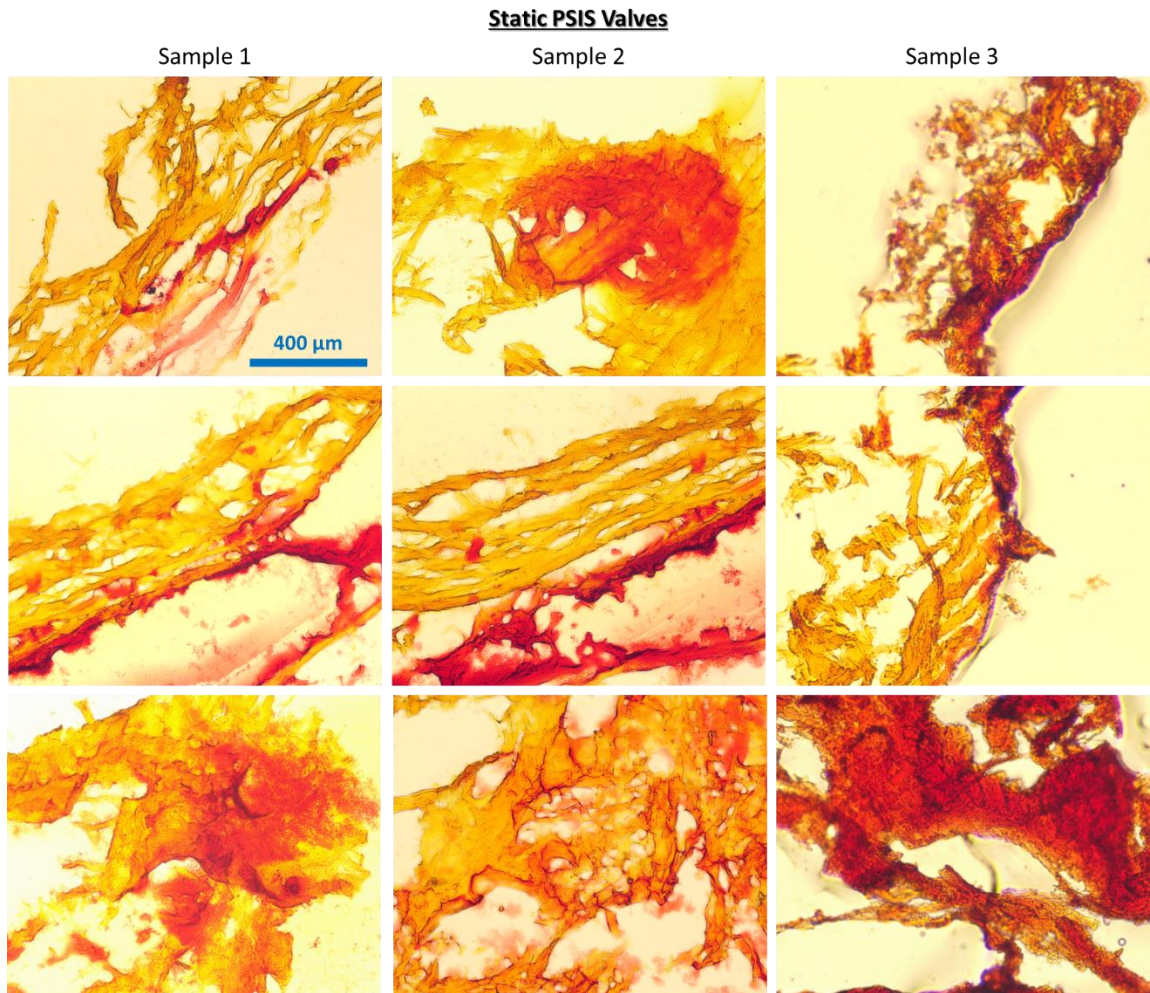
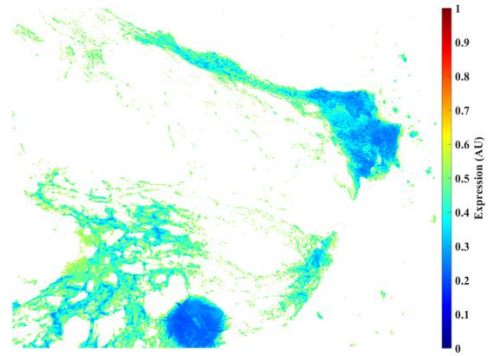
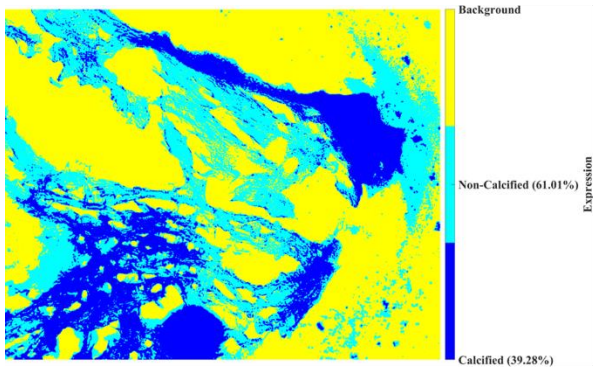


Figure 43. ARS images of statically conditioned valves. VECs and VICs were seeded in PSIS and placed in static environment with PC media for 7 days.

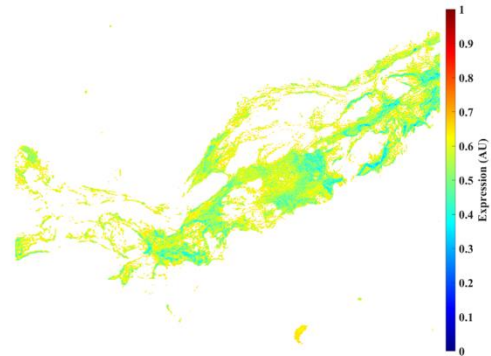
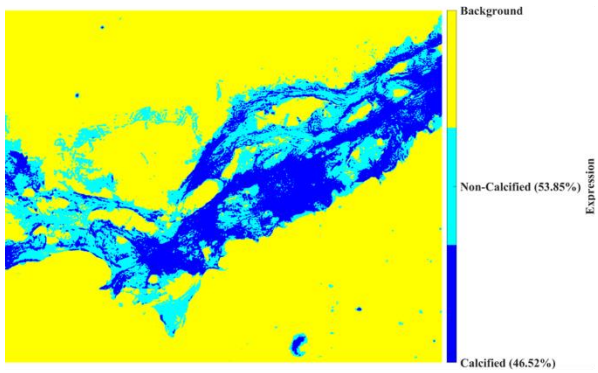
Table 6. ARS Quantification - Static Conditioned Samples

Static Calcification Quantification (AU)		
Sample 1	Sample 2	Sample 3
0.3681	0.4670	0.3109
0.3433	0.2904	0.3357
0.5000	0.3715	0.3165

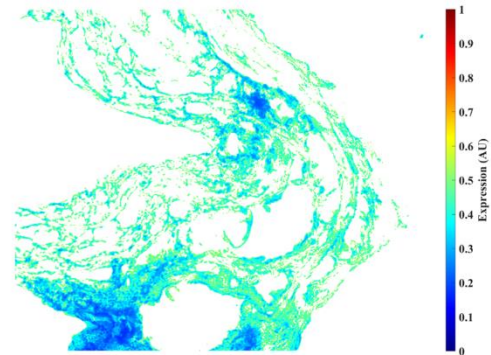
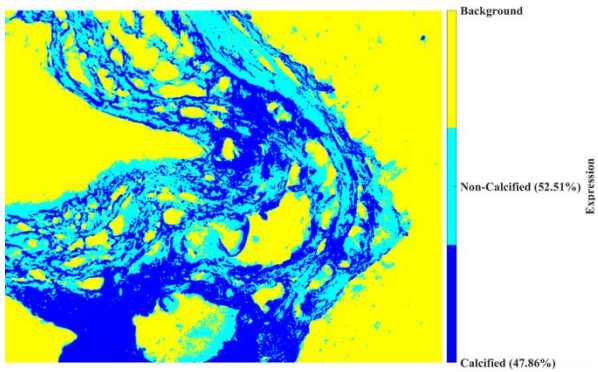
Bioreactor Sample 1



Calcified Intensity : 0.4243 +/- 0.0973 AU

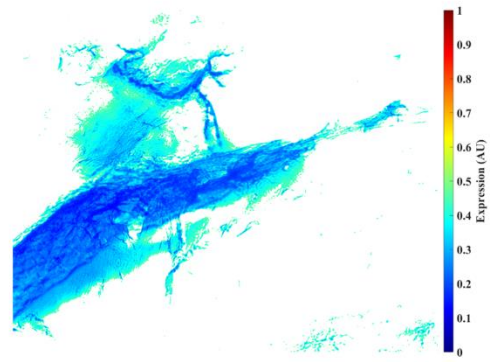
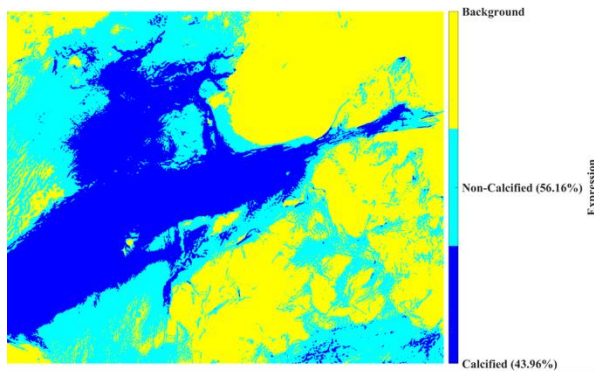


Calcified Intensity : 0.5694 +/- 0.0684 AU

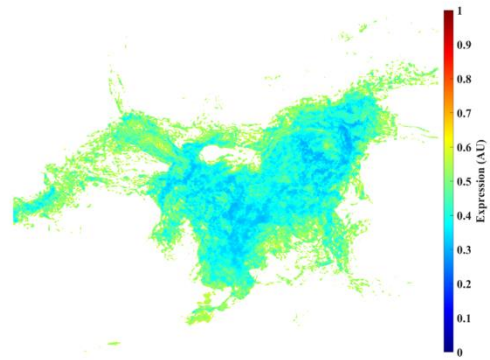
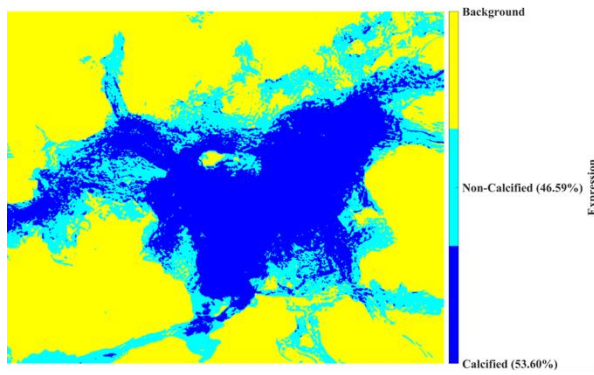


Calcified Intensity : 0.4163 +/- 0.0805 AU

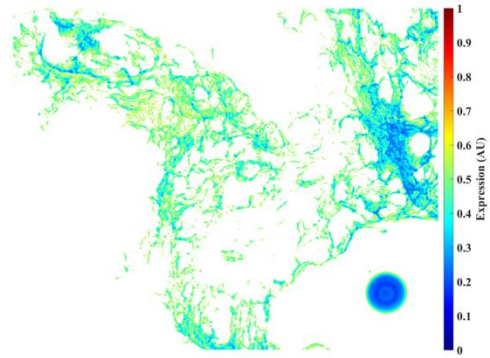
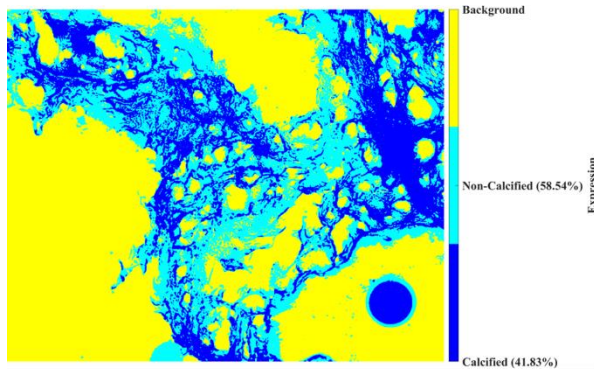
Bioreactor Sample 2



Calcified Intensity : 0.3118 +/- 0.0878 AU

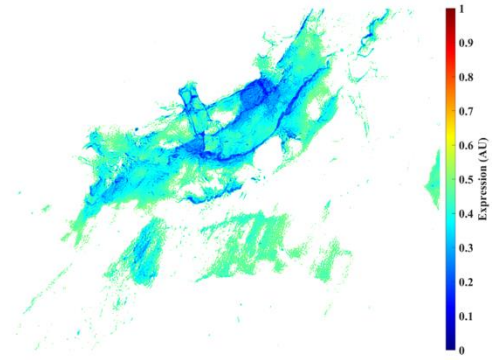
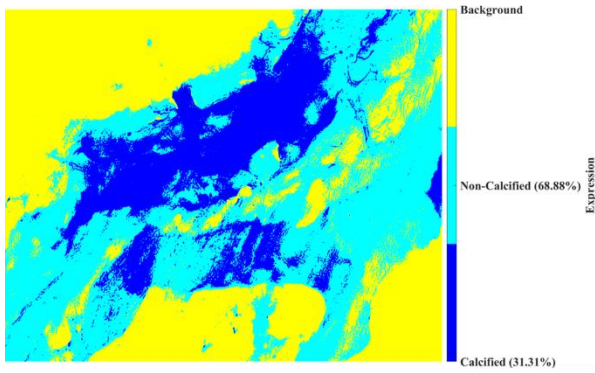


Calcified Intensity : 0.4455 +/- 0.0756 AU

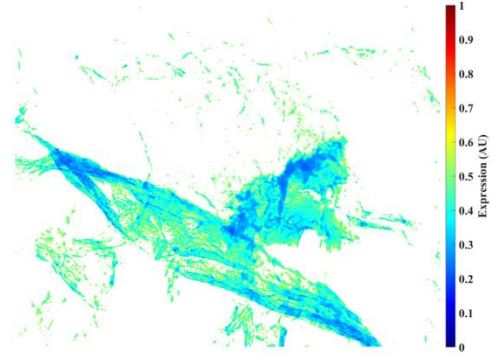
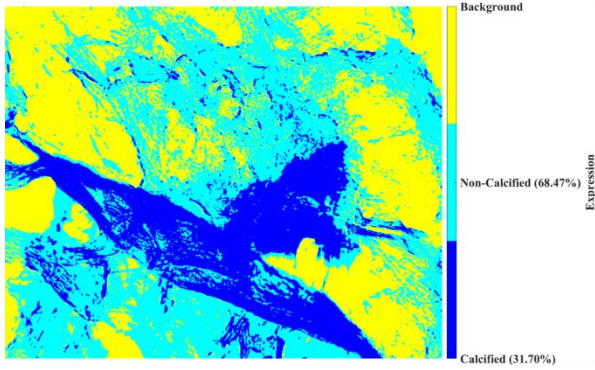


Calcified Intensity : 0.4526 +/- 0.0927 AU

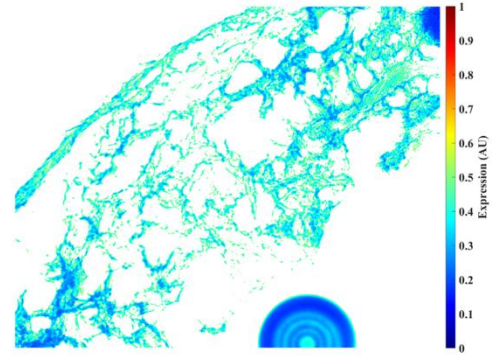
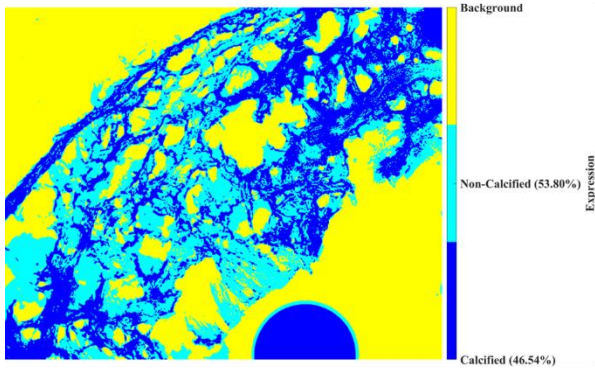
Bioreactor Sample 3



Calcified Intensity : 0.4071 +/- 0.0785 AU

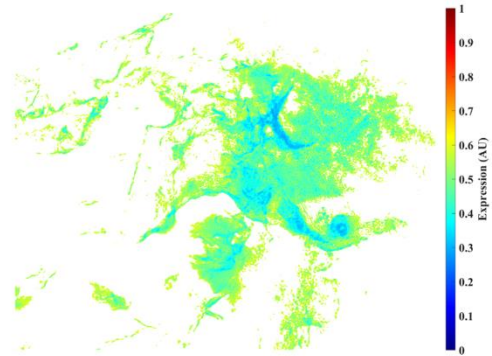
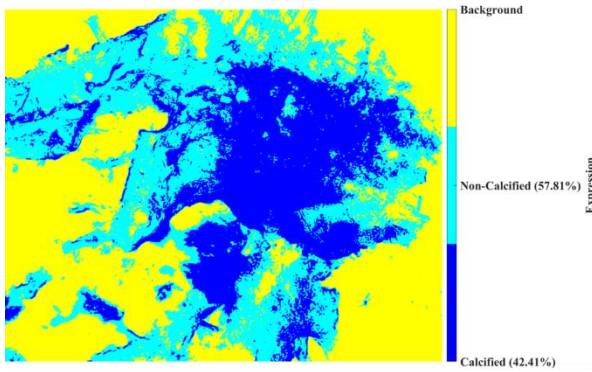
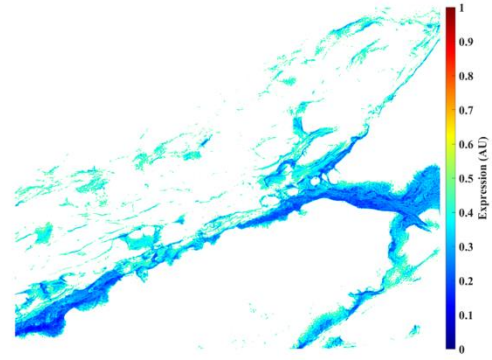
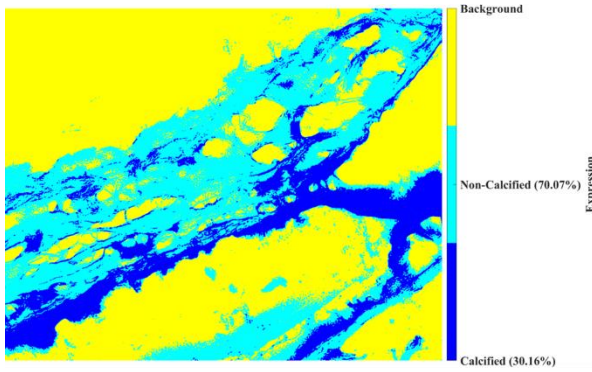
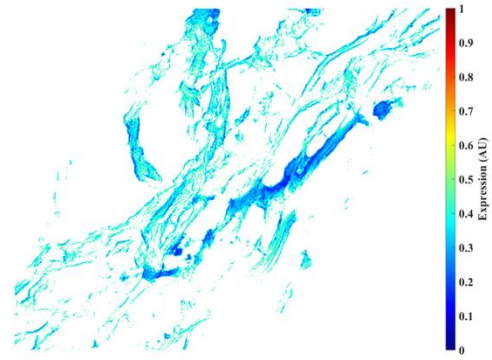
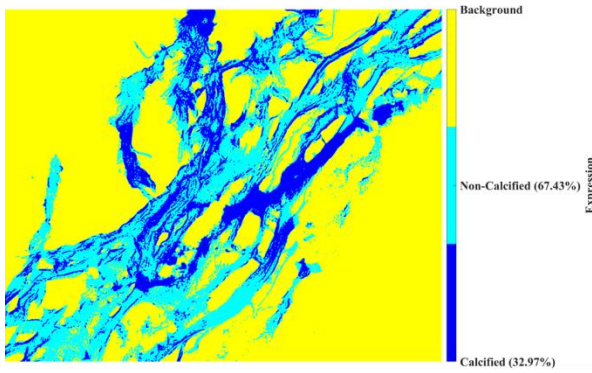


Calcified Intensity : 0.4169 +/- 0.0793 AU

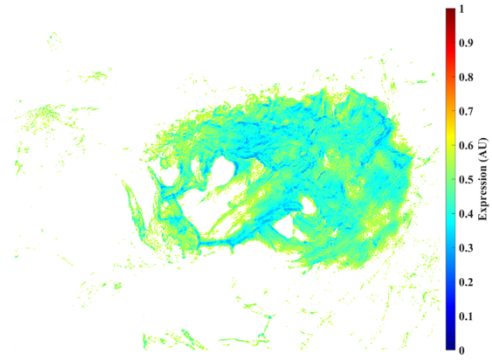
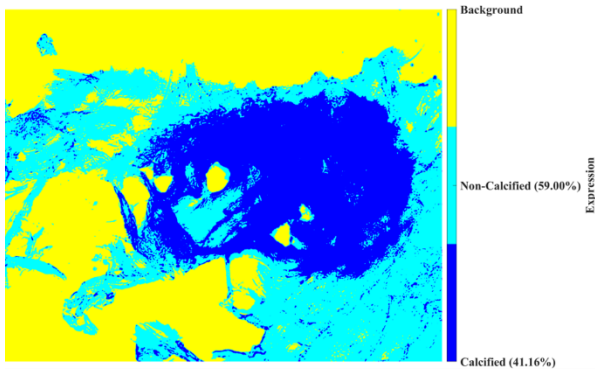


Calcified Intensity : 0.3836 +/- 0.0831 AU

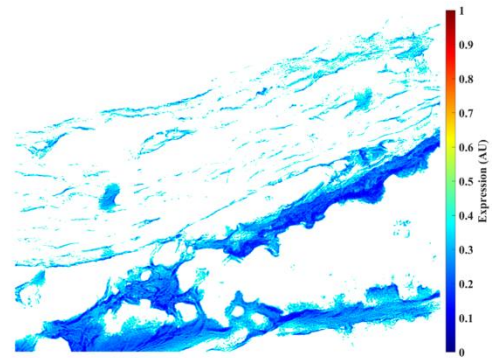
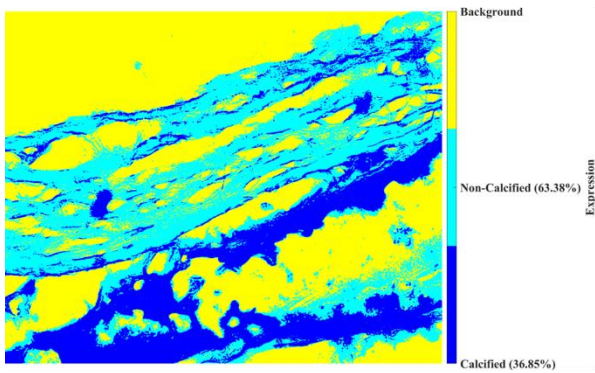
Static Sample 1



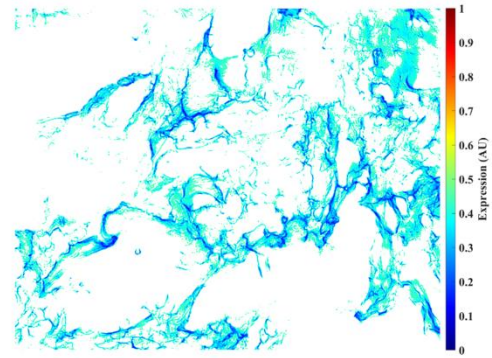
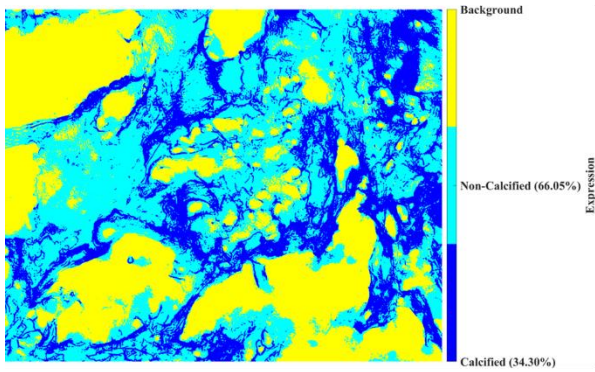
Static Sample 2



Calcified Intensity : 0.4670 +/- 0.0711 AU

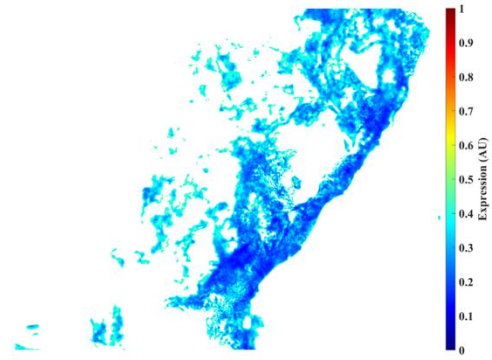
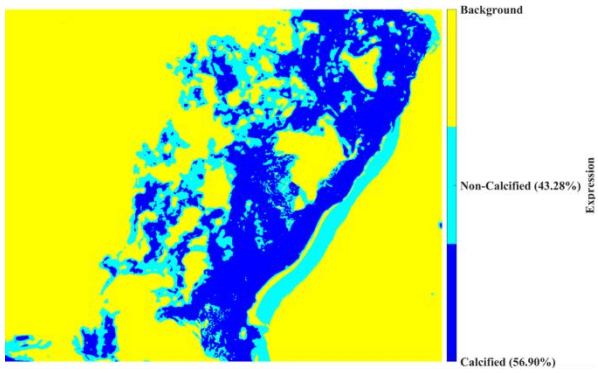


Calcified Intensity : 0.2904 +/- 0.0772 AU

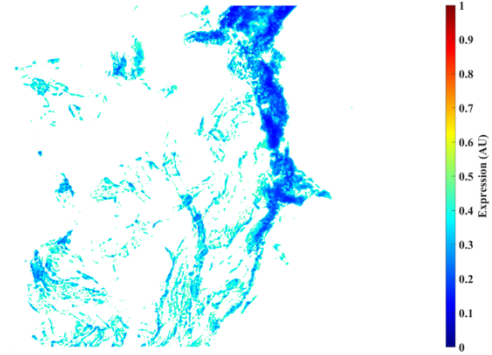
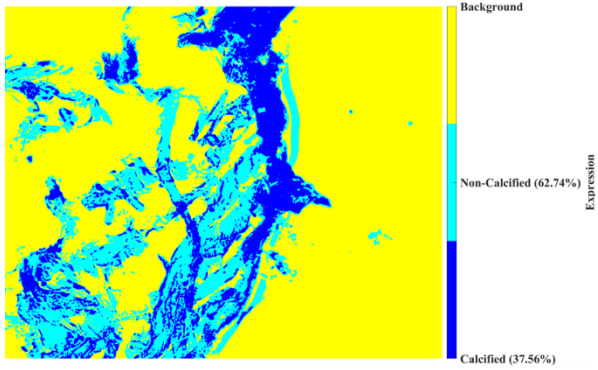


Calcified Intensity : 0.3715 +/- 0.0725 AU

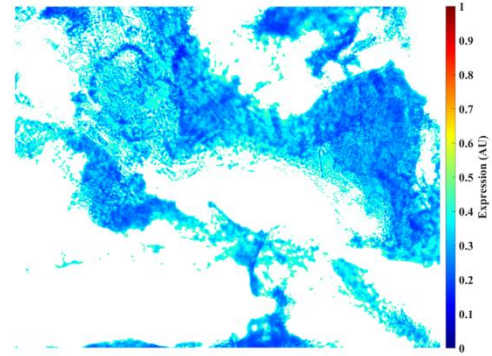
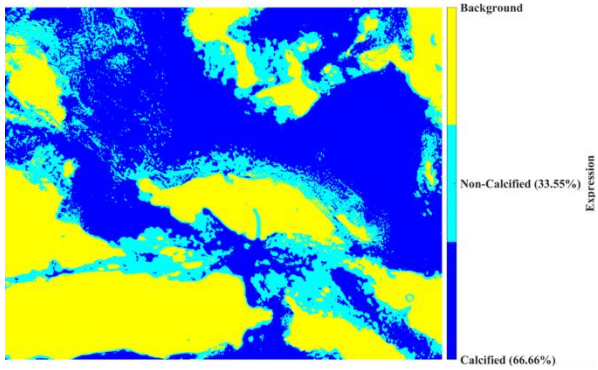
Static Sample 3



Calcified Intensity : 0.3109 +/- 0.0763 AU



Calcified Intensity : 0.3357 +/- 0.0869 AU



Calcified Intensity : 0.3165 +/- 0.0657 AU

Appendix VI: Immunofluorescent Stains

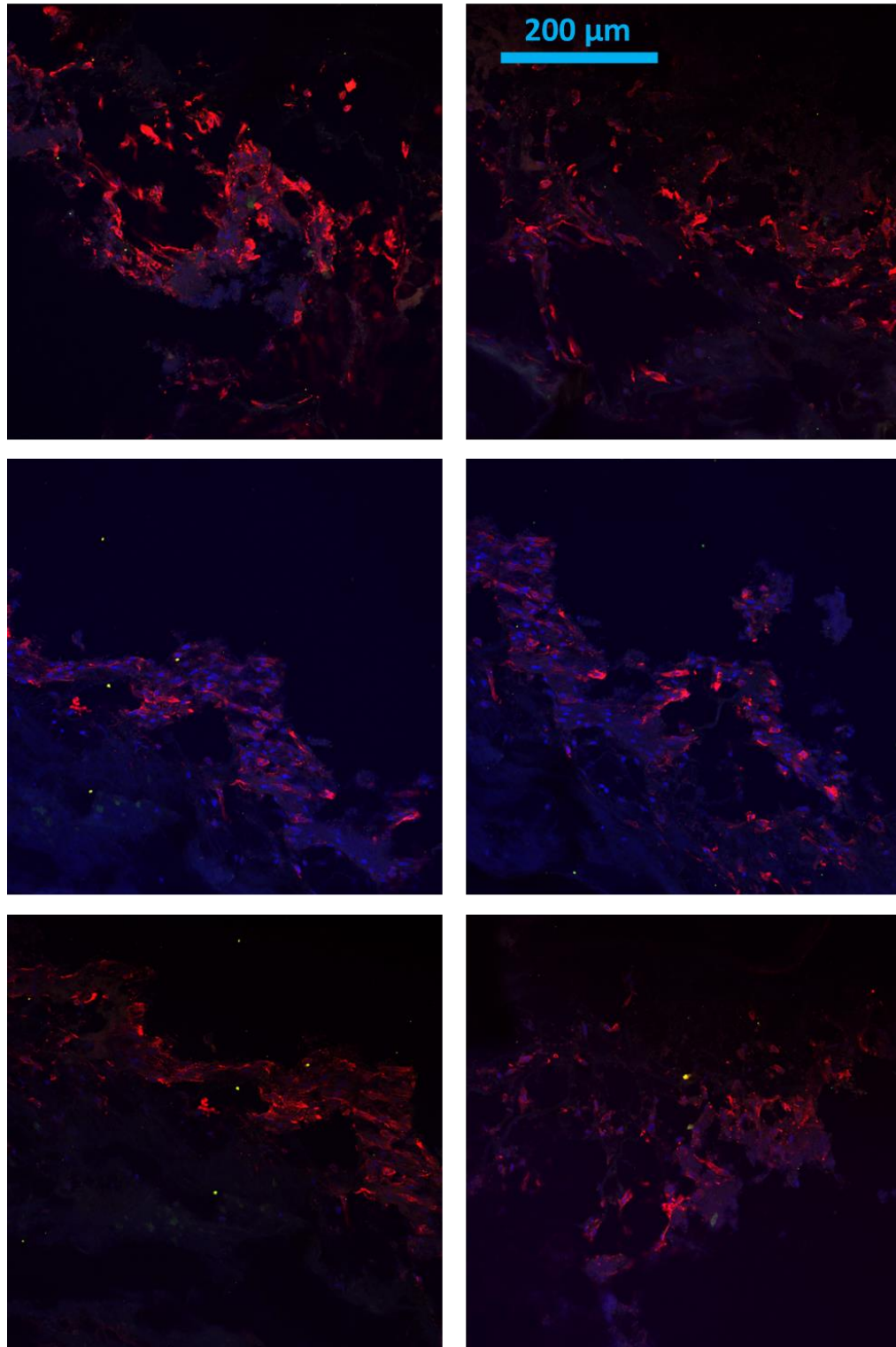


Figure 44. CD31 (green) and aSMA (red) immunofluorescent stains after conditioning in bioreactor with co-culture of VECs and VICs

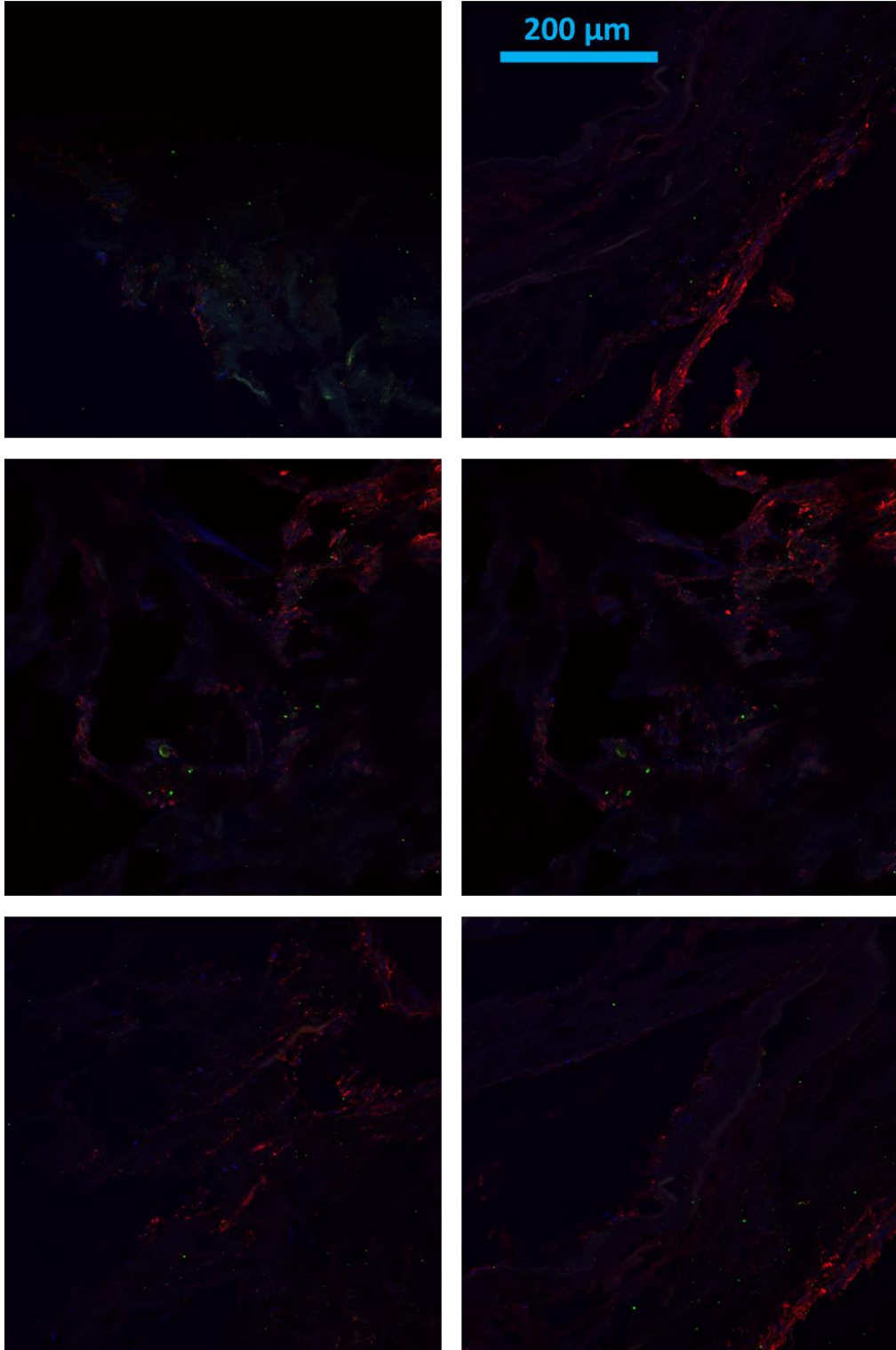


Figure 45. CD31 (green) and α SMA (red) immunofluorescent stains after conditioning in static with co-culture of VECs and VICs

MATLAB Code for immunofluorescent z-stack quantification
(Normalized to total tissue area):

```

%{
    Quantifying Normalized Tissue Code

    Originally By: Daniel Chaparro
    Edited By: Denise Hsu
    Further Edits By: Asad Mirza

    Last Updated On: 10/13/2022
%}
clear,clc,close all force
% Grab folder path of interest where image stacks are located
folder_path=uigetdir;
if folder_path==0
    error('Folder Not Selected, Stopping Code')
end
% Go into that folder
cd(folder_path)
% Grab all files that end in .nd2
f_all = dir('*.nd2');
%% Process Images

% Load neural network for denoising
if ~exist('net','var')
    try
        net = denoisingNetwork('DnCNN');
        net_loaded=1;
    catch
        net_loaded=0;
    end
end
% For each image found
full_loop=tic;
for ii = 1:length(f_all)
    image_loop=tic;
    % Grab the file name
    f=f_all(ii);
    % Parse the file name parts
    [filepath,name,ext] = fileparts(f.name);
    % Use BioFormats toolbox's bfoopen to open the image and access its data
    main = bfoopen([f.folder,'\',f.name]);
    chan = 3; % Number of channels images
    slices = size(main{1},1)/chan; % Number of slices in each image
    pix = 0.6215; %Microns per pixel
    pixz = 1.777; %Microns per Zstack
    % For each slice in the image file
    for n = 1:slices %slice number
        slice_loop=tic;
        fprintf('Processing Slice %1.0f out of %1.0f of Image %1.0f titled
%s\n',n,slices,ii,name)
        %----Indexing the channels from the main matrix----%
    end
end
end

```

```

rs = n*chan;    %red channel (asma)
gs = n*chan-1; %green channel (cd31)
bs = n*chan-2; %blue channel (DAPI)
%----Extracts channels from each slice of each image----%
imr{n} = main{1,1}{rs,1};
img{n} = main{1,1}{gs,1};
imb{n} = main {1,1}{bs,1};
%----Find only the area expressed by the molecule and exclude
%the non tissue portion of the image

% Locally brighten the image
denoisedimr = imlocalbrighten(imr{n});
if net_loaded
    % Apply neural network to image if the net is loaded
    denoisedimr = denoiseImage(denoisedimr,net);
end
% Apply median filter
denoisedimr = medfilt2(denoisedimr,[3 3]);
% Convert image from uint16 to uint8
denoisedimr = uint8(255*mat2gray(denoisedimr));
% Adjust contrast
denoisedimr = imadjust(denoisedimr);
% Threshold image - manual threshold
BW = denoisedimr > 15;
% Active contour
iterations = 100;
BW = activecontour(denoisedimr, BW, iterations, 'edge');
imr_filt{n}=imr{n}.*uint16(BW);

% Locally brighten the image
denoisedimg = imlocalbrighten(img{n});
if net_loaded
    % Apply neural network to image if the net is loaded
    denoisedimg = denoiseImage(denoisedimg,net);
end
% Apply median filter
denoisedimg = medfilt2(denoisedimg,[3 3]);
% Convert image from uint16 to uint8
denoisedimg = uint8(255*mat2gray(denoisedimg));
% Adjust contrast
denoisedimg = imadjust(denoisedimg);
% Threshold image - manual threshold
BW = denoisedimg > 15;
% Active contour
iterations = 100;
BW = activecontour(denoisedimg, BW, iterations, 'edge');
img_filt{n}=img{n}.*uint16(BW);

% Locally brighten the image
denoisedimb = imlocalbrighten(imb{n});
if net_loaded
    % Apply neural network to image if the net is loaded
    denoisedimb = denoiseImage(denoisedimb,net);

```

```

end
% Apply median filter
denoisedimb = medfilt2(denoisedimb,[3 3]);
% Convert image from uint16 to uint8
denoisedimb = uint8(255*mat2gray(denoisedimb));
% Adjust contrast
denoisedimb = imadjust(denoisedimb);
% Find complement of image
denoisedimb = imcomplement(denoisedimb);
% Threshold image - manual threshold
BW = denoisedimb < 150;
% Active contour
iterations = 100;
BW = activecontour(denoisedimb, BW, iterations, 'edge');
imb_filt{n}=imb{n}.*uint16(~BW);

%----Evaluates mean intensity of each optical section----%
avg_asma(ii,n) = mean(mean(imr_filt{n}>0));
avg_cd31(ii,n) = mean(mean(img_filt{n}>0));
avg_dapi(ii,n) = mean(mean(imb_filt{n}>0));
fprintf('Processing Slice %1.0f Finished in %3.2f
seconds.\n',n,toc(slice_loop))
end
% Go to the last row and only grab those values
avg_asma=avg_asma(end,:);
avg_cd31=avg_cd31(end,:);
avg_dapi=avg_dapi(end,:);
% Plotting
hold on
figure(1)
% Clear figure
clf
hold on
% Plot each color for molecule of interest
plot(avg_cd31,'g'),xlabel('Optical Section')
plot(avg_asma,'r'),xlabel('Optical Section')
plot(avg_dapi,'b'),xlabel('Optical Section')
ylabel('Fluorescence Intenstiy')
legend('CD31','ASMA','DAPI')
% Save the figure as a high quality png
file_name=[name '.png'];
print(gcf,file_name,'-dpng','-r300')
% Close figure
close all force
% Find ratio of image intensity across optical sections after normalizing
with
% total signal intensity found.
asma(ii,:) =
mean(avg_asma,2)./(mean(avg_asma,2)+mean(avg_cd31,2)+mean(avg_dapi,2));
cd31(ii,:) =
mean(avg_cd31,2)./(mean(avg_asma,2)+mean(avg_cd31,2)+mean(avg_dapi,2));
DAPI(ii,:)=
mean(avg_dapi,2)./(mean(avg_asma,2)+mean(avg_cd31,2)+mean(avg_dapi,2));

```

```
% Clear data for next image
clear avg_asma avg_cd31 avg_dapi imr img imb
fprintf('Processing Image %1.0f Finished in %3.2f
seconds.\n',ii,toc(image_loop))
end
fprintf('Total Processing time was %3.2f mins.\n',toc(full_loop)/60)
%% Export Image Intensity Data to Excel Sheet
T=table(asma,cd31,DAPI);
T.Properties.RowNames={f_all(:).name};
writetable(T,'Img_Results.xlsx','WriteRowNames',true,'FileType','spreadsheet')
```

VITA

CHIA-PEI DENISE HSU

Born Taipei, Taiwan

- 2004 – 2008 B.S. Mechanical Engineering and Biomedical Engineering
Carnegie Mellon University
Pittsburgh, PA
- 2007 Research Experiences for Undergraduates (REU)
The University of Akron
Department of Polymer Engineering
Akron, OH
- 2008 M.S. Mechanical Engineering
Carnegie Mellon University
Pittsburgh, PA
- 2009 – 2017 Product Specialist / Mechanical Engineer in industry
- 2017 – 2022 Teaching Assistant / Graduate Research Assistant
Florida International University
Miami, FL
- 2019 – 2022 Doctoral Candidate
Florida International University
Miami, FL
- 2022 Dissertation Year Fellowship
Florida International University
Miami, FL

PUBLICATIONS AND PRESENTATIONS (*indicates presenter)

Gonzalez BA, Herrera A, Ponce C, Gonzalez Perez M, Hsu CPD, Mirza A, Perez M, Ramaswamy S. Stem Cell-Secreted Allogeneic Elastin-Rich Matrix with Subsequent Decellularization for the Treatment of Critical Valve Diseases in the Young. *Bioengineering*. 2022; 9(10):587.

Hsu CPD, Tchir A, Mirza A, Chaparro D, Herrera RE, Hutcheson JD, Ramaswamy S. Valve Endothelial Cell Exposure to High Levels of Flow Oscillations Exacerbates Valve Interstitial Cell Calcification. *Bioengineering*. 2022; 9(8):393.

Gonzalez BA, Perez-Nevarez M, Mirza A, Perez MG, Lin YM, Hsu CPD, et al., Ramaswamy S. Physiologically Relevant Fluid-Induced Oscillatory Shear Stress Stimulation of Mesenchymal Stem Cells Enhances the Engineered Valve Matrix Phenotype. *Frontiers in Cardiovascular Medicine*. 2020; 7.

Hsu CPD, Hutcheson JD, Ramaswamy S. Oscillatory Fluid-Induced Mechanobiology in Heart Valves with Parallels to the Vasculature. *Vascular Biology*. 2020; 2(1), R59-R71.

Ruder WC, Hsu CPD, Edelman BD, Schwartz R, Leduc PR. Biological colloid engineering: Self-assembly of dipolar ferromagnetic chains in a functionalized biogenic ferrofluid. *Applied Physics Letters*. 2012; 101(6), 063701.

Ruder WC, Hsu CPD, Chou SY, Dawson JT, Gonzalez LM, Antaki JF, Leduc PR. Micropatterning Biomanufactured Single-Domain Nanoparticles using Self-Assembly to form Artificial Magnetosome Chains. *Biophysical Journal*. 2010; 98(3).

C.-P. D. Hsu*, J. Hutcheson, S. Ramaswamy. "Valve Endothelial Cell Secretions Augment Calcification by Valve Interstitial Cells". Oral presentation, 9th World Congress of Biomechanics 2022, July 10-14, Taipei, Taiwan

C.-P. D. Hsu*, B. Gonzalez, S. Ramaswamy. "Bio-scaffold Versus Synthetic Scaffold Interactions with Seeded Stem Cells in Dynamic Flow Culture Environments". ePoster presentation, 8th Heart Valve Society Annual Meeting 2022, March 3-5, Miami Beach, FL, USA

C.-P. D. Hsu*, A. Mirza, R. Matheny, S. Ramaswamy. "Tricuspid versus Mitral Performance of Cylindrical Porcine Small Intestinal Submucosa Valves". Video presentation, 7th Heart Valve Society Annual Meeting 2021, April 9, Miami Beach, FL, USA

C.-P. D. Hsu*, A. Tchir, J. D. Hutcheson, S. Ramaswamy. "Calcific Media Combined with Media from Oscillatory Flow-Conditioned Valve Endothelial Cells Leads to Valve Interstitial Cell Calcification". Video presentation, 52nd Biomedical Engineering Society Annual Meeting 2020, October 14-17, San Diego, CA, USA

C.-P. D. Hsu*, A. Mirza, R. Matheny, S. Ramaswamy. "Hydrodynamic Assessment of a Small Intestinal Submucosa Tubular Aortic Valve". Oral presentation, International Conference of Tissue-Engineered Heart Valves & 6th Heart Valve Society Annual Meeting 2020, February 14-16, Abu Dhabi, UAE